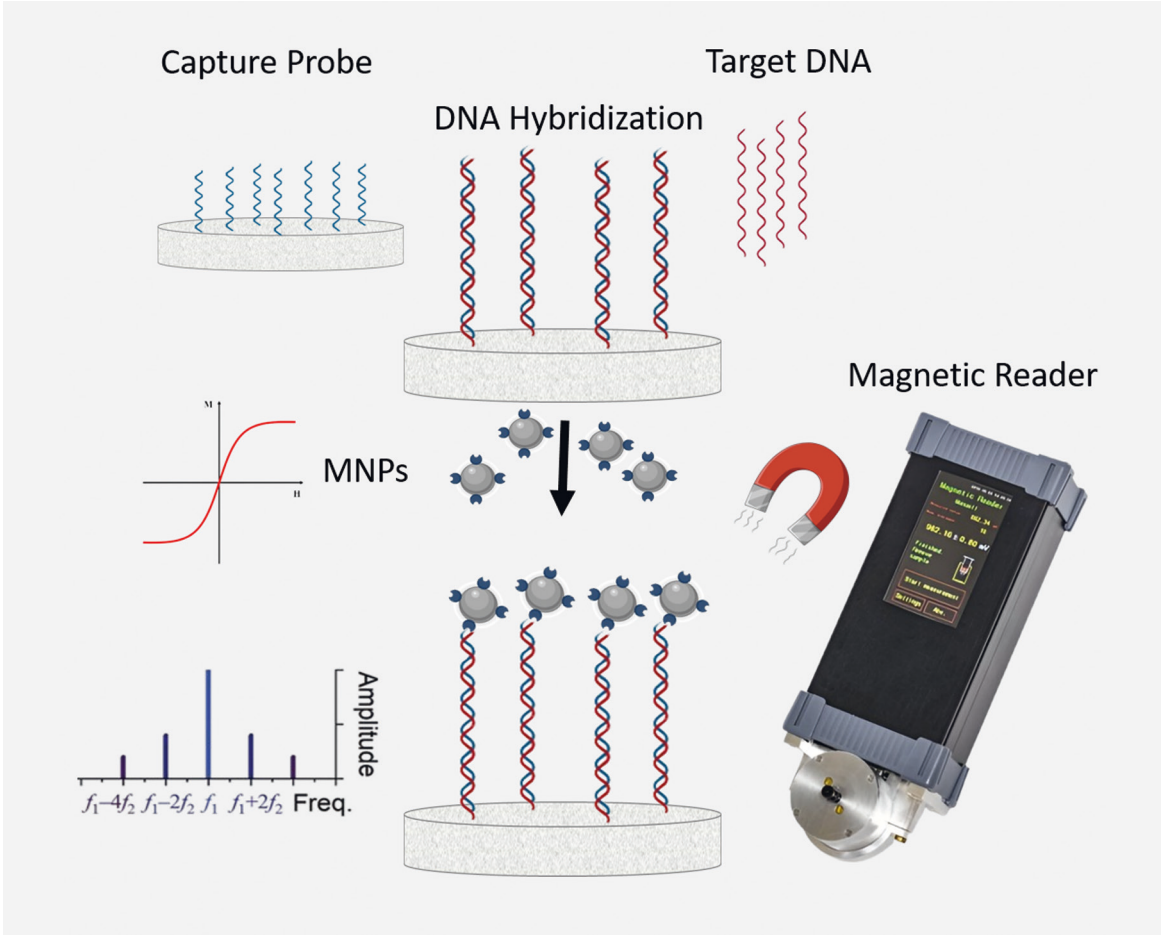

Development of Superparamagnetic Based Biological Sensor for the Detection of Brucella DNA Using Frequency Mixing Magnetic Detection

Abdalhalim Abuawad

Information
Band / Volume 113
ISBN 978-3-95806-836-0

Mitglied der Helmholtz-Gemeinschaft

JÜLICH
Forschungszentrum

Schriften des Forschungszentrums Jülich
Reihe Information / Information Band / Volume 113

Forschungszentrum Jülich GmbH
Institut für Biologische Informationsprozesse (IBI)
Bioelektronik (IBI-3)

Development of Superparamagnetic Based Biological Sensor for the Detection of Brucella DNA Using Frequency Mixing Magnetic Detection

Abdalhalim Abuawad

Schriften des Forschungszentrums Jülich
Reihe Information / Information Band / Volume 113

ISSN 1866-1777 ISBN 978-3-95806-836-0

Bibliografische Information der Deutschen Nationalbibliothek.
Die Deutsche Nationalbibliothek verzeichnet diese Publikation in der
Deutschen Nationalbibliografie; detaillierte Bibliografische Daten
sind im Internet über http://dnb.d-nb.de abrufbar.

Herausgeber und Vertrieb:	Forschungszentrum Jülich GmbH Zentralbibliothek, Verlag 52425 Jülich Tel.: +49 2461 61-5368 Fax: +49 2461 61-6103 zb-publikation@fz-juelich.de www.fz-juelich.de/zb
Umschlaggestaltung:	Grafische Medien, Forschungszentrum Jülich GmbH
Druck:	Grafische Medien, Forschungszentrum Jülich GmbH
Copyright:	Forschungszentrum Jülich 2025

Schriften des Forschungszentrums Jülich
Reihe Information / Information, Band / Volume 113

D 82 (Diss. RWTH Aachen University, 2025)

ISSN 1866-1777
ISBN 978-3-95806-836-0

Vollständig frei verfügbar über das Publikationsportal des Forschungszentrums Jülich (JuSER)
unter www.fz-juelich.de/zb/openaccess.

Abstract

Early detection of zoonotic diseases is essential in preventing the consequences of outbreaks and reemergence occurrences. Brucellosis is endemic in several countries and has re-emerged with a high prevalence rate in different locations, affecting livestock and public health sectors. Due to the limitations of conventional *Brucella* detection methods, including limited specificity, long incubation times and safety concerns, developing a rapid, selective and accurate technique for the early detection of *Brucella* in livestock animals is crucial to prevent the spread of the associated disease. In the present thesis, we introduce a magnetic nanoparticle marker-based biosensor using Frequency Mixing Magnetic Detection (FMMD) for the detection and quantification of *Brucella* DNA. Magnetic nanoparticles (MNPs) were used as magnetically measured markers to selectively detect the target DNA hybridized with its complementary capture probes immobilized on a porous polyethylene filter. Our sensor demonstrated a relatively fast detection time of approximately 10 min, with a detection limit of 0.09 fM when tested using DNA amplified from *Brucella* genetic material by means of Polymerase Chain Reaction (PCR). In addition, the detection specificity was examined using gDNA from *Brucella* and other zoonotic bacteria that may coexist in the same niche, confirming the method's selectivity for *Brucella* DNA. To enhance the practicality of the developed assay, we combined it with isothermal Recombinase Polymerase Amplification (RPA) and achieved rapid detection of 9 fM *Brucella* DNA in 25 minutes total assay time. In addition to isothermal DNA amplification in a water bath, we showed the feasibility of RPA directly inside our portable FMMD-based device. When being controlled by means of pulse width modulation (PWM), the inherently generated heat of the low frequency (LF) excitation coil of the magnetic reader can be utilized to serve as a constant temperature bath for RPA, thus enabling isothermal amplification inside the magnetic measurement head. We confirmed that RPA performs with high efficiency in the sensor unit of the FMMD device. In summary, the portability of the measurement device, the selective sensing of MNPs, the fast detection time, and the ability to deliver quantitative results make this biosensor a valuable tool for early on-site diagnosis and monitoring of *Brucella* infections in resource-limited settings.

Zusammenfassung

Die frühzeitige Erkennung von Zoonosen ist von entscheidender Bedeutung, um die Folgen von Ausbrüchen und Wiederausbrüchen zu verhindern. Brucellose ist in mehreren Ländern endemisch und ist mit einer hohen Prävalenzrate an verschiedenen Orten wieder aufgetreten, was Auswirkungen auf die Viehbestände und die öffentliche Gesundheit hat. Aufgrund der Einschränkungen herkömmlicher *Brucella*-Nachweisverfahren wie begrenzte Spezifität, lange Inkubationszeiten und Sicherheitsbedenken, ist die Entwicklung einer schnellen, selektiven und genauen Methode für den frühzeitigen Nachweis von *Brucella* in Nutztieren von entscheidender Bedeutung, um die Ausbreitung der Krankheit zu verhindern. In der vorliegenden Arbeit stellen wir einen auf magnetischen Nanopartikeln basierenden Biosensor vor, der Frequenzmischungs-Magnetdetektion (FMMD) für den Nachweis und die Quantifizierung von *Brucella*-DNA nutzt. Magnetische Nanopartikel (MNP) wurden als magnetisch gemessene Marker verwendet, um selektiv die Ziel-DNA nachzuweisen, die mit der auf einem porösen Polyethylenfilter immobilisierten komplementären DNA hybridisiert. Unser Sensor zeigte eine relativ schnelle Nachweiszeit von etwa 10 Minuten mit einer Nachweisgrenze von 0,09 fM, wenn er mit DNA getestet wurde, die aus dem genetischen Material von *Brucella* mittels Polymerase-Kettenreaktion (PCR) amplifiziert wurde. Darüber hinaus wurde die Spezifität unter Verwendung von gDNA von *Brucella* und anderen zoonotischen Bakterien, die in der gleichen Nische vorkommen können, untersucht und die Selektivität der Methode für *Brucella*-DNA bestätigt. Um die Praxistauglichkeit des neuentwickelten Assays zu verbessern, haben wir ihn mit Rekombinase-Polymerase-Amplifikation (RPA) kombiniert und einen schnellen Nachweis von 9 fM *Brucella* DNA innerhalb einer Gesamttestzeit von 25 Minuten erreicht. Zusätzlich zur isothermalen Amplifikation im Wasserbad haben wir die Machbarkeit von RPA direkt in unserer portablen FMMD-basierten Sensoreinheit gezeigt. Indem die inhärent erzeugte Wärme der niederfrequenten (LF) Anregungsspule des Magnetreaders mittels Pulsweitenmodulation (PWM) geregelt wird, kann der Messkopf als konstantes Temperaturbad für die RPA genutzt werden, um isothermale Amplifikation im Magnet-Messkopf zu ermöglichen. Wir konnten zeigen, dass RPA mit hoher Effizienz direkt in der Sensoreinheit des FMMD-Geräts funktioniert. Zusammenfassend lässt sich sagen, dass die Tragbarkeit des Messgeräts, die selektive Erfassung von MNPs, die schnelle Nachweiszeit und die Fähigkeit, quantitative Ergebnisse zu liefern, diesen Biosensor zu einem wertvollen Instrument für die frühzeitige Vor-

Ort-Diagnose und Überwachung von *Brucella*-Infektionen in ressourcenbeschränkten Umgebungen machen.

Table of Contents

Chapter 1

1. Introduction

In Palestine, animals, particularly milk-producing ones like sheep, goats and camels, are essential to many families as they rely on them as an important source of income. The communities that raise these animals live nomadic or semi-nomadic lifestyles, relying on grazing animals in mountainous and rural areas in search of pastures and water. Unfortunately, the low infrastructure in these areas, which are far from major cities, the lack of access to public health measures and the close contact with many animals make people living these lifestyles more likely to be infected by animal pathogens. Among these infections is brucellosis, a disease transmitted to humans through the consumption of unpasteurized milk and its products that seriously impacts economic and public health [1,2]. Brucellosis re-emerged after 2012 in Palestine with significant higher incidence rate in the south of the west bank and neighboring regions like Al-Naqab. The reported incidence rates were 26.2/100,000 in west bank and 33.5/100,000 in Al-Naqab according to Palestinian and Israeli ministries of health [3]. The reasons for the re-emergence of brucellosis are many such as socioeconomic factors, climate change and weak regional cooperation. Until now, the accurate and fast detection of infected animal samples in the field has been a major hurdle in implementing surveillance programs. Therefore, developing point-of-care (PoC) methods capable of detecting *Brucella* pathogen in the field is greatly needed to fight this serious disease. This thesis is written as a part of the Palestinian German Science Bridge (PGSB) which is funded by the German Ministry of Higher Education and Research (BMBF). The project is about the development of on-site magnetic based biological sensors for the detection of *Brucella spp.*

The importance of having a test that can rapidly detect the pathogen in the field is out of importance for this type of disease. It eliminates the need to transport samples from far areas to central labs in major cities which require additional time and cost. In addition, it helps and improves surveillance and control measures by enabling immediate identification and isolation of infected animals which reduces the spread of the disease between animals. Currently, the most common method used to detect *Brucella* pathogen at PoC is Rose Bengal Test (RBT). It

is a simple, rapid and cheap serological test based on the principle of antigen-antibody interaction. The stained antigens with rose bengal dye interact with antibodies of infected animals, resulting in visible agglutination in about 5 minutes [4]. However, it gives a high rate of false positive results due to cross-reactivity with other bacterial organisms especially in endemic areas [5,6]. RBT is considered a suitable test for initial screening, but it needs another lab-based highly specific test such as blood culture to confirm the result.

Based on the results of all methods used for brucellosis diagnosis, whether lab-based or PoC testing methods, the detection of *Brucella* DNA as a target molecule was proven to be efficient and accurate in terms of sensitivity, specificity and safety [7–9]. Detecting DNA addresses the limitations of other methods. It ensures high sensitivity as the DNA can be amplified from a very low amount to be detectable, using one of the several amplification methods, e.g. polymerase chain reaction (PCR). It ensures high specificity as it has unique nucleotide sequences which minimize the likelihood of cross-reactivity with other organisms. In addition, it is safer to analyze genetic material rather than live bacteria. In general, nucleic acid (NA) detection methods proved to be effective, and the most recent example was during the outbreak of SARS-CoV-2, which had made NA detection methods well-known. However, the requirements of sophisticated labs with different operational areas limit their practical use in on-site testing. Therefore, developing an appropriate assay for in-field testing of *Brucella* DNA is essential to provide a highly accurate and specific screening method.

The chemical stability, biocompatibility, and large surface area of nanoparticles make them very attractive materials for the on-site detection of many target analytes [10]. Mainly, magnetic nanoparticles (MNPs) have been widely used in several nucleic acid assays, including genomic DNA magnetic extraction, target enrichment, and DNA detection based on MNPs functioning as sensing elements [11]. The detection of MNPs can be achieved by using different methods such as susceptometry, relaxometry, and frequency mixing magnetic detection (FMMD) [12]. FMMD, with its portable magnetic reader is the technique used in this thesis to selectively detect and quantify magnetic nanoparticles (MNPs) [13]. The technique employs the mixing of magnetic fields at different frequencies at the nonlinear magnetization of MNPs, generating a distinct magnetic response signal at the sum and difference frequencies that enables the specific detection of MNPs.

In this thesis, we developed a new assay designed for the detection of *Brucella* DNA using FMMD technology with its portable magnetic reader. The core of this assay relies on the use

of MNPs, which serves as markers for sensing and quantifying the sequence-specific hybridization event between a capture probe immobilized on a polyethylene (PE) filter and its complementary target DNA.

A brief background information on the main topics is provided in Chapter 2. It begins with an overview of zoonotic diseases and their impact on public health and economic sectors, followed by a short review of brucellosis disease and the risk of reemergence in different countries. The conventional detection methods used to detect *Brucella* and their limitations are discussed. The isothermal amplification techniques and their role in PoC molecular diagnostic, focusing on recombinase polymerase amplification (RPA), are presented. The advantages of using MNPs in biosensing applications and the unique properties that make them suitable for PoC testing are discussed. Then, the specific phenomenon of superparamagnetism (SP) and superparamagnetic nanoparticles' (NPs) behavior when exposed to an external magnetic field is explained in detail. Finally, the basic principle of FMMD and the wide range of its applications in biosensing are presented.

Chapter 3 describes the reagents, oligonucleotide sequences, and genomic DNA used in this thesis, and covers all methodologies used for establishing the assay. Moreover, all the instruments utilized for FMMD measurement are presented, including the magnetic reader with its sensing entity (measurement head) and the systems used for automated measurements. Finally, the new implementation of a temperature controller into the measurement head for performing RPA amplification directly inside the measurement head in a temperature-controlled environment is explained.

Chapter 4 describes the establishment and validation of our magnetic assay for *Brucella* detection using synthetic oligonucleotide complementary targets. It covers the selection of new DNA target sequences and the design of capture probes using several in-silico tools. In addition, it provides the methods applied to PE filters, including surface functionalization and immobilization strategy. Several experimental conditions that would influence hybridization performance and magnetic measurement are investigated and discussed. The demonstration of the sensor's ability to quantify target DNA sequences with high sensitivity and specificity is addressed.

In Chapter 5, we evaluate the feasibility of our developed assay to detect DNA in clinically relevant samples by testing its performance with genomic DNA extracted from different infected animals. These extracted genomic DNA (gDNA) represent different bacterial species,

including *Brucella* pathogen and other non-related bacteria. It describes the strategies employed for DNA amplification, with a specific focus on PCR as a reference amplification method. In addition, strategies employed for ssDNA generation from dsDNA amplicons are discussed. Finally, the limit of detection and specificity are presented.

Chapter 6 introduces an advancement for our assay toward PoC detection by combining RPA amplification with FMMD. It presents all the steps involved in establishing the RPA assay, as well as the methods used for performing asymmetric RPA and their limitations. The new detection strategy based on using tailed primers to detect the whole amplicon is also discussed. All analytical performance experiments are presented and discussed.

Finally, chapter 7 presents another vital improvement to the FMMD technique in terms of field nucleic acid testing. Here, the thermal energy in the MH was utilized and controlled to perform RPA amplification inside our magnetic reader, without the need for additional instrumentation for the amplification process.

Chapter 2

2. Background

2.1. Zoonotic diseases

Among the 1400 species of human pathogens identified, 61% are known to be of animal origin [14]. These pathogens are the responsible agents of zoonoses, infections that can be transmitted from wild and domestic animals to humans. A wide range of pathogens, such as bacteria, viruses, parasites, etc., infect animals as the primary source of infection and are then introduced into humans through several modes of transmission [15]. Throughout history, many zoonotic diseases outbreaks such as severe acute respiratory syndrome (SARS), influenza A (H1N1), Middle East respiratory syndrome (MERS) and Ebola virus diseases have affected several countries, causing great loss of human life and a huge impact on global economics [16,17]. Until now, zoonoses are globally threatening both public health and economic sectors. The threat arises from the fact that they have the potential to cause new widespread outbreaks and become epidemic or pandemic. A recent example is the ongoing worldwide pandemic of COVID-19 that was caused by the SARS-CoV-2 virus, leading to more than 775 million confirmed cases and about 7 million deaths [18].

Due to the complex nature of zoonotic diseases and factors such as globalization, urbanization, climate change, and increased human-wildlife interaction, preventing such diseases is very challenging [19–21]. However, some control and prevention programs have been implemented, including testing, vaccination, and public health measures to reduce the risk of transmission [15,22]. In all programs, regular animal surveillance of wild and domestic animals is an essential step to achieve an effective measure, particularly for diseases that have the potential to reemerge.

2.1.1. Brucellosis

Brucellosis is one of the most common global zoonotic diseases caused by bacteria of the genus *Brucella.* Of the 12 *Brucella* species*, Brucella melitensis, Brucella abortus, Brucella suis* and *Brucella canis* are the four species related to human infections [23]. These species mainly infect milk-producing animals in livestock, such as cattle, sheep, goats, and camels, resulting in significant losses to animals and a reduction in milk production. The infection is transmitted to humans through direct contact with the infected animals or the consumption of their products. According to a recent study by the Centers for Disease Control and Prevention organization (CDC), the new estimated global incidence rate of human brucellosis is about 2.1 million new cases yearly, which differ from the previously thought number of 500,000 cases estimated by WHO [24]. Although the control measures that have been taken were effective in reducing brucellosis infections many regions, the disease is still endemic in several developing countries in the Middle East, Asia, Africa and Southern Europe [25,26]. Figure 1 shows the heat map of global annual incidence of human brucellosis.

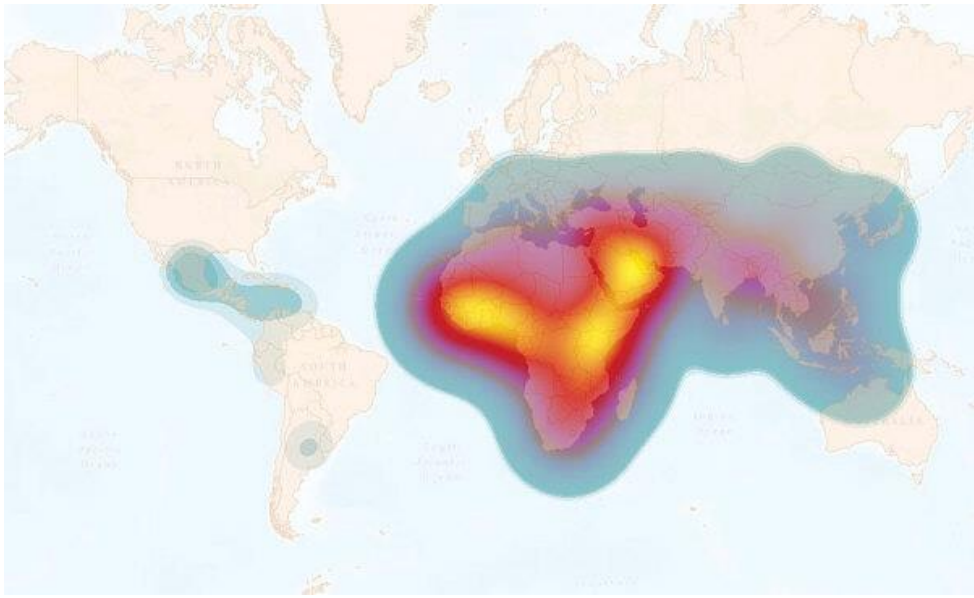

Figure 1. Heat map illustrating the global annual incidence of human brucellosis per 1 million people [24].

For many years, numerous studies showed an increased incidence rate of brucellosis in different geographical areas, highlighting the high risk of a reemergence of this disease [3,27]. Even in

countries that have been declared free of brucellosis, reemergence was reported by local *Brucella* strains, and in many countries such as Germany, France and United Kingdom, imported *Brucella* species originating from endemic regions were identified [28–30]. Preventing the spread of the disease through rigorous surveillance and control programs is essential to reduce the infection rate and minimize the economic and public health burden of this severe disease.

2.1.2. Conventional detection methods

Brucellosis infection can be diagnosed by directly detecting the whole bacteria, its DNA, an antigen, or indirectly by measuring the antibody and immune response [31]. The direct isolation of the whole *Brucella* bacteria from specimens like bone marrow, joint fluid and tissues by blood culture method is considered gold standard in terms of diagnostic specificity. However, it has limitations such as low diagnostic sensitivity (10 to 90%), prolonged incubation time (up to 4 weeks) and safety concerns [32]. Due to these limitations, serological assays like the Rose Bengal Test (RBT) and the Standard Agglutination Test (SAT) were used as rapid and safe tests for the detection of *Brucella* antibodies. Despite their simplicity, these serological methods suffer from low specificity due to cross-reactivity with other bacterial organisms, as well as from low sensitivity at the early stage of infection [6,33]. Nucleic acid amplification tests (NAATs) like polymerase chain reaction (PCR) and its variants were proven to be more sensitive, specific, and safe than other conventional methods, which makes them a reliable alternative [34,35]. However, the requirements of sophisticated labs with different operational areas and stationary expensive equipment limit their practical use in the on-site testing of *Brucella*. Thus, the development of a suitable assay for the in-field testing of *Brucella* DNA is crucial to ensure a highly accurate and specific screening method.

2.2. Isothermal nucleic acid amplification techniques

2.2.1. Overview

Isothermal amplification techniques have revolutionized molecular diagnostics by enabling the detection of specific DNA or RNA sequences with high sensitivity and specificity in PoC scenarios [36,37]. These isothermal techniques offer the advantages of simplicity and speed compared to PCR [38,39]. In addition, they have a single operating temperature to support the various enzymatic processes involved in DNA or RNA amplification, which makes integration

into a field-detection platform feasible, without the need for expensive sophisticated thermal cycling equipment. Figure 2 shows an overview of isothermal nucleic acid amplification methods based on their reaction temperature.

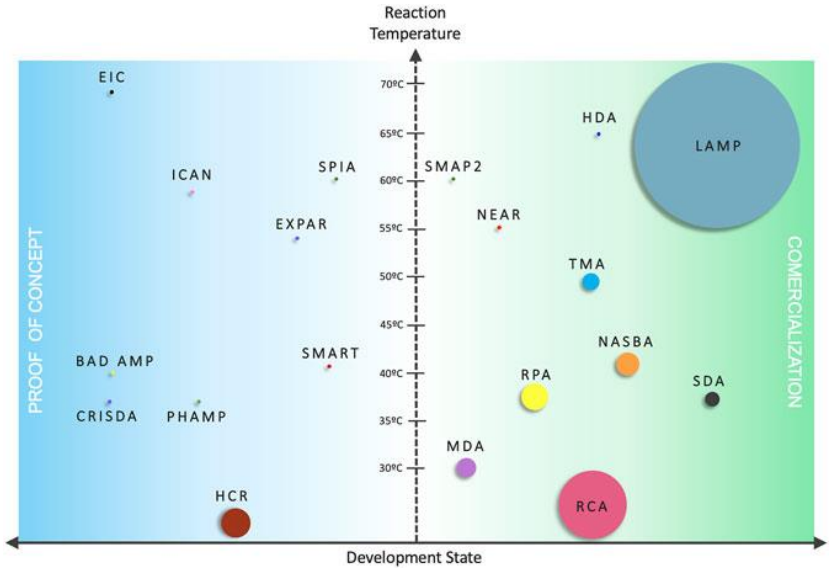

Figure 2. Isothermal nucleic acid amplification methods based on their reaction temperature [40].

Among these techniques, major attention has been paid to Loop-Mediated Isothermal Amplification (LAMP), Rolling Circle Amplification (RCA), Recombinase Polymerase Amplification (RPA) and many more alternatives to PCR [40]. LAMP amplification can detect as low as one single copy with high specificity due to the use of multiple primer sets that bind different regions on template DNA. In addition, its amplification products can be detected through simple visualization methods like turbidity, which makes it more popular than other methods [41]. RCA has a low incubation temperature

e around 23°C and simple requirements are needed for amplification such as one single primer and DNA polymerase [42]. RPA offers a rapid amplification time of 20 minutes with high sensitivity and specificity. The most important feature of LAMP, RCA and RPA is that the initial denaturation of templates is not required like other methods such as Strand Displacement Amplification (SDA) [40]. However, each of these techniques has its own disadvantages. LAMP requires a complex assay design due to the number of primers sets used. RCA is limited to circular templates and long fragments only. RPA can be costly due to the high price of the commercial kits. In general, the selection of an isothermal amplification method relies on the

requirements of the assay, such as the type of nucleic acid target, the time needed, the place of testing, cost and the readout method.

2.2.2. Recombinase polymerase amplification

In 2006, Piepenburg et al. developed a novel isothermal amplification approach called Recombinase Polymerase Amplification (RPA) to detect *Staphylococcus aureus* DNA without the need for thermal denaturation of the template and thermal cycler equipment [43]. This approach includes additional components such as a recombinant enzyme (T4 UvsX), Strand-displacement DNA polymerase (bacillus subtilis Pol I), Single Stranded DNA-Binding proteins (SSBs) and Polyethylene Glycol (PEG) [44]. The mechanism of the RPA process involves first the formation of the recombinase-primer complex when the recombinase enzyme T4 UvsX binds to the forward and reverse primer sequences in the presence of ATP, PEG and loading factor T4 UvsY protein. Once the complex is formed, it scans the genome to find the homologous sequences. When the target site is found, a D-ring loop structure forms through the strand chain exchange reaction initiated by the recombinase-primer complex. This interaction is stabilized by the SSBs proteins that bind to the displaced strands, which prevent primer dissociation. Finally, the recombinase dissociates, leaving the 3` end of the primers, and the synthesis of new strands starts by DNA polymerase [45]. Figure 3 shows the principle of RPA amplification.

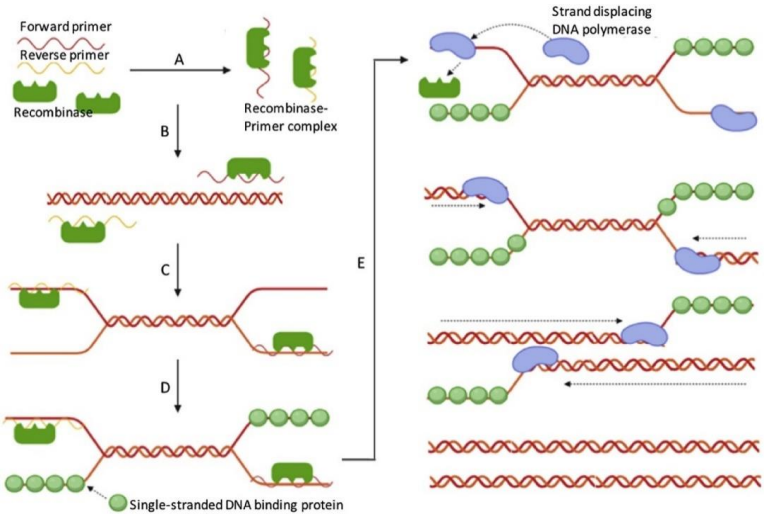

Figure 3. RPA principle. A) The formation of primer-recombinase complex. B) Recognition of homologous sequences. C) Strand chain exchange. D) Single-stranded DNA binding proteins binding to displaced strand. E) DNA polymerase binding to the 3`end of the primers and extension [46].

The whole RPA amplification process operates at a constant temperature, typically between 37°C and 42°C. However, other studies demonstrated that RPA amplification can still produce detectable signals even at low temperatures such as 25°C [47,48]. RPA amplification is considered as the fastest method compared to other isothermal techniques, with an reaction time between 20 and 40 min [40]. Other studies showed the capability of RPA to amplify DNA in less than 10 min [49,50]. In terms of sensitivity, RPA can detect as low as one single copy, which is similar to the performance of PCR [51]. RPA can also be directly performed in several sample types such as milk, urine, serum and pleural fluids, even in the presence of known PCR inhibitors [45]. Another important feature is the long-term stability of its reagents. They can be stored up to 12 weeks at 25°C with the same efficiency. In addition, it can be used in lyophilized form, which is very beneficial for PoC testing [52]. The features of RPA amplification make it an attractive technology for several molecular diagnostic applications. It has been widely used for the detection of pathogens in fields such as the food industry, agriculture, water testing, and veterinary medical diagnostics [53]. However, it suffers from some issues such as the formation of primer dimer due to the length of primers (30-35 bp), nonspecific amplification, the need for primer screening of several pairs, and the cost of their kits, which are currently manufactured and sold by only one company (TwistDx, UK).

2.3. Magnetic nanoparticles

2.3.1. Structure

In the last decade, the widespread use of nanoparticles has advanced medical diagnostics, particularly in biosensing applications. Their characteristics such as chemical stability, biocompatibility, and large surface area make them highly attractive materials for the on-site detection of various target analytes [10]. Among nanoparticles, magnetic nanoparticles (MNPs) have been widely used in several assays, such as DNA magnetic extraction, target enrichment, and pathogen detection based on MNPs functioning as sensing elements [11]. What makes magnetic nanoparticles different from other nanoparticles is their distinct characteristic, which is being magnetic. This allows us to manipulate or separate them using an external magnetic field, or using them as labels by measuring their selective magnetic response. The most common type of MNPs are superparamagnetic iron oxide nanoparticles (SPION), which are synthesized in the form of magnetite (Fe_3O_4) or maghemite (γ- Fe_3O_3) surrounded by a thin amorphous oxide layer and the shell, see Figure 4.

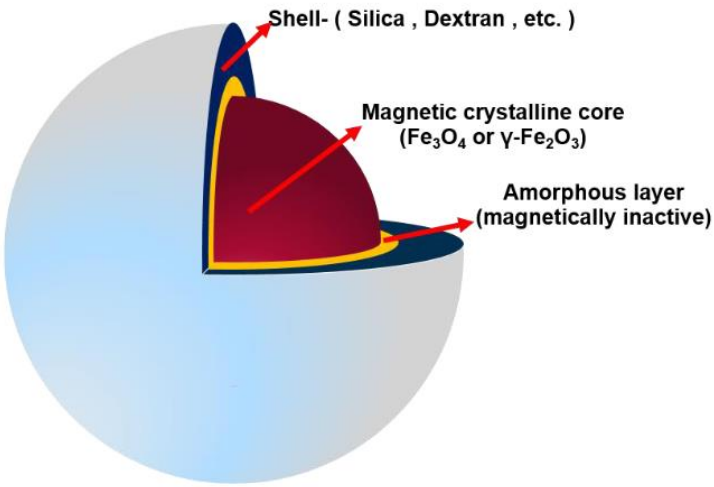

Figure 4. Single core MNP model. Adapted from Ali Pourshahidi dissertation [54].

For MNP biosensing assays, it is important to coat plain MNPs with a protective shell on the surface to prevent them from agglomeration due to magnetostatic and van der Waals interactions. Moreover, the shell can make them hydrophilic and biocompatible. In addition,

this shell can be functionalized with different molecules such as carboxylic acid, amines and streptavidin, which make them beneficial for immobilizing a various types of capture biological molecules like ssDNA oligonucleotide probes, enzymes, aptamers and antibodies [10].

MNPs have advantages over other nanoparticles in biosensing assays, as they are highly responsive and controllable when a magnetic field is applied, leading to highly selective and rapid target detection [55]. The first advantage is that they have a high saturation magnetization, which leads to a strong response, allowing fast detection. Moreover, their specific magnetic response allows for accurate and efficient detection, as most of the molecules that lead to nonspecific interaction in complex biological media are nonmagnetic. Furthermore, they exhibit higher stability and lower background noise, compared with other optical nanoparticles [56]. These advantages make them good candidates for reliable field detection of DNA.

2.3.2. Superparamagnetic nanoparticles

What is important in magnetic biosensing applications is the behavior of MNPs when exposed to external magnetic field. Superparamagnetic NPs are particles that can be magnetized in the presence of a magnetic field, and demagnetize quickly when the magnetic field is removed [55]. The explanation for that is a magnetic phenomenon called superparamagnetism (SP), which is a unique behavior that happens to ferromagnetic and ferrimagnetic materials when their sizes are reduced to a few nanometers in the single domain region (see Figure 5) [57].

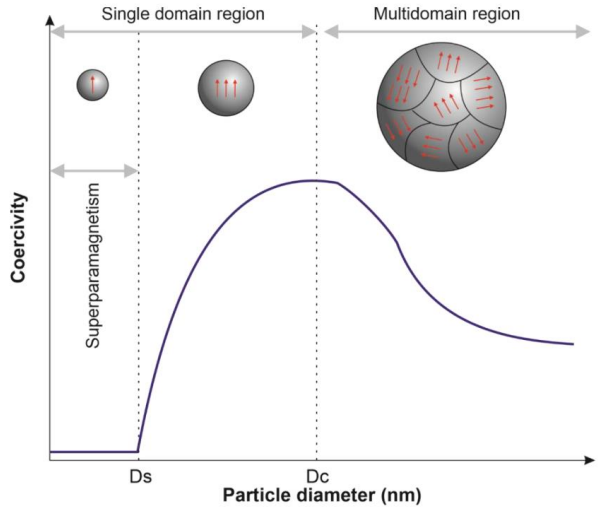

Figure 5. MNP transition from superparamagnetic to multidomain region based on particle diameter. The red arrows show the orientation of the domains [57].

At this small size and in the absence of an external magnetic field, the magnetic moments of the material point randomly in all directions. Once a magnetic field is applied, the magnetic moments respond and align in the same direction as the magnetic field applied, see Figure 6. When removed, the magnetic moments flip back to random orientation due to the thermal energy, and the net magnetic moment becomes zero [58].

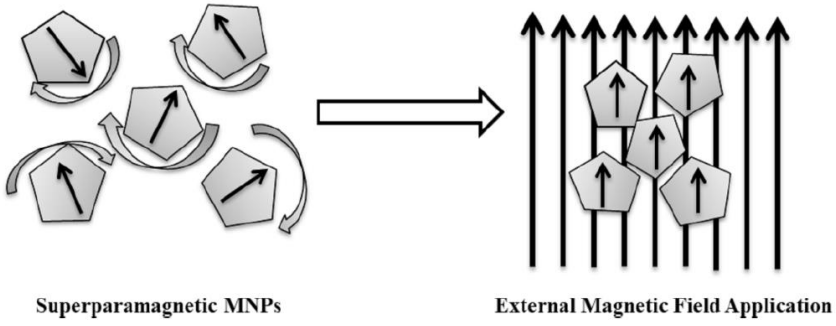

Figure 6. Magnetic moment orientations of superparamagnetic NPs in the absence (left) and presence (right) of an external magnetic field [59].

They exhibit non-linear magnetization curve with zero hysteresis, see Figure 7. The loss of magnetization makes them different from ferromagnetic NPs that become permanently magnetized after removing the external magnetic field. Having this type of MNP that can be temporarily magnetized makes them more preferred than other MNPs types, particularly for biomedical applications.

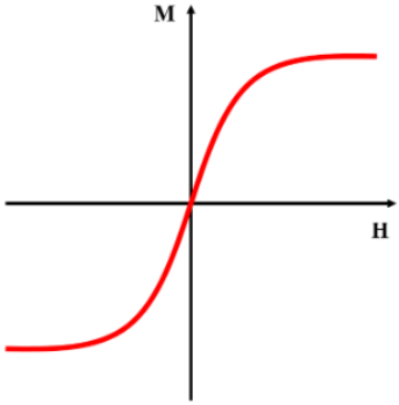

Figure 7. The magnetization curve of superparamagnetic NPs.

2.4. Frequency mixing magnetic detection

Frequency mixing magnetic detection (FMMD) is the technique employed to detect and quantify the superparamagnetic NPs markers used in this dissertation. The core of this technique relies on the magnetic response of superparamagnetic NPs or of magnetic beads (MBs) that exhibit nonlinear magnetic properties by measuring the harmonic distortions in the detected signal. The principle of FMMD is explained in Figure 8. Here, the sample containing MNPs is exposed to a dual-frequency magnetic excitation field, a high frequency f_1 and a low frequency f_2. Once the MNPs are exposed to such a field, their nonlinear magnetization response leads to a distorted time-varying magnetization, generating various new sum and difference mixing frequencies [13].

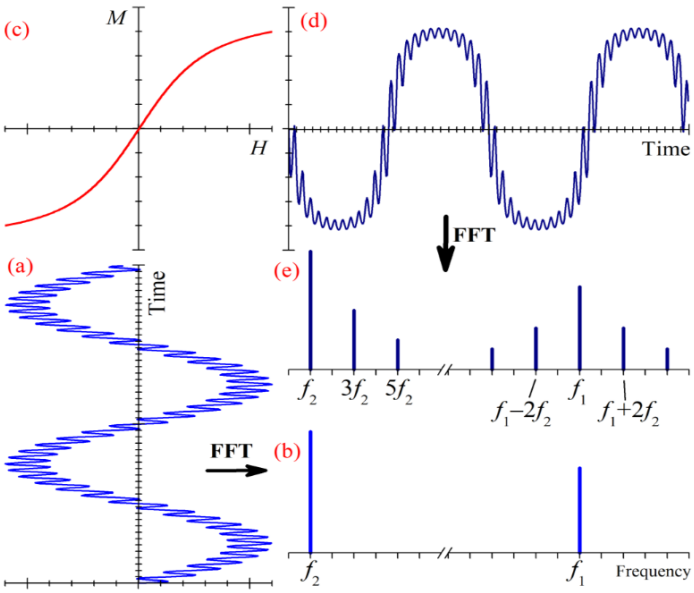

Figure 8. Graphical illustration of frequency mixing principle. a) The superparamagnetic NPs are exposed to a magnetic field consisting of two frequency components high frequency (f_1) and low frequency (f_2). b) The excitation frequency spectrum exhibits two distinct lines. c) The non-linear magnetization curve of superparamagnetic NPs. d) The distorted time-dependent magnetization of superparamagnetic NPs. e) The multi-harmonic frequency spectrum of the response signal.

This technique uses ABICAP immunofiltration columns as a vertical flow system with a volumetric capacity of 750 µl. The ABICAP columns contain a porous sintered polyethylene filter (PE) as a solid surface for immobilizing biological capture molecules. These columns come with two sizes of PE filters, ∅ 5 × 5 mm and ∅ 5 × 2.5 mm. Both sizes are suitable for binding a large number of biological molecules. Compared to lateral flow assays, this vertical flow system is independent of the sample volume and has a higher binding capacity, which allows for a more sensitive and wider detection range. In addition, it provides a quantitative result.

FMMD, with its portable magnetic reader, has been widely used as a selective technique for quantifying MNPs in different immunoassay applications. It was used as a PoC technique to rapidly detect of SARS-CoV-2-specific antibodies in 170 sera sample patients, obtaining a high sensitivity of 97% and a specificity of 92% in 21 min of total assay time [60]. It was also used to quantify plant viruses in less than 30 minutes, obtaining a wider dynamic detection range

compared to ELISA [61]. Furthermore, a competitive magnetic immunoassay was applied in FMMD to quantify Aflatoxin B1 in contaminated crops, and a detection limit of 1.1 ng comparable to the cELISA reference method was achieved [62]. Antibiotics in milk were also detected using the same competitive magnetic immunodetection [63]. Many other analytes were quantified using this technique, such as proteins in human blood and bacterial antigens [64,65]. Recently, multiplex detection of different particles was demonstrated, showing the potential of this technique to detect multiple analytes in a single assay [66–68]. The advantages of the FMMD technique make it a promising tool for rapid and selective detection of various analytes in research settings.

Chapter 3

3. Reagents, instruments, and methods

This chapter provides a description of the reagents, oligonucleotide sequences, genomic DNA, and methodologies used in the development of our magnetic biosensor assay for the detection of *Brucella* DNA. It covers the selection of the DNA target, the design of hybridization capture probes, and primers using several bioinformatics tools. In addition, it provides the methods applied to PE filters, including surface functionalization and immobilization for establishing the assay. Additionally, the labeling and measurement of MNPs by FMMD are explained.

The chapter also describes the strategies employed for DNA amplification with a specific focus on both PCR as a reference and the isothermal RPA amplification as a point-of-care (PoC) amplification method. It covers combining RPA amplification with FMMD magnetic detection for the on-site quantification of amplified *Brucella* DNA. In addition, the experiments performed to detect authentic *Brucella* genomic DNA from other unrelated genomic DNA are explained.

Moreover, all the instruments utilized for FMMD measurement are presented, including the magnetic reader with its sensing entity (measurement head) and the systems used for automated measurements. Finally, the new implementation of a temperature controller into the measurement head for performing RPA amplification directly inside the measurement head in a temperature-controlled environment is explained.

3.1. Reagents

1-Ethyl-3-(3-dimethylaminopropyl) carbodiimide (EDC), BupH MES-Buffered Saline Packs containing 0.1 M 2-(N-morpholino) ethanesulfonic acid, 0.9% sodium chloride at pH 4.7 (MES), phosphate-buffered saline (PBS) (10 mM phosphate, 150 mM sodium chloride, pH 7.3 to 7.5), and (10×) bovine serum albumin in PBS (BSA) were purchased from Thermo Fisher

Scientific (Erlangen, Germany). The organic compound ethylenediamine (EDA), betaine solution, and gold nanoparticles with 40 nm size were obtained from Sigma-Aldrich Chemie GmbH (Taufkirchen, Germany). Phusion® High-Fidelity DNA Polymerase, dimethyl sulfoxide (DMSO), and lambda exonuclease kit were purchased from New England Biolabs GmbH (Frankfurt am Main, Germany). All solutions were prepared in ultrapure deionized water (Millipore, Merck, Darmstadt, Germany).

Sintered polyethylene filters (PE) with ∅ 5 mm × 2.5 mm size and about 20 µm pore size, ABICAP immunofiltration columns were obtained from Senova Gesellschaft für Biowissenschaft und Technik mbH (Weimar, Germany). The superparamagnetic nanoparticles (MNPs) used were both of type Synomag®-D, one has a streptavidin surface (Product code: 104-19-701) and the other has a plain surface (Product code: 104-00-701), and both have the same hydrodynamic diameter (70 nm). The MNPs were obtained from Micromod Partikeltechnologie GmbH (Rostock, Germany). TwistAmp® Liquid Basic kit was obtained from TwistDx™Ltd (Maidenhead, United Kingdom). GeneRuler Low Range DNA Ladder, and DNA Gel Loading Dye (6X) were purchased from Thermo Fisher Scientific™ (Langerwehe, Germany). ROTI ® Prep PCR Purification, and Agarose standard powder were obtained from Carl Roth GmbH (Karlsruhe, Germany). RedSafe DNA stain (20.000 X) was obtained from Hiss Diagnostics GmbH (Freiburg im Breisgau, Germany).

3.2. Oligonucleotide sequences

All the designed single-stranded DNA (ssDNA) sequences, including target, non-target, control and capture probe, along with their modifications used in this work, were synthesized by biomers.net GmbH (Ulm, Germany), which are shown in Table 1. We used the letters “T” to refer to the target (complementary), “P” capture probe, and “C” control (non-complementary), followed by a number which indicates the sequence length.

Table 1. The designed target and capture probe sequences with their modification.

Oligonucleotide Name	Sequence (5′ to 3′)	Modification (5′)	Length (bp)
T (164)	GCTGTAGTGGCGAATTAACTTGTGGTTTGGTATGG GCAAAAAATCTTCAGCTTTAGGAGCGAAACCGAA GGTGGAGTGGTTCCCCCATCAAGGTTTCGCGACG CCAAGATGGAGGTTTTTTGCCATATCCCGAAGGG ACGCAGTGTATTTTGCTTCTGAATGTG	Biotin	164
T (50)	GGTATGGGCAAAAAATCTTCAGCTTTAGGAGCGA AACCGAAGGTGGAGTG	Biotin	50
C (50)	TTCAAGTAGTCCAGGAGCCGTAAGGGATTGGACA CCACGTGCAGTCACAG	Biotin	50
P (50)	CACTCCACCTTCGGTTTCGCTCCTAAAGCTGAAGA TTTTTTGCCCATACC	COOH	50
P (40)	CACTCCACCTTCGGTTTCGCTCCTAAAGCTGAAGA TTTTT	COOH	40
P (30)	CACTCCACCTTCGGTTTCGCTCCTAAAGCT	COOH	30
P (20)	CACTCCACCTTCGGTTTCGC	COOH	20

3.3. Bacterial template DNA for amplification

To assess our magnetic sensor's capability to detect authentic *Brucella* genomic DNA and discriminate against unrelated genomic DNA, we conducted experiments using extracted genomic DNA from different bacterial species responsible for different livestock zoonotic diseases, which may influence the accuracy of diagnostic test. The list of bacterial species is shown in Table 2.

Table 2. The bacterial genomic DNA from different bacterial species.

Pathogen	Zoonotic disease	Animal reservoir	Clinical symptoms
Brucella melitensis	Brucellosis	Cattle, goats, sheep, camels	Abortion, infertility, stillbirth [69].
Chlamydia	Chlamydiosis	Cattle, goats, sheep, pigs	Abortion, epididymitis, stillbirth [70].
Campylobacter fetus subsp. venerealis (Cfv)	Bovine genital campylobacteriosis	Cattle	Abortion, infertility, early embryonic death [71].
Campylobacter fetus subsp. fetus (Cff)	Bovine genital campylobacteriosis	Cattle, sheep	Abortion, infertility, early embryonic death [71].
Salmonella enteritidis	Salmonellosis	Wild rodents, poultry	Fever, septicemia, gastroenteritis [72]
Escherichia coli (APEC)	Colibacillosis	Poultry	Septicemia, mortality depletion, thymus [73].

3.4. Magnetic reader

To utilize the FMMD technique, a specific magnetic reader instrument was used to perform the magnetic measurement. The magnetic reader employs a unique setup consisting of two key components: the electronic excitation and readout circuit, and the measurement head, see Figure 9. The electronic circuit is responsible for the synthesis of low and high-frequency signals, and for the generation of the currents to the excitation coils by means of power amplifiers. The measurement head is the core of this setup, where the PE column filter containing MNPs is exposed to the dual-frequency magnetic excitation field, and where the magnetic response signal from the MNPs is picked up.

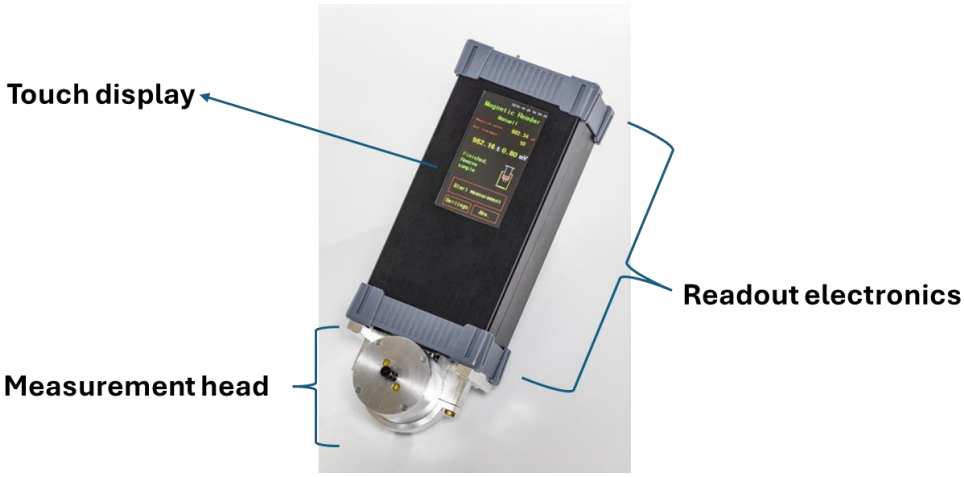

Figure 9. The magnetic reader instrument.

The measurement head is the actual sensing entity comprised of low-frequency driving and high frequency excitation coils, along with a detection coil. The design involves three coils, the high- and low-frequency coils tightly wound together, with a differential wound detection coil (measurement coil and reference coil) placed in the center; see Figure 10. In addition, temperature and light sensors are included for monitoring the measurement head's temperature and for sample in/out tracking. An aluminum housing of 5 mm encloses all the coils and sensors to prevent the surrounding high-frequency electromagnetic noise from being detected by the coils.

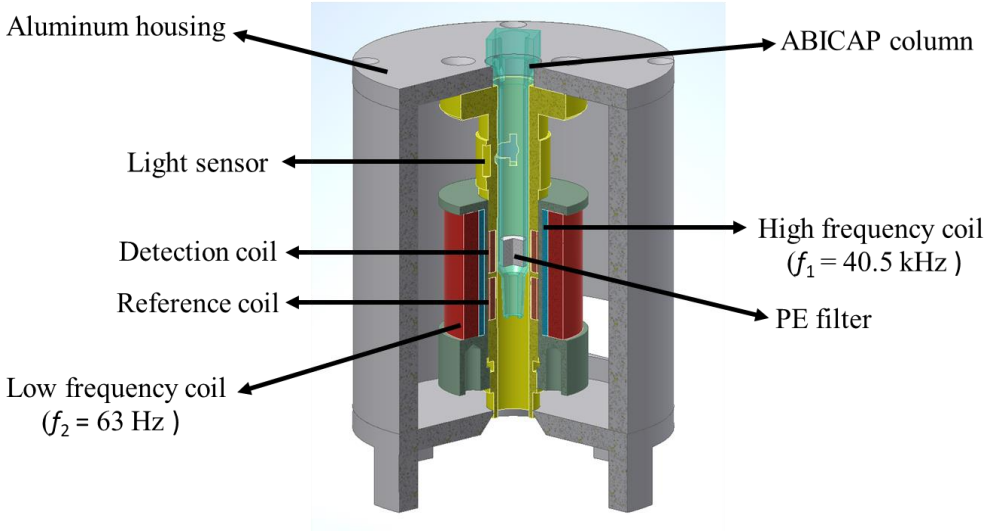

Figure 10. The measurement head 3D assembly comprises the different coils and their positions.

For magnetic detection, the PE filter column containing superparamagnetic nanoparticles is inserted inside the measurement head from the top opening, so that the PE filter is in the center of the detection coil. Once the PE filter is inserted, the superparamagnetic nanoparticles are subjected to a time-varying magnetic field comprising two distinct excitation frequencies. Specifically, a low frequency (f_2= 63 Hz with a field amplitude of 16 mT) was utilized to drive the beads to magnetic saturation, while a high frequency (f_1 = 40.5 kHz with an amplitude of 1.3 mT) probed the magnetization state. Due to the non-linear and non-hysteretic magnetization properties of the superparamagnetic particles, their response generated various new sum and difference mixing frequencies. Among these mixing frequencies, the frequency $f_1 + 2f_2$ exhibited the highest response signal. Consequently, this frequency was selected for sensing and quantifying streptavidin-conjugated magnetic nanoparticles. The response signal is synchronously detected at this mixing frequency. For a given type of MNP, it yields quantitative information about the amount of MNPs in the PE filter.

3.5. Automated measurement

In order to facilitate the measurement of multiple PE filter samples, an automated system of taking the columns in/out of the measurement head was implemented to improve the measurement procedure of the PE filter columns. The first system used was an old industrial micro-robot arm system (Mitsubishi Movemaster EX RV-M1), see Figure 11A. Here, the

robotic arm was programmed to perform precise movement from the rack to the upper opening of the measurement head, where columns were inserted for magnetic measurement. However, the robot turned out to be somewhat unreliable, which can be attributed to its age of approximately 25 years. Therefore, a new robotic system was constructed by modifying a 3D printer (Comgrow Creality 3D Printer - Ender-3), see Figure 11B. This system was programmed to perform the same automated measurement task as the robotic arm, introducing a cost-effective and affordable alternative to the old robot.

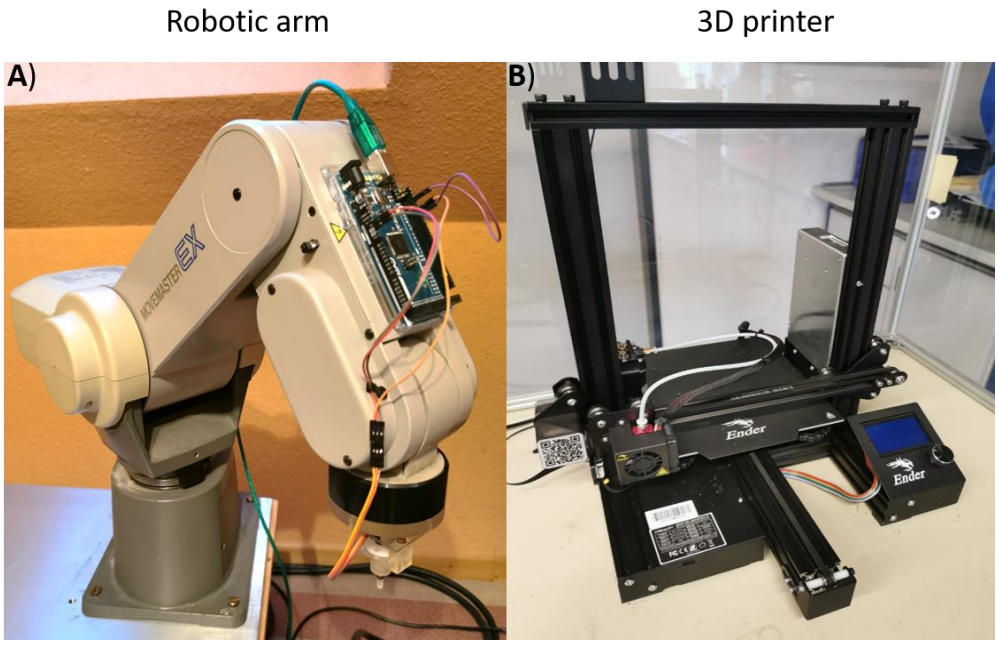

Figure 11. The instruments are used for automated measurement. A) The micro-robot arm system. B) The 3D printer Ender-3 system.

To handle the columns, a grabber shape piece was designed, 3D printed and attached to the robot arm, see Figure 12A. Then, a rotor motor was implemented to the grabber. This motor allowed the grabber to rotate and expand its grip when inside the column, enabling it to securely hold and extract the column from its position. This rotational capability with adjustable width allowed to take out the columns from the rack, put them into the measurement head, and put them back into the rack with secure holding. The grabber was attached to the robotic arm and to the 3D printer and tested for the automated measurement, see Figure 12B and 12C.

Additional images of the systems and of the movement of the samples can be found in the supplementary materials, see Figures S1, S2 and S3.

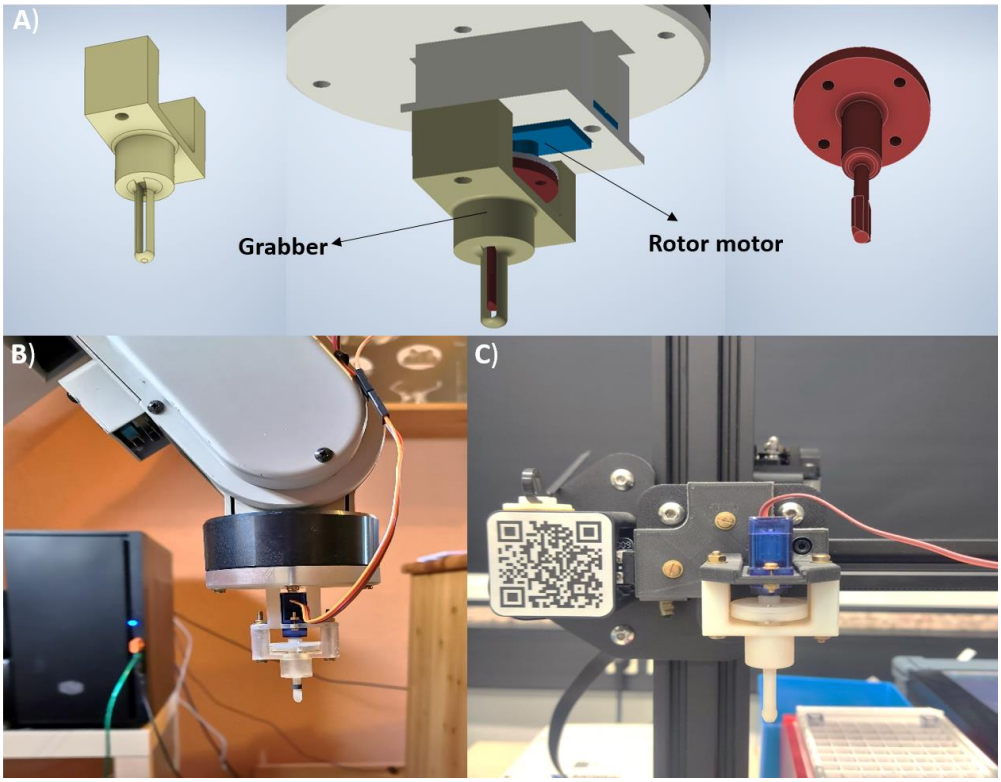

Figure 12. The grabber with rotor motor designed for taking ABICAP column filters. A) The 3D model of the designed grabber. B) The grabber is attached to the robotic arm. C) The grabber is attached to the 3D printer.

3.6. Magnetic Detection of DNA Target

3.6.1. Target selection and probe design

To identify and select a highly abundant target within the genome, the DNA repeats in the referenced genome *Brucella melitensis bv. 1 str. 16M* were predicted utilizing the online in silico tool 'Find Repeats' for small genomes, accessible on the Softberry website (http://www.softberry.com). Following this prediction, repeats exceeding 5 copies in the genome and having more than 70 bp in length were specifically chosen for subsequent

screening. The conservation of the selected repeats across *Brucella* genomes was then confirmed by subjecting them to the BLAST tool (https://blast.ncbi.nlm.nih.gov/Blast.cgi), using them as queries against all completed representative genomes of *Brucella spp*. To assess the specificity of the identified targets, the chosen sequences were used as queries against entire available genomic sequences in the nucleotide collection database, excluding all genomic sequences that existed in *Brucella* genus. Any sequence that did not fulfill the two conditions a) specificity to *Brucella* genus and b) conservation across all *Brucella* strains, were excluded from further analysis. Finally, the sequence characterized with minimal variations was chosen for DNA amplification and capture probe design to ensure the highest degree of specificity and sensitivity.

For capture probe design, the capture probes complementary to the least variation sequences within the selected target were designed for hybridization reaction. To determine the optimal size, four different lengths (50 bp, 40 bp, 30 bp, and 20 bp) of capture probes were designed. To ensure the specific binding of the capture probes to the intended target DNA, a non-complementary DNA sequence (50 bp) was synthesized and used as control in our validation experiments.

For the examination of secondary structures, we used the Unfold web server (DNA folding form) to predict secondary structures for all sequences [74]. Furthermore, the online software tool Oligoanalyzer was used to screen the potential formation of the hairpin, self-dimer, and heterodimer structures.

3.6.2. Polyethylene filter surface functionalization

In preparation for the magnetic detection assay, the PE filters were functionalized to enhance the reactivity of its surface, see Figure 13. The PE filters were first subjected to an oxidation process inside a plasma oven and treated for 5 minutes to activate the surface. The plasma conditions were controlled at 50 sccm oxygen flux and 50 W power, as recommended by [75]. The plasma oven used was the oxygen Plasma generator 100-E obtained from PVA TePla Analytical Systems GmbH (Westhausen, Germany).

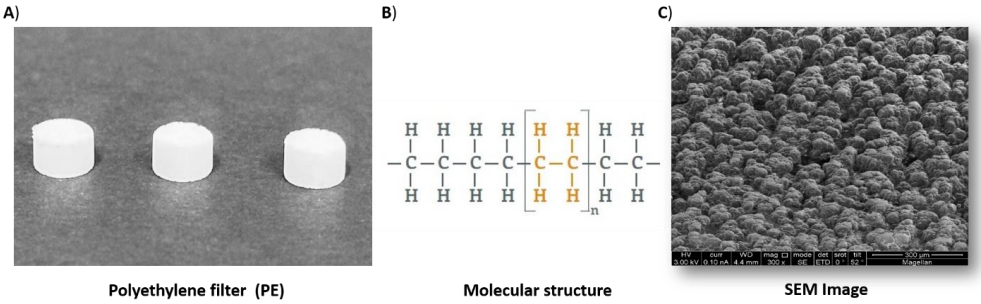

Figure 13. A) Sintered polyethylene filter with ∅ 5 mm × 2.5 mm size. B) Molecular structure of PE. C) SEM image shows the polymer structure.

For surface amine functionalization, the activated filters were incubated in a diluted ethylenediamine (EDA) solution at 1% concentration for 1 hour with shaking at 15 rpm speed at room temperature. Following the incubation, the PE filters were washed with distilled water and left to dry at room temperature.

3.6.3. Polyethylene filter preparation

To facilitate the diffusion of the solutions through the filters' pores, the PE filters were inserted inside the ABICAP columns, placed in a desiccator, and incubated in 99% ethanol solution under negative pressure to remove air bubbles, see Figure 14. The filters were then washed with distilled water to clear any alcohol from the PE filter and stored at room temperature for further use [61].

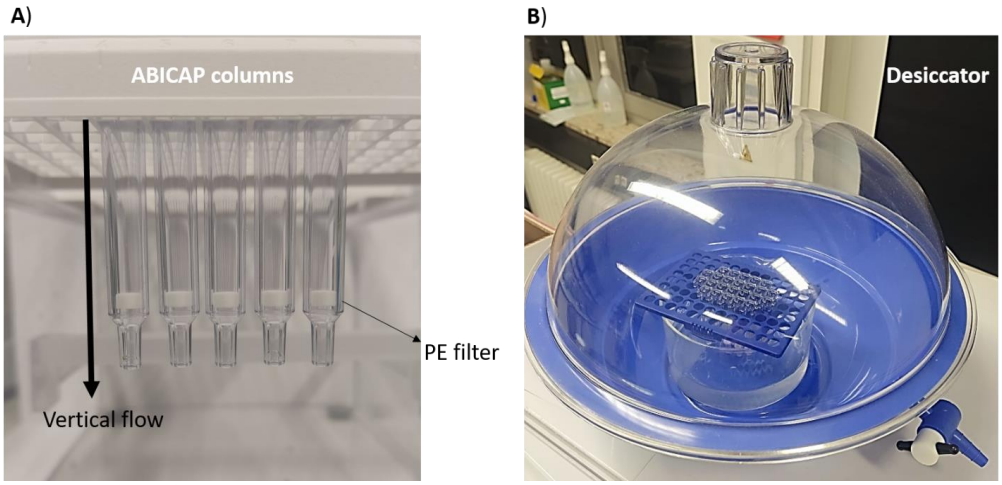

Figure 14. A) ABICAP columns with inserted PE filters. B) Desiccator.

3.6.4. Capture probe immobilization

For the immobilization of carboxylate-modified capture probes onto the aminated surface of PE filters, the coupling reagent EDC (10 mg) was first added to a solution containing 10 µl of capture probes and 450 µl MES buffer for activation of the carboxyl group. Then, the activated capture probes solution was added to the PE filters for the formation of the covalent amide bond between the activated carboxyl groups and amine groups on the PE surface. The filters were closed with caps at the bottom and incubated at room temperature for the desired incubation time. After incubation, any non-immobilized capture probes were removed by washing the PE filters with 750 µl of (1×) PBS by gravity flow.

To prevent the nonspecific binding of the MNPs and DNA sequences, the PE filters were incubated with 500 µl of (1%) BSA substance for 1 hour, blocking the potential nonspecific interactions.

3.6.5. DNA hybridization and magnetic labeling

For hybridization reaction between capture probes and DNA target, a volume of 10 µl of complementary or noncomplementary 5′-biotinylated ssDNA sequences was mixed with 290 µl of (10×) PBS buffer. The solution was added to the column filters for the hybridization reaction

and incubated at room temperature for the desired incubation time. Subsequently, the PE filter was then washed with 750 µl (1×) PBS buffer to remove non-hybridized DNA sequences.

After hybridization reaction, the MNPs are used as labels for sensing the hybridization between the capture probes and target sequences. In this study, magnetic nanoparticles are functionalized with a streptavidin shell which binds specifically to biotinylated DNA target. For the labeling assay, 15 µl of magnetic beads of the stock solution (5 mg/ml) was added to 400 µl (10×) PBS buffer and mixed by pipetting. The solution was added to the column filters and incubated for the desired time at room temperature. After incubation, a washing step was performed using 750 µl (1×) PBS buffer to remove unbound magnetic nanoparticles. Finally, PE filter columns were inserted inside the measurement head for magnetic measurement.

3.6.6. Software and data analysis

The software used to measure the magnetic response generated from magnetic nanoparticles is (GetriggerteFFTAnalysator), version V18.2, designed in LabVIEW environment by Dr. Stefan Achtsnicht. In this software, the magnetic response measurements are presented as signal amplitudes output, see Figure 15.

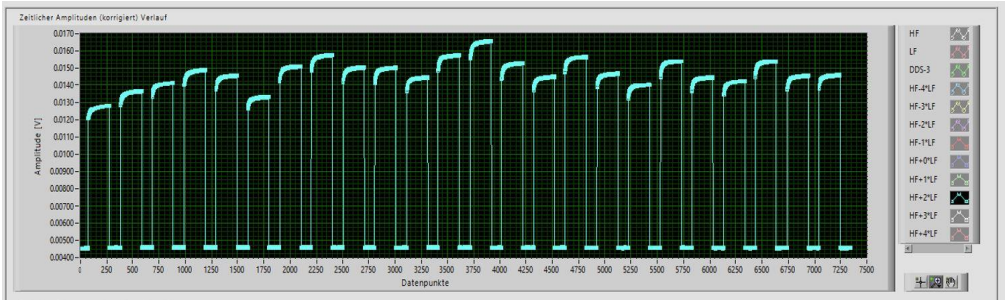

Figure 15. Measurement signal amplitude display.

In addition, the software tracks the temperature inside the measurement head and the readout electronics in real time, see Figure 16.

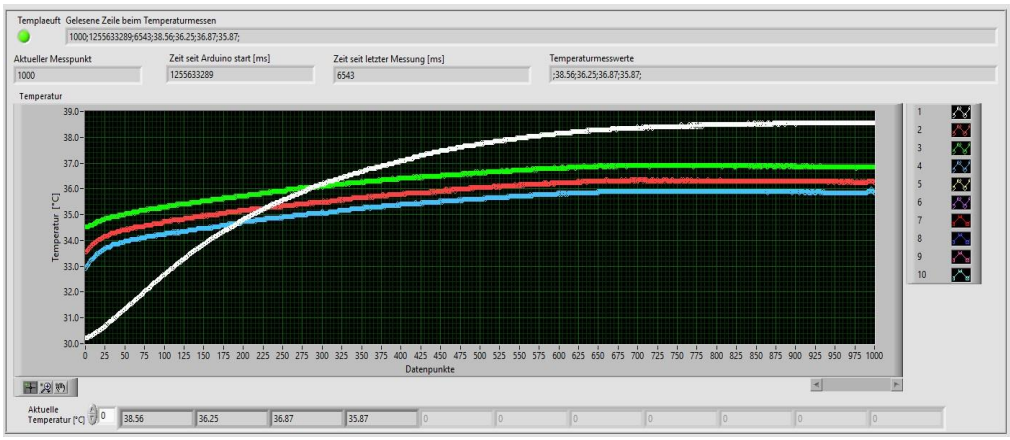

Figure 16. Temperature measurement display. Green, red and blue show the temperature reading inside the magnetic reader. White is for the measurement head temperature.

Furthermore, the software allows monitoring the insertion of the ABICAP columns into the measurement head with a light sensor, see Figure 17.

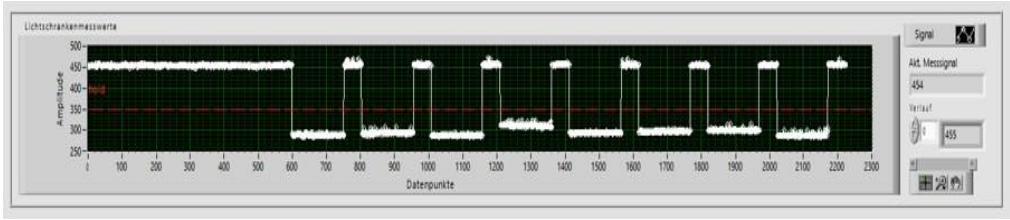

Figure 17. Light sensor display. The upper signal indicates the absence of an ABICAP column. Lower signals indicate the presence of an ABICAP column.

The measured signal amplitudes, including the mean and standard deviation, were fitted to the nonlinear Hill function using software (OriginPro 2019, V 9.6, Northampton, MA, USA) according to the equation

$$y = end\,\frac{x^n}{k^n + x^n} \tag{1}$$

where y equals the measured signal amplitude (corrected for blank value measured without sample), *end* is the signal in the limit of high concentration, x is the concentration of ssDNA target, k is the value of target concentration that yields half of the maximum signal, *end*/2, and n is the Hill coefficient. For $0 \leq y < end$, equation (1) can be analytically inverted, yielding

$$x = k\left(\frac{y}{end-y}\right)^{\frac{1}{n}} \quad (2)$$

For quantification, the inverted Hill function (2) was used to determine and quantify the unknown concentration *x* of ssDNA from the measured offset-corrected signal *y* (obtained after subtracting blank values from measured signals).

For the limit of detection (LOD) determination, the following equation was used:

$$LOD = Blank + 3 \cdot StDev(Blank) \quad (3)$$

3.7. Magnetic Detection of Amplified *Brucella* DNA

3.7.1. Primer design

Forward and reverse primers were designed to amplify the selected target sequence to obtain 84 bp target DNA that is complementary to the capture probes. The forward primer was designed to bind to the adjacent sequences of the complementary capture probe to avoid the binding of primer sequences to the probes, which may lead to false positive results, see Figure 18.

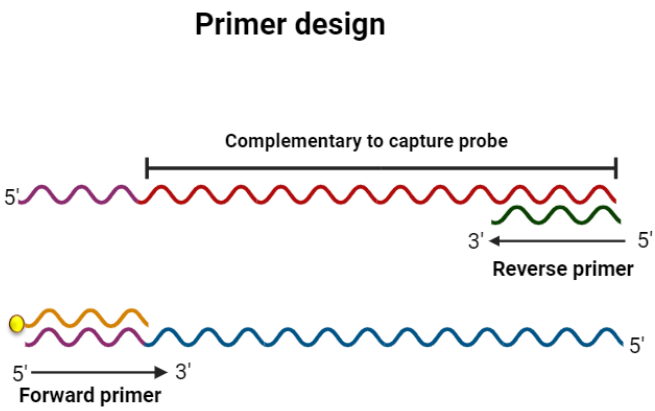

Figure 18. Schematic representation of forward and reverse primers binding sites. Created with BioRender.com.

3.7.2. PCR optimization

The PCR reaction conditions were optimized to select the best annealing temperature and primer concentration to ensure an efficient amplification. Gradient PCR was first performed using a range of annealing temperatures (55°C, 57.5°C, 60°C, 62.7°C, 65.9°C, 67°C, 68°C) to identify the temperature at which the amplification was maximized. The PCR was performed with a range of primer concentrations (0.5, 1, 1.5, 2 and 2.5 µM) to select the optimal ratio to avoid insufficient amplification and the appearance of nonspecific amplification. The optimal concentration and temperature were then determined by assessing the intensity and specificity of PCR bands. The image processing software ImageJ was used to analyze gel bands.

Following optimization experiments, *Brucella* genomic DNA was amplified in 50 µL of PCR mixture contained 0.75 µM of both forward and reverse primers, 200 µM of dNTPs, 2 µL of DNA, 1× Phusion HF buffer, and 1 unit of Phusion DNA Polymerase. The cycling conditions were: initial denaturation at 95°C for 10 min, followed by 30 cycles of 95°C for 30 s, 60°C for 20 s, and 72°C for 5 s, and final extension at 72°C for 10 min.

3.7.3. Agarose gel electrophoresis

A 3% agarose gel was prepared by dissolving agarose powder in 1× Tris-borate-EDTA (TBE) buffer. Then, the gel was stained with RedSafeTM nucleic acid staining solution for visualization of DNA fragments. 6 µL of PCR amplicons were loaded on gel at 100 V for 1 hour. A DNA ladder with a size range between (25-700 bp) was used as a marker to estimate the size of amplicons. The visualization was done using ChemiDoc™ XRS Imaging System.

3.7.4. Generation of ssDNA sequences

To generate the ssDNA complementary target from the dsDNA PCR amplicons, three different methods were tested to select the proper method that yielded a high ssDNA amount. The first method was heat and cool, where the PCR amplicons (50 µl) were heated to 95°C for 5 minutes to denature dsDNA, followed by rapid cooling on ice for 4 minutes, see Figure 19A. The second method was lambda exonuclease treatment. 1 µl of lambda exonuclease enzyme and 5 µl of reaction buffer were mixed with (50 µl) of purified and unpurified PCR amplicons and incubated inside a thermo shaker at 37°C for 15 minutes, see Figure 19B. The last method was streptavidin-coated magnetic beads, where the (50 µl) of biotinylated DNA amplicons were

captured by Synomag®-D streptavidin-magnetic nanoparticles for 15 minutes, then transferred to a MACS column placed in a strong magnetic field force for separation using MiniMACS™ Separator. While the MACS column was inside the separator, an alkaline treatment using NaOH at 0.5 M concentration was applied for 5 minutes to break the hydrogen bonds between the dsDNA strands. After alkaline treatment, the MACS column was removed and washed with 300 µl of 1× PBS buffer to elute the desired ssDNA strand, see Figure 19C.

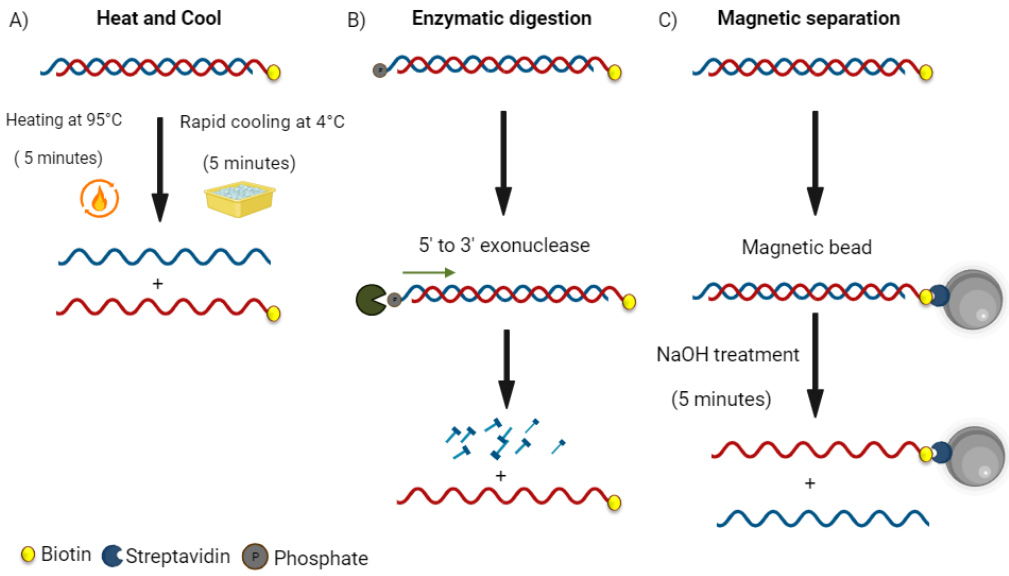

Figure 19. DNA denaturation strategies to generate ssDNA target. A) Heat and cool method. B) Lambda exonuclease treatment. C) Magnetic separation. Created with BioRender.com.

3.7.5. Detection of PCR amplified DNA by FMMD

After obtaining the ssDNA target sequences through lambda exonuclease digestion, the generated complementary ssDNA strands were mixed with 250 µl of (10×) PBS hybridization buffer and then added to the PE filter. The hybridization was carried out through gravity flow, which takes about 1.5 minutes for our PE filter. After hybridization, the PE filter was washed out with 750 µl (1×) PBS buffer to remove unbound ssDNA target. For magnetic labeling, 15 µl of MNPs mixed with 400 µl (10×) PBS buffer were added to the PE filter column and incubated

for 3 minutes. Finally, the PE filter was washed with 750 µL of (1×) PBS to remove unbound nanoparticles and inserted into the magnetic reader for magnetic measurement.

3.8. Magnetic Detection of RPA products

3.8.1. Primer design and primer screening

As the primer amplification performance and primer design criteria are different in recombinase polymerase amplification (RPA) than in PCR, the primers were designed based on recommendations for primer design consideration provided by (TwistDx, UK). A new set of RPA forward and reverse primers specific to the selected target DNA were manually designed to choose the best candidate primer pair. The NCBI Primer-Blast tool was used to evaluate the specificity and the potential binding sites of the primers. In addition, the primer sequences were aligned against all *Brucella* genome sequences to confirm their conservation among all *Brucella spp*.

The primer pair choice influences the assay's amplification performance. Therefore, an experimental screening process was conducted on all primers using *Brucella* genomic DNA to identify the most optimal primer pair. This screening focused on assessing their specificity and efficiency in amplification. All the RPA bands were analyzed by (ImageJ) software.

3.8.2. RPA amplification

The RPA amplification was performed in 50 µl of total solution. The master mix was prepared by combining 2× reaction buffer (20 µl), dNTPs (9.2 µl), 10× basic E-mix (5 µl) and (2.4 µl) of each primer. The master mix was then vortexed and briefly spun. Then, a 20× core reaction (2.5 µl) was added to the tube lid, mixed by 10× full inversions followed by spinning. To initiate the RPA amplification, (2.5 µl) of magnesium acetate (MgOAc) and (1 µl) of genomic DNA were added to the tube lid and kept separate, mixed by 6× full inversions, and spun. The reaction tubes were placed in a heat block at 37°C for 4 minutes, mixed and incubated for 30 minutes.

3.8.3. Asymmetric RPA amplification

Asymmetric recombinase polymerase amplification (ARPA) was employed to amplify our desired ssDNA target strand. The forward primer F2 was used as an access primer (high concentration), while the reverse primer R1 was used as a limiting primer (low concentration), see Figure 20. In this experiment, the master mix was prepared first by the addition of all

components of RPA amplification except primers. Then, the mixture was added to separate tubes containing different primer concentration ratios (1:20, 1:40, and 1:60). The ARPA reactions were incubated at 37°C for a duration of 30 minutes. After the amplification, the amplified products were first purified and then subjected to gel electrophoresis at 3% agarose concentration to check the presence of the expected ssDNA strand.

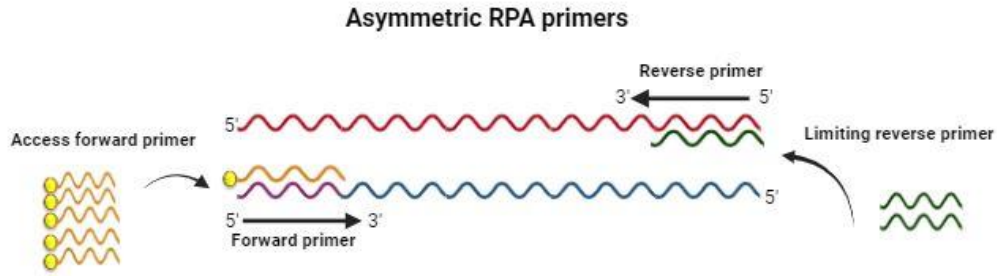

Figure 20. Schematic illustration of asymmetric RPA. Created with BioRender.com.

3.8.4. Magnetic detection of asymmetric recombinase polymerase amplification (ARPA) amplified DNA.

After the generation of the ssDNA target by ARPA amplification, the reaction tubes (50 µL) were immediately mixed with 250 µl of (10×) PBS hybridization buffer and transferred to the ABICAP column with the capture probes P (50) for hybridization reaction. The hybridization was done by gravity flow at a flow rate of ~200 µL/min, followed by a washing step with 750 µl of (1×) PBS. The magnetic detection was done first by labelling the hybridized strand by the addition of 15 µl of Synomag®-D magnetic nanoparticles for 3 minutes to enable the binding of streptavidin MNPs to the biotinylated target. Secondly, the ABICAP columns were washed with 750 µl of (1×) PBS to remove unbound MNPs. Finally, the columns were inserted in the measurement head of a magnetic reader for performing the magnetic measurement.

3.8.5. Tailed primers and capture probe design

An alternative primer design was employed to detect the whole amplicon amplified by RPA amplification. We designed two reverse primers (R7 and R8) with a short oligonucleotide sequence at their 5` ends. The length of the tail sequence was 20 bp for the R7 primer and 15 bp

for the R8 primer. A C3 spacer is incorporated between the primer and tail to stop the elongation of amplification by the DNA polymerase enzyme, see Figure 21.

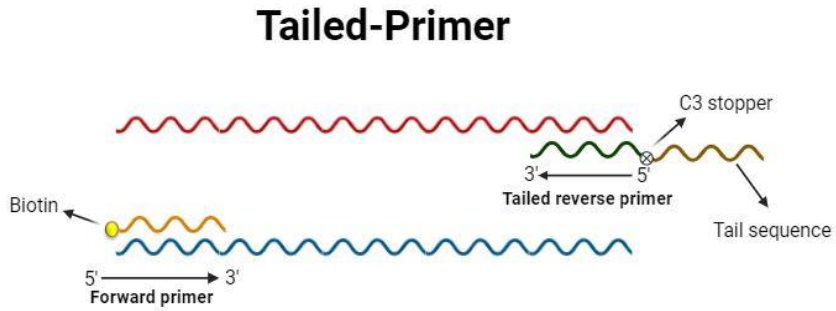

Figure 21. Scheme of tailed primer design. Created with BioRender.com.

A new capture probe complementary to the tail sequence of two reverse primers was designed to capture the amplicon through a hybridization reaction. As the capture probe sequence is relatively short (20 bp), a poly-T sequence of 15 bp was additionally introduced to the 3`ends of the capture probe. This enhances its potential binding capacity and accessibility for an efficient hybridization with amplicons.

3.8.6. Tailed primers selection and primer dimer reduction

The two designed reverse-tailed primers (R7 and R8) were screened with the RPA forward primers (F2, F3 and F4) to select the most specific and efficient primer pair for RPA amplification. The selected optimal primers were then tested using different methods to reduce the formation of primer dimers. Organic additives, such as dimethyl sulfoxide (DMSO) and betaine, were tested at different concentrations (10, 5, 3, 1%) and (1, 0.5, 0.25, 0.1M), respectively. In addition, primer concentration optimization was performed at concentrations of (150, 300, and 450, 600 nm). All RPA products were then purified and loaded onto gel at 100 V for 1 hour. The intensity and specificity of the RPA products were assessed using image processing software (ImageJ).

3.8.7. Magnetic detection of tailed RPA DNA

Once the primer dimer formation was eliminated, the RPA amplification conditions were systematically optimized to achieve the highest amplification performance. The RPA reaction was performed at different temperatures, from 21°C to 42°C, to determine the optimal incubation temperature. The influence of the cofactor MgOAc concentration on RPA amplification was investigated by varying the concentration within the range of 6 to 36 mM. The reaction time for RPA amplification was tested to identify the best time duration to achieve maximum product yield. The reaction times tested were 2, 5, 10, 15, and 30 min.

Following our optimized isothermal RPA conditions, the magnetic detection of amplified DNA was evaluated on the PE filter immobilized with a capture probe complementary to the tail sequence P (tail) at 5 µM concentration. First, the amplified DNA was mixed with 250 µl of 10× PBS buffer and pipetted to the PE filter, allowing a hybridization reaction by gravity flow. Subsequently, the filter was washed with 750 µl (1×) PBS to remove unbound target DNA, followed by magnetic nanoparticle labeling for 3 minutes and then a last washing step to remove unbound MNPs

3.9. Isothermal amplification in temperature-controlled measurement head

3.9.1. Pulse width modulation temperature controller

A 2-point PWM feedback controller for LF-amplitude duty cycle adjustment and therefore controlled heat supply was implemented in the Arduino microcontroller software of the magnetic reader. The temperature sensor used for feedback control was a DS18B20 sensor, mounted on the LF-coil surface inside the measurement head. The suggested control algorithm incorporates two distinct, freely selectable error-ranges. A first, wider error-range for tuning the temperature in the desired interval and a second, narrower error-range within which the temperature is kept during the FMMD measurement process. This makes it generally possible to heat up the amplification environment with maximum power fed to the LF-coil, but then regulate the heat with e.g., only half maximum power.

The conditional equivalent logic for the duty cycle regulation within these error ranges based on the temperature difference between the measured output temperature and the set desired temperature input value followed the scheme in Figure 22 below:

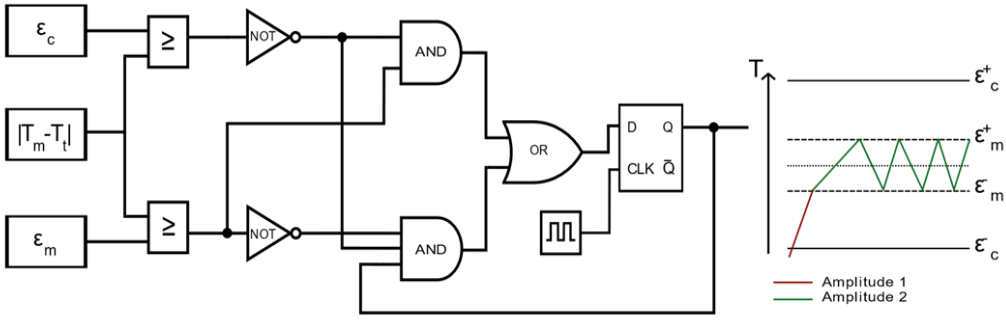

Figure 22. Equivalent logic for a PWM controller with differentially adjustable heating and measurement LF amplitude, and schematic of controlled temperature using this logic.

Here, ε_c denotes the allowed temperature error range during heat up and tuning and ε_m denotes the allowed temperature error range during the FMMD measurement. T_m is the measured temperature at the LF-coil surface and T_t is the set controller target temperature. The output of this equivalent logic states the condition that determines if the LF-amplitude is turned on or off with a first amplitude setting (Amplitude 1) or a second amplitude setting (Amplitude 2), different from the first one. Software-wise, this logic was implemented into the Arduino microcontroller using multi-tasking programming with a time-slicing scheduling technique to account for the wait time of the temperature sensor and measurement readout.

3.9.2. RPA inside the measurement head

The RPA for positive control reactions was performed following the manufacturer's recommendation in the TwistAmp® Liquid Basic kit, with slight adjustments by reducing the reagent quantities to create a total volume of 25 µl. In the RPA reaction, a master mix was prepared containing 3.5 µl of oligo mix primers, 12.5 µl of 2× reaction buffer, 2.5 µl of 10× basic E-mix, 2.75 µl of dNTPs, and 1.25 µl of 20× core reaction. After mixing, 2 µl of MgOAc and 1 µl of positive control DNA were added to start the reaction. The RPA reaction was carried out at desired incubation temperatures and time inside the measurement head.

After the amplification, the RPA product was purified using ROTI ® Prep PCR Purification kit through column centrifugation to remove reaction components. For the visualization of RPA products, 10 µl of the purified amplicons were analyzed using agarose gel electrophoresis on 2% agarose gel in 1× TBE buffer at 100 V for 1 hour. The visualization was done with ChemiDoc™ XRS Imaging System (Bio-Rad Laboratories Co., Ltd., California, USA).

Chapter 4

4. Superparamagnetic Nanoparticle-based DNA Sensor for the Detection of *Brucella* Spp.

The chapter is partly based on the original publication by the author [76].

4.1. Target selection

Selecting an appropriate DNA marker for amplification and detection techniques is crucial in ensuring the efficiency of the assay. The choice of DNA marker can impact the overall performance, including accuracy, specificity and sensitivity [77,78]. Thus, several key characteristics should be taken into consideration when selecting a good target. These characteristics include the abundance of the DNA marker with a sufficient amount within the genome, uniqueness and conservation across target organisms. Among different DNA candidate sequences, studies have shown that targeting the repetitive sequences that exist in bacterial genomes provides greater analytical sensitivity compared with other DNA sequences [79,80]. This can be explained by the natural presence of these repeats in multiple copies throughout the bacterial genomes [81] [82]. As a result, the potential binding sites for the primers are more frequently available compared with single copy sequence, which can lead to more efficient amplification, resulting in higher sensitivity.

In this study, the strategy used to select a suitable DNA marker for the *Brucella* pathogen, which is our present model of interest, was based on screening and targeting sequence repeats found in multiple copies across the *Brucella* genome. The in-silico tool (Find repeats) was used to predict repeat sequences in the referenced genome *Brucella melitensis bv. 1 str. 16M*. The tool generated 70 repeat sequences with different lengths and copy numbers. Out of the repeats analyzed, 38 repeats had more than five copies and 70 bp length. These repeats were then subjected to the BLAST tool to assess the specificity and conservation across all *Brucella*

genomes. Any sequences that did not fulfill the two conditions were excluded. Among the 38 repeats analyzed, we selected the target sequence below.

5′-

AGGCTGTAGTGGCGAATTAACTTGTGGTTTGGTATGGGCAAAAAATCTTCAG CT TTAGGAGCGAAACCGAAGGTGGAGTGGTTC-3′

The selected target sequence is highly conserved among all *Brucella* representative genomes, with 5-6 copies distributed across the two chromosomes. Moreover, the percent identity exceeds 95% among all *Brucella* genera, see Table 3.

Table 3. DNA target copy numbers and distribution in Brucella genome.

***Brucella* strains**	**Accession numbers**	**Percent identity**	**Number of copies**	
			Chr.1	Chr.2
Brucella melitensis bv. 1 str. 16M	NC_003317.1 NC_003318.1	(95- 100) %	5	1
Brucella abortus 2308	NC_007618.1 NC_007624.1	(95-98.8) %	4	1
Brucella suis 1330	NC_004310.3 NC_004311.2	(95-98) %	5	1
Brucella ovis ATCC 25840	NC_009505.1 NC_009504.1	(95-98) %	5	1
Brucella canis ATCC 23365	NC_010103.1 NC_010104.1	(95-98) %	5	1
Brucella microti CCM 4915	NC_013119.1 NC_013118.1	(95-98) %	5	1
Brucella ceti TE10759-12	NC_022905.1 NC_022906.1	95%	5	1
Brucella inopinata strain 141012304	NZ_LT605585.1 NZ_LT605586.1	(91-96) %	3	1

Chr: Chromosome.

4.2. Principle of DNA magnetic assay

The developed assay is based on the magnetic measurement of superparamagnetic nanoparticle markers to selectively detect *Brucella* DNA using frequency mixing magnetic detection. The detection relies on the sequence-specific hybridization event between the immobilized capture probe on an amine-modified PE filter and its complementary biotinylated target DNA. The principle of the targeted detection of our designed magnetic nanoparticle-based DNA sensor is illustrated in Figure 23.

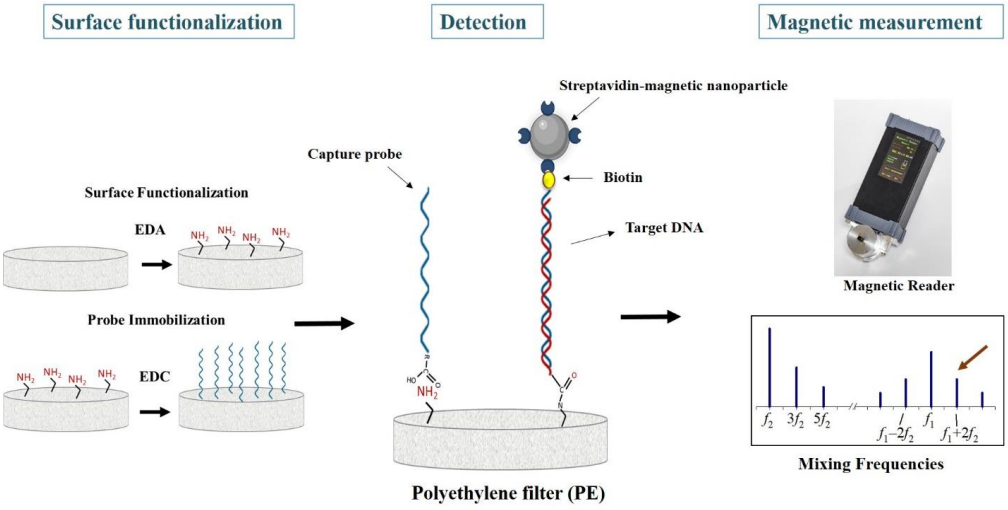

Figure 23. Magnetic nanoparticles-based DNA sensor for the detection of *Brucella* DNA. The red arrow marks the frequency mixing component that is demodulated.

In the presence of the *Brucella* target sequence, the designed complementary capture probe binds selectively to the DNA target sequence, forming a hybridized structure. Magnetic detection of this hybridization event is achieved using magnetic nanoparticles as markers. Streptavidin-functionalized nanoparticles will bind to the target DNA by streptavidin–biotin interaction, thus enabling detection and quantitation of the DNA target analyte.

4.3. Polyethylene surface functionalization and probe immobilization

The selection of an appropriate immobilization strategy for coupling capture probes onto solid support is crucial for developing label-based nucleic acid assays [83]. The stability of the probe–surface bonds, the good orientation and the specific coupling are the main factors that

impact the efficiency of the hybridization assay. To meet these requirements, the covalent bonding method is preferred, as it ensures a proper vertical orientation where the end of the DNA capture probe can be specifically attached to the solid surface. In addition, it also promotes the formation of stable bonds between the modified probe and the functionalized solid surface [84]. In our study, we selected the well-established one-step EDC chemistry for the covalent bonding of the capture probes onto the PE surface. EDC allows efficient crosslinking by activating carboxyl groups, allowing them to form a stable amide bond with amine-functionalized solid surfaces with very high efficiency [85,86]. This method ensures specific and stable attachment of the capture probes with proper orientation on the surface.

Due to the absence of reactive sites on the surface of polyethylene filters, they need to be modified to generate reactive functional groups. A previous study showed that PE can be modified for the covalent immobilization of antibodies using ω-aminocellulose carbamate as a coating agent [87]. However, this modification requires the complex synthesis of ω-aminocellulose carbamate prior to its adsorption. In our study, we employed a simpler approach for PE modification. First, the PE filters were activated to generate reactive sites like oxygen and hydroxyl groups, and then functionalized with two different commercial coating agents to introduce amine groups to the PE surface that enable the coupling with carboxylate-modified capture probes. The coating agents used are at first polyethyleneimine (PEI) and then ethylenediamine (EDA), which are shown in Figure 24.

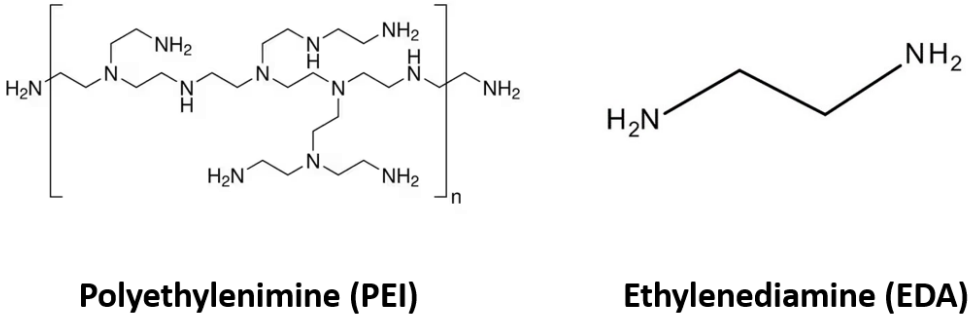

Figure 24. The coating agents used for PE surface functionalization [88].

To validate the presence of amine groups on functionalized PE filters with the two coating agents, we tested the PE filters with ninhydrin reagent. Ninhydrin is an organic compound used for the analysis of amino acids, peptides and proteins to detect the amines group visually [89].

It forms a purple color called Ruhemann's purple (RP) when it reacts with free amine groups [90]. In our study, the filters were immersed in a 0.2 % ninhydrin solution diluted with ethanol, and then incubated at 80°C for 15 minutes for reaction. Following the incubation, the filters were dried and observed for color appearance. Figure 25 shows the transition in color for modified and non-modified PE filters. The modified filters showed a purple color with different contrast, while no changes occurred to the non-modified filters. By comparing the modified filters, the filters coated with PEI showed a darker color than the EDA. This is due to the presence of a higher amount of amine group in PEI polymer as shown in Figure 24. Overall, this result confirms the successful functionalization of the PE filters with amine groups.

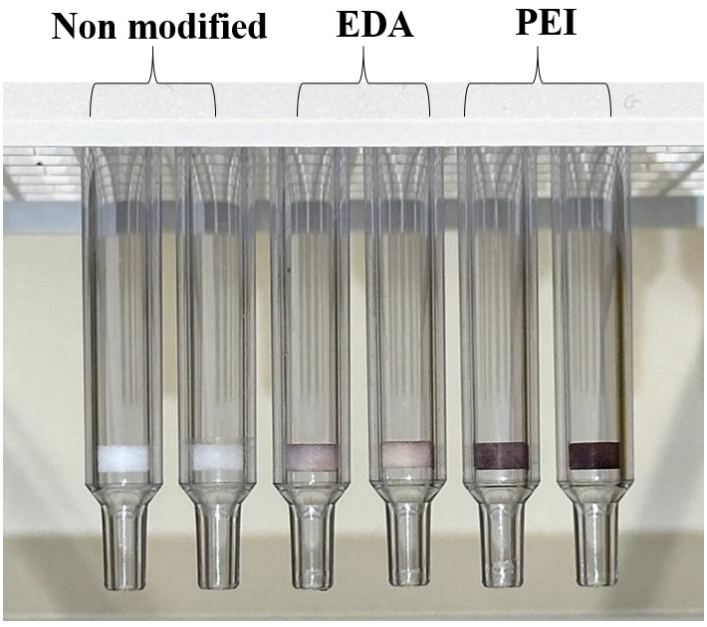

Figure 25. The transition in color from white to purple for the modified and non-modified PE filters using ethylenediamine (EDA) and polyethyleneimine (PEI) coating agents.

The covalent binding of the capture probes on the functionalized PE filters was investigated. First, the PE filter modified with PEI coating agent was tested using carboxyl-modified capture at 10 µM concentration on PE filters with EDC, filters without EDC, and non-modified filters to perform coupling reactions. The preliminary result demonstrated the success of surface functionalization as the non-modified filters showed a very low magnetic signal. However, the PE filters without EDC showed a very high signal, similar to those with EDC, see Figure 26.

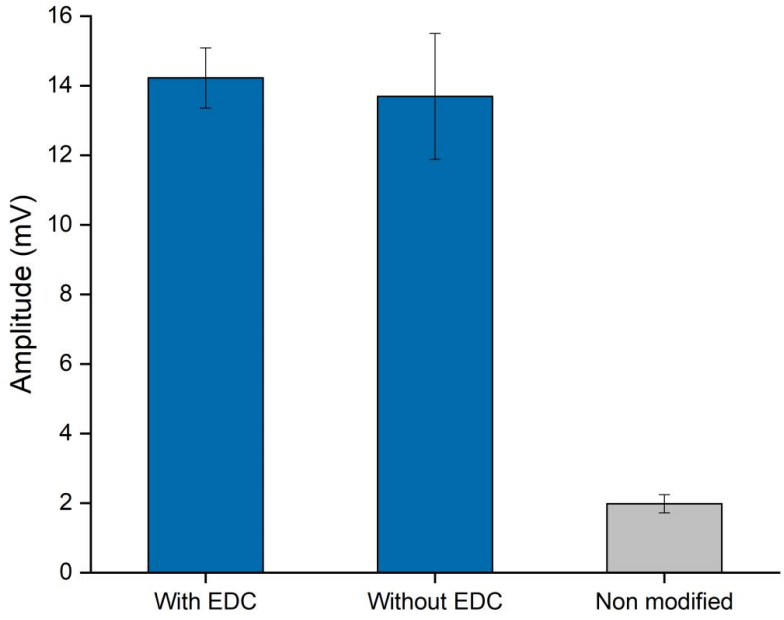

Figure 26. The signal amplitudes of target DNA in the presence and absence of the EDC crosslinker on PE filters coated with PEI. Error bars represent the standard deviation of two independent measurements.

This high signal value, which leads to false positive results, can be explained by the nonspecific binding of MNPs or biotinylated target DNA to the amine-functionalized surface. Therefore, we conducted an experiment by testing only the streptavidin-coated magnetic nanoparticles on the modified PE filter, and the result showed the same high signal amplitude, see Figure S4 in the supplement. We concluded that the binding occurred through the electrostatic interaction between the negatively charged functional groups on streptavidin protein and positively charged amine groups on the PE filter.

As a result, we decided to use another coating agent that should be smaller in size and have less amine groups (less positivity). Therefore, we selected the organic compound ethylenediamine (EDA) which has a simple chemical structure which contains primary amine groups at the ends as a new coating agent. Here, the same coupling strategy was performed using capture probes at a concentration of 10 µM on both filters with EDC and without EDC. Subsequently, target and nontarget ssDNA sequences at a concentration of 5 µM were tested for hybridization reaction, and filters without capture probes were used as a control.

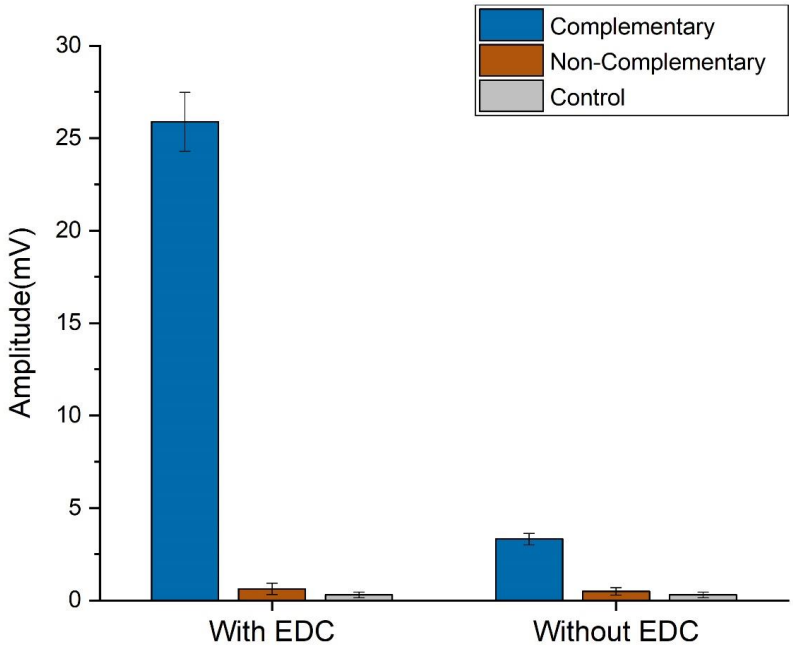

Figure 27. The signal amplitudes of target and nontarget DNA in the presence and absence of the EDC crosslinker on PE filters coated with EDA. Error bars represent the standard deviation of three independent measurements.

As shown in Figure 27, in the presence of EDC crosslinker, the signal amplitude of complementary target DNA is substantially higher compared to both the nontarget and control. In the absence of EDC, the signal amplitude showed only a slight increase compared to the nontarget and control. This slight increase might be to the electrostatic interaction between the negatively charged phosphate groups in the DNA and the positively charged amine groups present on the functionalized surface. By comparing the magnetic signals of the target and non-target DNA in the presence or absence of EDC, we assume that the attachments of the ssDNA capture probes onto the PE filter occurred through EDC covalent bonding chemistry, rather than electrostatic interaction. The finding also confirmed that the designed capture probes exhibited high specificity towards the target DNA, as the average magnetic signals of nontarget DNA were very low. Following these results, we selected EDA as a coating agent for our PE filter surface modification.

To validate and visualize the binding and distribution of the capture probes on the PE filters, another capture probe, having the same sequence and length but with biotin modification at the

3′ end, was employed on modified and non-modified filters using the same EDC coupling strategy. Streptavidin-conjugated gold nanoparticles (40 nm) were used as labels to improve contrast for visualization under a scanning electron microscope (SEM). Figure 28A and Figure S5 in the supplement show the SEM image of the bound gold nanoparticles with the immobilized capture probes on an amine-functionalized PE filter. However, no bound gold nanoparticles were observed on non-functionalized PE filters, as shown in Figure 28B and Figure S6 in the supplement. This confirms the successful binding of the probes on the functionalized PE filters.

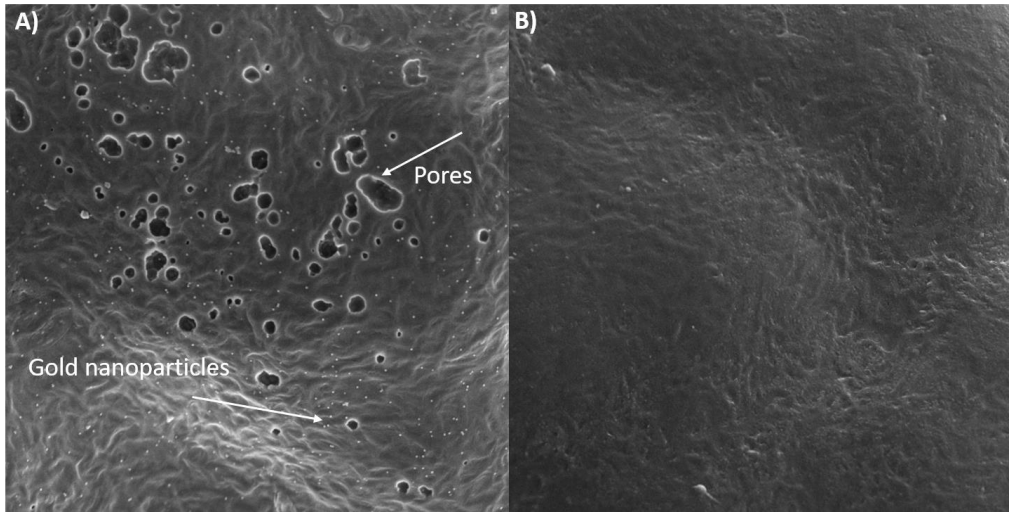

Figure 28. A) SEM image of gold nanoparticles bound to the immobilized capture probes on an amine-functionalized PE filter. B) non-functionalized PE filters. Scale bar = 5 µm.

4.4. Adjusting probe parameters

The quantity and distribution of bound ssDNA probes on a solid surface are key factors in achieving efficient hybridization between the immobilized ssDNA probes and their complementary targets [91]. Thus, optimizing probe parameters to ensure the best hybridization kinetics is needed to avoid undesirable behavior that would influence the DNA duplex formation, such as steric hindrance and electrostatic repulsion that occur at high probe concentration, and signal reduction at low probe concentration [92].

Previous reports have investigated the influence of the immobilization time on DNA target detection, showing that a longer immobilization time may allow more capture probes attachments to the solid surface, which enhances the hybridization efficiency by increasing the density of probes available for DNA binding and thus increasing the signal values [93,94]. Therefore, we first optimized the immobilization time of our capture probes to find the optimal time. Here, the immobilization was done for different duration times (15, 30, 60, 120, 180 minutes) using a capture probe at 10 µM concentration and DNA complementary target at 5 µM concentration. As shown in Figure 29, the signal amplitudes showed negligible differences at all times tested with a relatively high standard deviation at 15 min. This indicates that the attachments and coupling reaction of the probes on the PE filter using EDC crosslinker is rapid. As a result, we selected 30 min as an optimal immobilization time for our further assays.

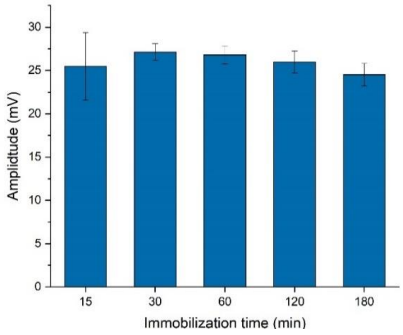

Figure 29. Effect of the immobilization time on signal amplitude. Error bars represent the standard deviation of three independent measurements.

After the immobilization time selection, we optimized our assay's probe concentration by testing various concentrations of the capture probes, ranging from 1 µM to 50 µM. As shown in Figure 30A, increasing the concentration of the capture probes increased the signal amplitude. This clearly indicated that a high amount of probe molecules bound on the PE filter enhanced the hybridization efficiency between the probes and their target DNA, thus increasing the signal amplitude. The signal amplitude was the lowest when a low probe concentration (1 µM) was tested. When a very high concentration of probe (50 µM) was tested, a possible interference due to steric hindrance was not observed, and the signal amplitude obtained was the highest. This observation can be explained by the availability of an abundant surface area on the PE filter to bind large amounts of capture probe. This explanation is supported by the

SEM image in Figure 28A, which demonstrates relatively large distances between adjacent probes distributed on the PE filter.

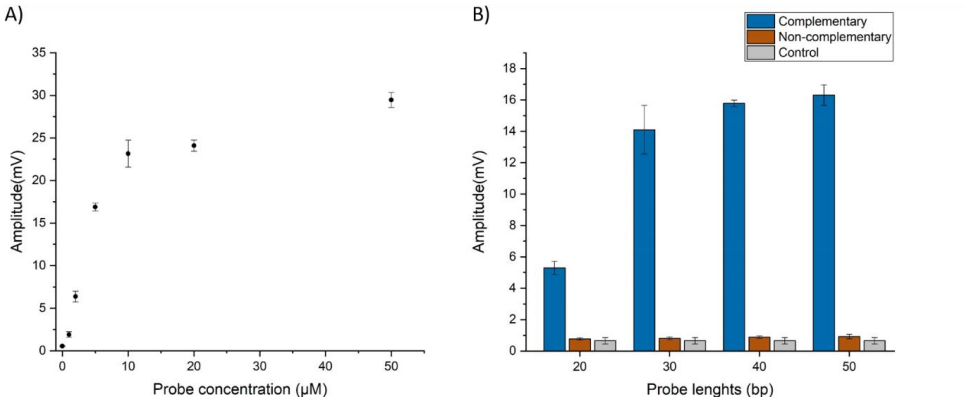

Figure 30. A) Effect of probe concentration on signal amplitude. B) Effect of probe length on signal amplitude. Error bars represent the standard deviation of three independent measurements.

For selecting a suitable probe concentration for our assay, we took into account that the assay would be used mainly in developing countries where a low cost is an essential factor. Therefore, a low amount of probe concentration and a high signal-to-background ratio were considered as criteria for our selection. As a result, the 5 μM concentration was selected for further optimization experiments as a compromise, yielding the highest signal amplitude per probe concentration, as shown in Figure 30A.

We decided to examine another factor that has a significant impact on determining the specificity and sensitivity of DNA hybridization: the length of the attached capture probes. Previous studies on DNA microarrays have demonstrated a significant influence of probe length on signal strength [95–97]. The results of these studies confirmed that using longer probes provides higher detection sensitivity compared to shorter probes. In principle, longer probes are easier to reach and bind to their complementary DNA sequences away from the PE filter surface. This increases the probability of hybridization, and thus the detection sensitivity. Additionally, higher numbers of hydrogen bonds are formed in duplex DNA, resulting in more stable hybrids. However, long probes are more prone to cross-hybridization with non-specific DNA sequences than short probes [98]. Thus, it is critical to find a trade-off between binding efficiency and binding specificity by evaluating several probe lengths.

For our magnetic DNA biosensor, we designed four probes of different lengths (20 bp, 30 bp, 40 bp, and 50 bp) to detect the conserved sequence with minimal variations within the selected target sequence. Hybridization and magnetic sensing were conducted using target and non-target DNA sequences at a concentration of 5 μM. Figure 30B shows the performance of the designed probes in terms of signal amplitude. The signal amplitudes obtained were higher when capture probes with lengths of 50 bp, 40 bp, and 30 bp were used. However, a significant reduction of about 50% in signal amplitude was observed when a probe with 20 bp length was used. Hence, we selected the length of 50 bp as a proper probe length for the following experiments.

4.5. Optimization of DNA hybridization

Determining the optimal ionic composition is crucial to ensure the best hybridization environment that will lead to a stable duplex formation. Since ssDNA capture probes are negatively charged, the presence of cations is essential to compensate for total negative charge, minimizing the electrostatic repulsions between immobilized probes [99]. Additionally, higher salt concentrations ensure a more stable duplex by increasing the association rate between the capture probe and DNA [100]. To evaluate the impact for our assay, several concentrations of the PBS hybridization buffer were prepared (10×, 6×, 4×, and 2×), and a distilled water solution was used as a control. A target and a nontarget sequence at 5 μM concentration were mixed with the prepared solutions and incubated for 1 h to allow the hybridization. The impact of the ionic strength of the PBS buffer on the signal amplitude is shown in Figure 31A. Results demonstrated that the signal amplitudes decreased with decreasing saline concentrations of the PBS buffer. By comparing the signal amplitudes of all ion-containing solutions with that of the distilled-water solution (without ions), we could confirm the significance of ions in enhancing hybridization efficiency, as all solutions containing salt exhibited higher signal amplitudes. From the result, 10× PBS buffer yielded the highest signal amplitude; thus this saline concentration was selected as optimal for the subsequent experiments.

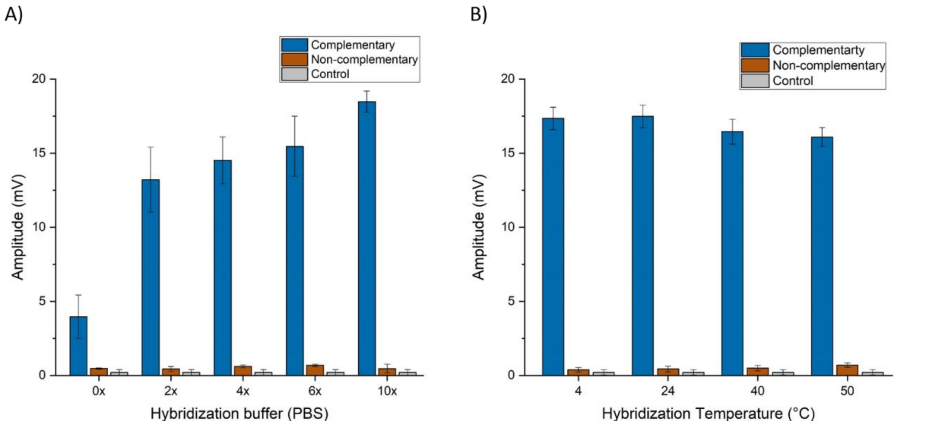

Figure 31. (A) Effect of ionic buffer strength on signal amplitudes. (B) Effect of temperature on signal amplitudes. Error bars represent the standard deviation of three independent measurements.

Assessing the assay ability to detect the desired target at different temperatures is crucial, particularly when the goal is to develop a point-of-care (PoC) testing assay intended to be used in the field under different environmental temperatures. Thus, we examined the temperature impact on our DNA sensor's signal amplitude, using both target and nontarget DNA sequences. The DNA sequences were incubated for detection at hybridization temperatures ranging from 4°C to 50°C for 1 hour. As shown in Figure 31B, the signal amplitudes obtained were almost equivalent at all hybridization temperatures tested. This indicated that the performance of our developed sensor is consistent in a wide range of hybridization temperatures, which in future PoC applications may minimize any possible influence of the external temperature both in cold and hot geographical regions of the world.

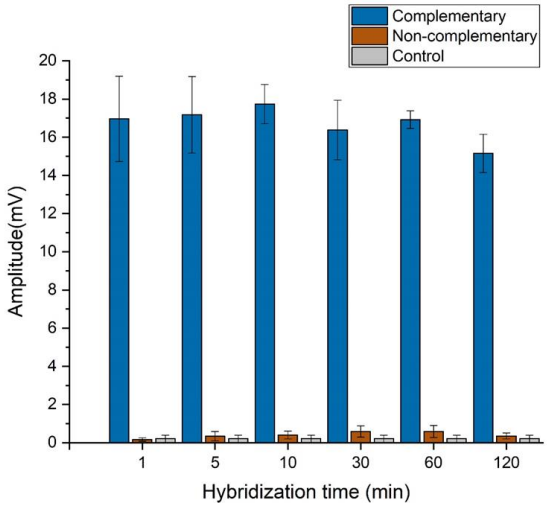

Figure 32. Detection time of the hybridization reaction. Error bars represent the standard deviation of three independent measurements.

Furthermore, to investigate the detection speed and the influence of the hybridization time on signal amplitude, we incubated DNA target and nontarget sequences for different lengths of time. Some samples were added to the PE filters, and hybridization was carried out without incubation by gravity flow, at a flow rate ~200 µL/min. This process took about 1.5 min. Other samples were incubated for 5, 20, 30, 60, and 120 min after the PE filters were closed with caps at the bottom so that the samples did not drop out of the columns. Figure 32 shows the effect of hybridization time on signal amplitude. It can be seen that the signal amplitudes obtained were high across all hybridization times and no significant differences were measured when the target DNA was used. However, the signal amplitudes were very low at all hybridization times when the nontarget DNA was used. The results highlight that our sensor works rapidly and is capable of detecting the target DNA in 90 s of hybridization time.

4.6. Magnetic sensing optimization

To evaluate the specificity of magnetic nanoparticles binding to the biotinylated target DNA, we tested another type of MNPs of identical size and specifications, but lacking a streptavidin shell (plain). PE filters containing a complementary DNA target were first tested at 5 µM concentration for hybridization reaction, and then magnetic labeling was done using MNPs with and without streptavidin shell. As seen in Figure 33A, the signal amplitudes of the magnetic nanoparticles with the streptavidin shell were remarkably higher than those without. This result

confirms that the binding of the MNPs to the biotinylated target DNA is selective through biotin–streptavidin interactions.

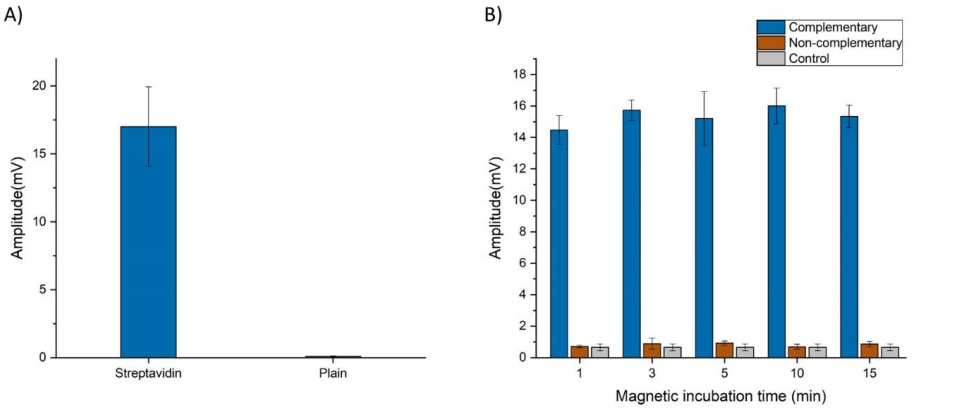

Figure 33. The selectivity of the binding of MNPs to biotinylated target DNA. (b) Effect of the MNPs incubation time on signal amplitude. Error bars represent the standard deviation of three independent measurements.

To further ensure the maximal binding capacity of magnetic nanoparticles to biotinylated target DNA, the magnetic nanoparticles were added to PE filter samples containing target and nontarget sequences and tested at various incubation times (1, 3, 5, 10, and 15 min). The impact of the magnetic nanoparticle incubation time is shown in Figure 33B. Notably, high signal amplitudes were observed across all incubation times when the target DNA was used. In contrast, only a very low signal amplitude, at the same level as that of the control samples, was measured when the nontarget DNA was used. For our assay, we determined 3 min of magnetic nanoparticle incubation time as optimal, ensuring the efficient binding of nanoparticles to DNA target.

4.7. Analytical performance

Under the previously optimized conditions, the sensitivity and dynamic detection range of our proposed DNA magnetic sensor were evaluated. Specifically, capture probes with a length of 50 bp were immobilized on polyethylene (PE) filters at a concentration of 5 µM for 30 minutes, followed by blocking with BSA for 1 hour. After immobilization, serial dilutions of single-stranded DNA (ssDNA) targets ranging from 9.8 nM to 5 µM were prepared. Triplicate samples of each concentration were mixed with 290 µl of 10× phosphate-buffered saline (PBS). In addition, blank samples without the ssDNA targets were prepared to determine the limit of

detection (LOD). The samples were added to the PE filters, and hybridization was carried out through gravity flow at a flow rate of 200 µL/min. After the hybridization, the magnetic nanoparticles were incubated for 3 min to allow their binding to biotinylated DNA. Finally, the samples were inserted into the measurement head of our portable magnetic reader to measure the signal amplitudes.

After magnetic measurement, a calibration curve was generated by fitting the mean and standard deviation of each ssDNA concentration after subtracting the background values using the Hill function presented in Equation (1). The resultant fitting parameters are k = 0.49182, end = 0.01573 and n = 1.04392.

As shown in Figure 34, the signal amplitudes increased with higher ssDNA target concentrations. The limit of detection was determined based on Equation (3) and was about 19 nM, with a linearity from 19.5 nM to 312.5 nM, a sensitivity of (22.1 ± 1.2) mV/µM, and a detection range from 19 nM to 1650 nM.

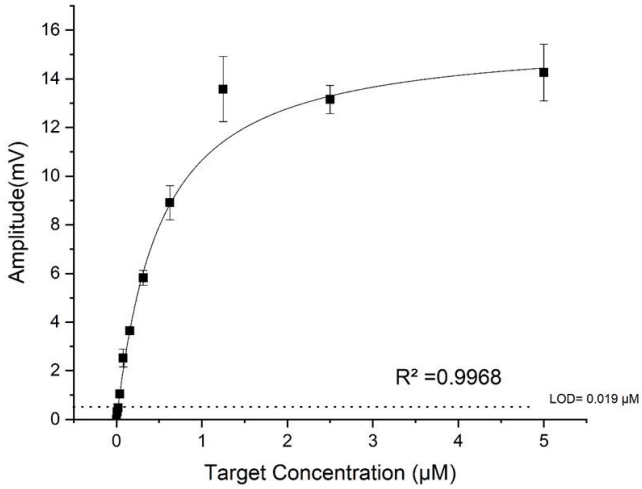

Figure 34. Fitted calibration curve of the measured signal amplitudes at different synthetic ssDNA concentrations. The LOD was determined using equation (3). Error bars represent the standard deviation of three independent measurements.

4.8. Reproducibility

In addition, intra and inter-day assays were performed to evaluate the reproducibility and repeatability of the sensor using synthetic ssDNA at different concentrations. The coefficient of variations (CV) was then calculated for each concentration, and a value of less than 10 % was obtained, showing the good reproducibility performance of the assay Table 4.

Table 4. The coefficient values of *Brucella* DNA assay.

ssDNA concentration	**Intra-assay (n=4)**			**Intra-assay (n=4)**		
	Mean (V)	**S. D**	**CV**	**Mean (V)**	**S. D**	**CV**
5 µM	0.01474	0.00121	8.22	0.01494	0.00105	7.008
1 µM	0.0099	0.00092	9.29	0.0103	0.00074	7.184
0.5 µM	0.00847	0.00065	7.6	0.0088	0.00063	7.15

4.9. Long term stability and regeneration

To evaluate our DNA magnetic assay in terms of long-term stability, we stored the PE filters with 500 µl of 10× PBS buffer in refrigerator at +4°C for a period of 4 weeks. The hybridization and magnetic detection for triplicate samples were performed each week. As shown in Figure 35A, no reduction was found after the first week, and only a slight reduction of about 7.42% in the magnetic response was observed in the second week. The reduction increased to 25.48% in the third week and 35.32% in the fourth week. This result indicates that our DNA magnetic assay has high stability and is suitable for long term application.

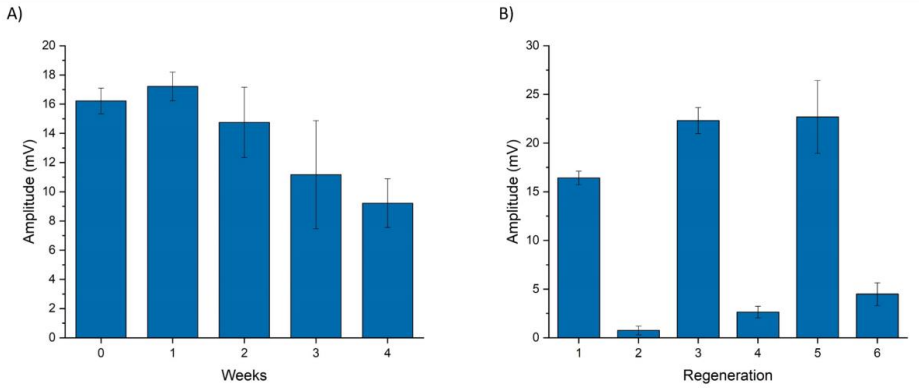

Figure 35. A) Stability of the PE filters at different weeks of storage. B) Regeneration performance of the PE filters. Error bars represent the standard deviation of three independent measurements.

As this assay is intended for large-scale testing, regeneration is desirable to ensure sustainability by reducing costs, waste, and materials for each test. The regeneration was investigated for the PE filters by employing chemical treatment using sodium hydroxide (NaOH). NaOH treatment is a common method used to disrupted the hydrogen bond between duplex DNA [101,102]. Here, NaOH at 0.5 M concentration was used to dissociate the hybridized DNA from the immobilized capture probe for 5 minutes. The PE filters were then washed with 1× PBS buffer to remove NaOH. After washing, 5 µM of target DNA was added to the PE filters for hybridization, followed by magnetic labeling for 3 minutes. For the first regeneration step, the signal amplitude decreased after adding NaOH, indicating the dissociation of target DNA from the capture probe, see Figure 35B. The signal amplitude increased after the rehybridization with target DNA for the second and third regeneration steps. Noticeably, the signal amplitudes were higher in the 2nd and 3rd generation steps than in the initial magnetic response. We assume that this increase in signal amplitude is due to the addition of more MNPs in each step, and the potential of MNPs to bind to the PE filter increases, and thus, signal amplitude increases. This can be seen in the NTC samples after the addition of NaOH, in which the signal amplitude increased. We also observed that adding NaOH affected the PE filter's flow rate. The first step's flow rate slowed to around 4 minutes, and 10 minutes for the second regeneration step. The slow flow rate allows more time for target DNA to hybridize to capture probe, which increases the signal amplitudes. As a result, that regeneration test showed that the PE filters can be used more than once. However, increasing the signal amplitude and the flow rate might be considered before using the filter for another test.

Overall, the analytical performance of our proposed assay showed the ability to detect and quantify *Brucella* DNA at low concentrations with a broad detection range, making it suitable for the early and accurate diagnosis of brucellosis in field applications.

Chapter 5

5. Magnetic Detection of Amplified *Brucella* DNA

After the development and validation of our magnetic assay for *Brucella* detection using synthetic oligonucleotide targets, we demonstrated the sensor's ability to detect and quantify target DNA sequences with high sensitivity and specificity. However, to assess its utility in practical applications, further evaluation with clinically relevant samples is necessary.

In this study, our objective is to evaluate the feasibility for our assay to detect DNA in real samples by testing its performance with DNA extracted from different infected animals. These extracted genomic DNA (gDNA) represent different bacterial species including *Brucella* pathogen as well as other non-related bacteria.

The chapter is partly based on the original publication by the author [74].

5.1. Primer design and PCR optimization

Forward and reverse primers were designed to amplify the selected target DNA sequence, yielding an 84 bp DNA fragment complementary to the capture probe P (50). The primer sequences with their modifications are listed in Table 5.

Table 5. The designed primer sequences with their modification.

Primer	**Sequence (5′ to 3′)**	**Modification (5′)**	**Length (bp)**
F1	AGGCTGTAGTGACGAATTAACTTGTGG	Biotin	27
R1	GAACCACTCCACCTTCGGTTTCGCTCC	No modification	27
R2	GAACCACTCCACCTTCGGTTT CGCTCC	Phosphate	27

The forward primer has been modified with biotin at its 5' end to enable the specific binding to the streptavidin-magnetic nanoparticles. To ensure that the forward primer sequence, which generates the ssDNA target strand, does not hybridize with the capture probe, the forward primer was designed to bind to an adjacent sequence that does not contain a sequence complementary to the capture probe, see Figure 36. As a result, the double standard PCR amplicon amplified will consist of two strands: one target strand that contains the biotinylated primer sequences, which is complementary to the capture probes, and the other is non-complementary.

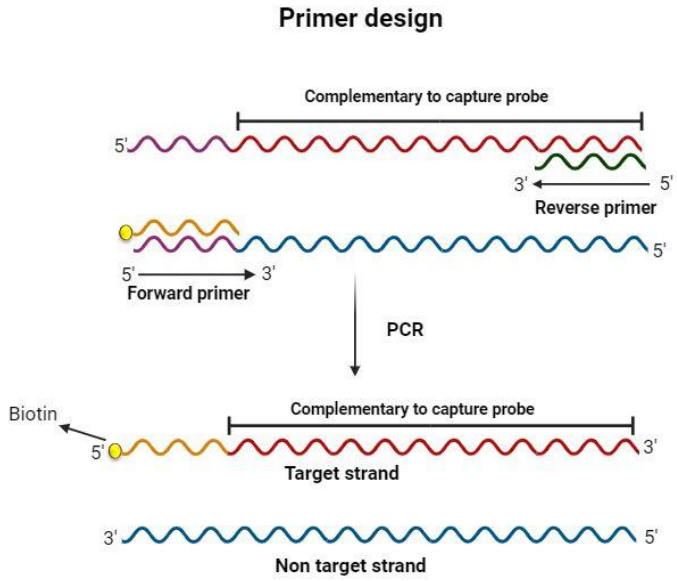

Figure 36. Schematic representation of the locations where primers bind within the target sequence and the resulting amplified DNA produced from PCR. Created with BioRender.com.

In order to evaluate and optimize the amplification reaction with the new primers, we first performed a gradient PCR reaction by testing multiple annealing temperatures ranging from 55 to 68°C. The PCR reaction was performed in 50 µl reaction tubes, with each tube containing the new primer pairs (F1/F2) and all mixtures of PCR while varying only in the annealing temperatures. The result showed that the band intensities of amplicons were high at all temperatures from 55 to 65.9°C, and no bands were observed at the higher temperatures 67°C and 68°C. Thus, we selected 60°C as a suitable annealing temperature, see Figure S7 in the supplement. This result also confirmed the successful amplification of *Brucella* genomic target DNA with the new primers, as the expected PCR fragment with 84 bp length was observed.

After selecting a suitable annealing temperature, the primer concentration optimization was performed to select the optimal ratio. Selecting an optimal ratio is needed for our assay as the concentration of primers influences the yield, sensitivity and specificity. Therefore, optimizing the primer ratio is important to maximize the yield of desired DNA amplicons, increase sensitivity and minimize the potential for nonspecific binding. As shown in Figure 37, the expected bands on agarose gel were observed at 0.5, 1 and 1.5 µM primer concentrations without nonspecific amplification. However, the intensities of the bands of 0.5 µM were lower than at 1 and 1.5 µM. When higher primer concentrations were tested, nonspecific bands were observed at 2 and 2.5 µM. As a result, we selected 1 µM as a suitable primer concentration.

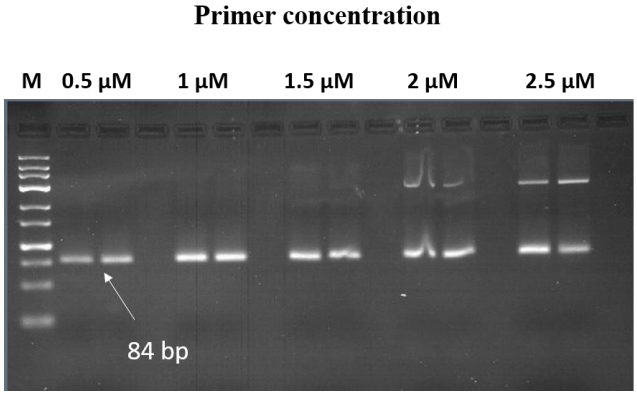

Figure 37. Optimization of primer concentrations. M: Marker.

5.2. Generation of ssDNA sequences

For the detection of PCR amplified *Brucella* DNA, the biotinylated ssDNA target strand, which is complementary to the capture probe, needs to be generated from dsDNA amplicons. This generation allows hybridization between the capture probe and ssDNA target and further magnetic sensing. Here, we investigated three different denaturation strategies to select a suitable method that yields a high biotinylated ssDNA amount. The first method used is heat and cool, where the PCR amplicons are incubated at high temperature, followed by rapid cooling. This method is cost-effective and used in many molecular biology applications as a simple way to generate ssDNA from dsDNA [103,104]. In our study, the PCR tubes (50 µL) were heated at 95°C for 5 minutes to break the hydrogen bonds between the complementary

strands, resulting in the separation of the two ssDNA strands. After separation, the tubes were immediately cooled on ice for 4 minutes to slow down the reannealing of the two strands. The tubes were then mixed with 250 µl of 10× PBS hybridization buffer and immediately added to the PE filter for hybridization reaction and magnetic detection.

The second strategy used was lambda exonuclease treatment, where the PCR amplicons are digested by lambda exonuclease enzyme by targeting the phosphorylated strand from the 5′ to the 3′ end. This strategy is widely used in aptamer selection method due to its efficient and specific generation of ssDNA strand [105,106]. For our PCR reaction, we used a new reverse primer (R2) which has the same sequence as (R1) but with phosphate modification at its 5′ end. This modification allows lambda exonuclease to digest the non-complementary strand generated by this primer, while leaving the captured biotinylated ssDNA target strand in the reaction. Before the digestion reaction, some samples were purified while others were kept unpurified to check the enzyme's activity in both reactions. For lambda exonuclease digestion, we incubated both purified and unpurified PCR products with lambda exonuclease enzyme at 37°C with different duration times of 5, 10 and 15 minutes. Following enzymatic digestion, gel electrophoresis was performed to evaluate the band intensities. As shown in Figure 38, a significant change in band intensities and migration rates was clearly observed at all incubation times. This indicated the efficient digestion of PCR amplicons using lambda exonuclease enzyme. These changes can be explained firstly by the fact that ssDNA has lower molecular weight, which results in faster migration through agarose gel compared to dsDNA. Secondly, the weaker band intensity of ssDNA to dsDNA can be attributed to the lesser amount of red safe stain incorporation into ssDNA strand [105]. Comparing the band intensities of the purified and non-purified samples, the unpurified samples showed a weak band of the same size as dsDNA, which might be an indication of the incomplete digestion of the dsDNA. In addition, 5 minutes incubation time was sufficient for complete digestion. The digested PCR amplicons were mixed with 250 µl of 10× PBS buffer and added to the PE filter for hybridization reaction and magnetic detection.

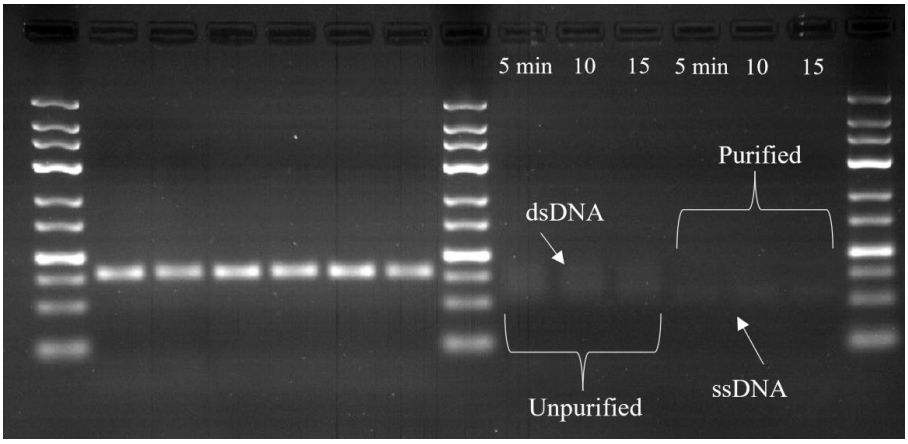

Figure 38. Agarose gel image of Lambda exonuclease digestion of purified and unpurified Amplicons at different incubation times 5, 10 and 15 minutes. M: Marker.

The last strategy used was magnetic separation, where the PCR amplicons were incubated with Synomag®-D streptavidin-coated MNPs for capturing biotinylated amplicons. After capturing, the mixture was transferred to a MACS column placed in a magnetic separator, followed by alkaline treatment to break the hydrogen bonds between the dsDNA strands. After the separation of the non-biotinylated strand, the MACS column was removed from the magnetic separator, and the biotinylated ssDNA strands bound to MNPs were eluted with 300 µL of 10× PBS buffer in Eppendorf tubes for hybridization reaction and magnetic detection.

Following the generation of ssDNA strand from the three strategies used, the generated ssDNA target strands were added to the PE filters to hybridize with complementary capture probes P (50) at 5 µm concentration. The hybridization reaction was carried out by gravity flow. Then, any unhybridized DNA strand was washed away by 750 µL of 1× PBS buffer. After washing, the PE filters were labeled with MNPs and incubated for 3 minutes, followed by a final washing step to remove unbound MNPs. Finally, the PE filters were inserted into the magnetic reader to measure the magnetic response.

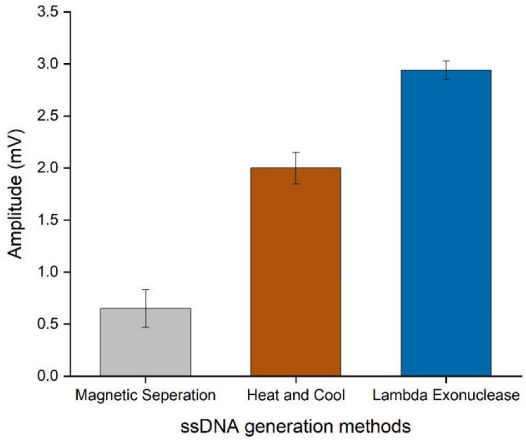

Figure 39. Measured signal amplitudes of the ssDNA generation methods used in this study. Error bars represent the standard deviation of three independent measurements.

Figure 39 shows the different signal amplitudes obtained from the three strategies tested. The signal amplitude obtained from lambda exonuclease treatment was the highest compared with other methods, while magnetic separation was the lowest. This indicates that lambda exonuclease yielded higher ssDNA amounts, resulting in the highest signal amplitude. In contrast, the low yield of ssDNA amount for the heat and cool and magnetic separation methods can be attributed to variations in their efficiency in separating dsDNA. For the heat and cool method, the ssDNA strands favor hybridization in solution rather than on-surface hybridization due to the mobility and accessibility of its complementary strands. In addition, the hybridization rate in solution is faster than on solid surface [107]. For magnetic separation, the significant reduction of signals can be explained by the possible denaturation of streptavidin molecules from the surface of MNPs due to the harsh alkaline treatment with NaOH that has an influence on the loss of tertiary structure [106,108]. In addition, it might also be explained by the insufficient magnetic separation force on the small MNPs, which resulted in the loss of MNPs through washing step. As a result, we selected lambda exonuclease digestion as a suitable method for generating the ssDNA target strand from the amplified PCR products.

5.3. Limit of detection and specificity

To test the ability of our assay to detect authentic *Brucella* genomic DNA, we conducted a serial dilution ranging from 5 to 5 × 10^6 copies of the template. The diluted samples were then subjected to PCR amplification using F1 and R2 primers, followed by gel electrophoresis for visualization, see Figure S8 in the supplement. Subsequently, the amplicons were then treated with lambda exonuclease to generate complementary ssDNA through the digestion of the nontarget strand amplified by the reverse primers R2 modified with a phosphate group. Finally, the generated target ssDNA strand was added to 250 µL of 10× PBS buffer for hybridization reaction and FMMD magnetic measurement.

As shown in Figure 40, our assay was capable of detecting the *Brucella* target DNA at all concentrations ranging from 5 to 5 × 10^6 copies, exhibiting high signal amplitude. However, the signal amplitudes were notably low when five copies of the genome were tested, similar to those observed for the non-template control (NTC). These results indicated that the assay has high sensitivity in detecting amplified *Brucella* DNA, being sensitive to amounts as low as 55 copies (0.09 fM).

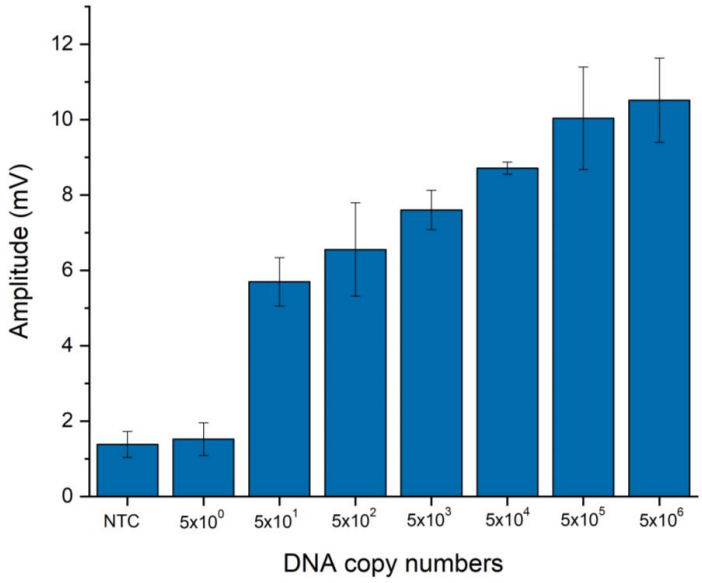

Figure 40. The signal amplitudes for different copy numbers of amplified *Brucella* DNA. Error bars represent the standard deviation of three independent measurements.

Furthermore, the assay specificity was also evaluated by analyzing the PCR-amplified products in the presence of genomic DNA from various bacterial strains, including *Campylobacter fetus subsp. venerealis (Cfv)*, *Campylobacter fetus subsp. fetus (Cff)*, *Ovax Chlamydia vaccine*, *Escherichia coli (APEC)*, and *Salmonella enteritidis*. The selection of these bacterial species was based on their potential to interfere with *Brucella* detection, as they can coexist in animal samples subjected to examination. Notably, while the assay showed a specific high signal when examining *Brucella melitensis* gDNA, all non-related bacterial genomes exhibited a very low signal amplitude, ensuring the specificity of the primers and capture probes toward *Brucella* DNA, as shown in Figure 41 and Figure S9 in the supplement.

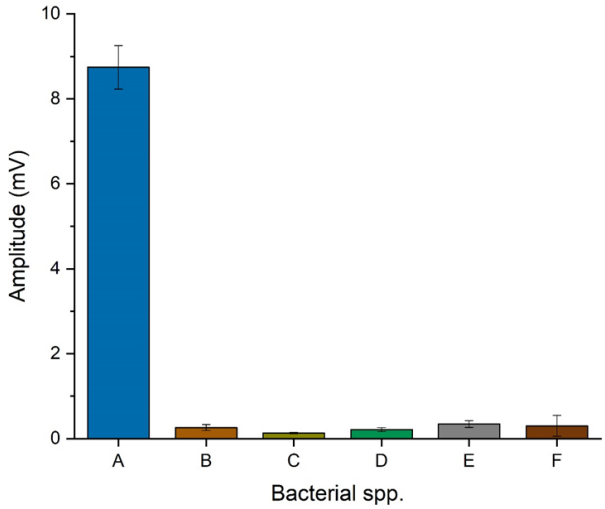

Figure 41. The signal amplitudes for *Brucella melitensis* and non-related bacterial genomic DNA amplified by PCR. (A) *Brucella melitensis* at 2 ng/µL, (B) *Ovax Chlamydia* at 5 ng/µL, (C) *Campylobacter fetus subsp. venerealis* (Cfv) at 27 ng/µL, (D) *Campylobacter fetus subsp. fetus* (Cff) at 55 ng/µL, (E) *Escherichia coli* (APEC) at 83 ng/µL, (F) *Salmonella enteritidis* at 84 ng/µL. Error bars represent the standard deviation of three independent measurements.

Chapter 6

6. Magnetic Detection of RPA Amplified DNA

To enhance usability of our developed DNA magnetic assay for field testing, we combined Recombinase Polymerase Amplification (RPA) with frequency mixing magnetic detection. We chose RPA for its rapid amplification time compared to other isothermal amplification methods. By combining RPA with our magnetic assay, which demonstrated rapid detection time within 10 minutes, we could enhance the capability of our assay in detecting *Brucella* pathogen by allowing a fast amplification and magnetic detection using our portable magnetic reader at point of care.

In this chapter, the development and integration of RPA with FMMD are introduced in detail. We establish the RPA assay and the steps involved, such as primer design and primer screening, to select suitable specific primer pairs. Following primer selection, we include an asymmetric RPA technique to simplify the generation of ssDNA complementary strands without the need for other separation methods. The design and limitations of asymmetric RPA are discussed. Then, a new detection strategy of amplified DNA using new primers with tail sequences for amplification and magnetic detection to overcome the issue of asymmetric RPA is presented. In addition, the different methods used to eliminate the nonspecific binding of primers are discussed. Finally, all optimization steps for enhancing RPA reaction, such as incubation temperature and time and its effect on the magnetic signal, are presented.

6.1. RPA primer design and screening

RPA amplification has a constant amplification temperature between 37°C and 42°C, which makes primer design criteria different from PCR that mainly based on the primers' melting temperature (Tm) [109]. RPA amplification requires longer primer, usually between 30-35 bp length [110]. However, several studies have shown that shorter primers below 25 bp and even PCR primers were able to amplify their desired products [111–113]. The long RPA primer is

important for the T4 UvsX protein to form a stable nucleoprotein filament complex that binds to the complementary DNA sequences. However, the longer the primer, the higher the potential to form a secondary structure or primer artifacts. In addition, there is no bioinformatics software for RPA primer design.

Although RPA amplification requires only two primers compared to other isothermal amplification methods like LAMP, an experimental primer screening for several designed primers is recommended to select the optimal primer candidate.

Based on our previous results of PCR amplification, the primer pair (F1/R2) designed to amplify *Brucella* DNA generated a product of 84 bp, which is considered as a suitable length based on the recommendation of the manufacturer (TwistDx) for keeping the amplicon length less than 500 bp. In order to keep the product length and to perform primer experimental screening, we designed new forward primers (F2 and F3) with longer sizes, the sequences are listed in Table 6.

Table 6. The designed Forward primer sequences with their modification for screening.

Primer	**Sequence (5′ to 3′)**	**Modification (5′)**	**Length (bp)**
F2	CTGTAGTGACGAATTAACTTGTGGTTTGG	Biotin	29
F3	AGGCTGTAGTGACGAATTAACTTGTGGTTTGG	Biotin	32

RPA amplification was performed by screening the forward primers F1, F2 and F3 against the reverse primer R1 using *Brucella* genomic DNA. The primers were added to separate tubes at 600 nM final concentration. Then, the master mix containing 2× reaction buffer (20 µl), dNTPs (9.2 µl), 10× basic E-mix (5 µl) and 20× core reaction (2.5 µl) were added to the tubes. To initiate the RPA reaction, 2.5 µl of magnesium acetate and 1 µl of *Brucella* gDNA (0.02 ng/µl) were added to each tube. The tubes were then placed in a heat block at 37°C for 30 minutes. After RPA amplification, we purified the RPA amplicons with a column-based purification kit and analyzed them by gel electrophoresis at 2% concentration to evaluate the primers' performance.

As shown in Figure 42, the PCR primer pair (F1/R1) and the RPA primers (F2/R1) and (F3/R1) were successfully able to amplify the DNA target with their amplicon expected sizes. However,

nonspecific amplification products were observed in all primer pairs tested. This appearance of nonspecific bands is common in RPA amplification due to the mismatch tolerability and lower constant temperature of amplification, where the primers have lower binding stringency compared to PCR [53]. This lower binding stringency allows the recombinase enzyme to form the nucleoprotein complex on template DNA, even when the primers are partially bound on different genomic locations. Another explanation is that our selected target DNA is a repeat sequence, which makes the probability of having multiple DNA fragments that have partial sequences within the genome high compared to a single copy target. For primer pair selection, F2/R1 showed fewer DNA fragments and was therefore selected for the next optimization experiments.

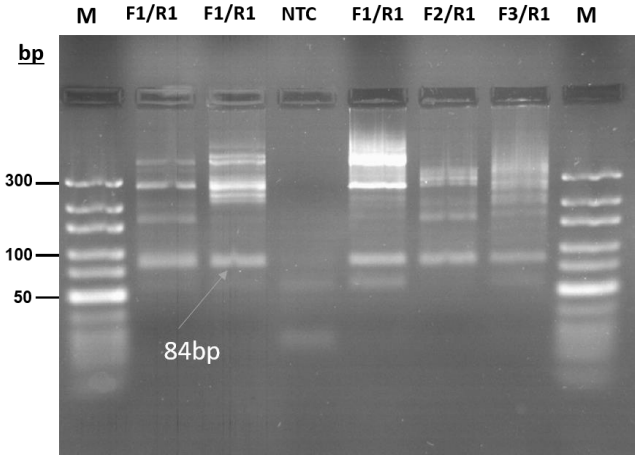

Figure 42. Screening of primer pairs by RPA amplification. M: Marker

After primer pair selection, we performed RPA amplification using a lower concentration of primers (F2/R1) to evaluate the effect on the appearance of nonspecific products. The concentrations tested were 150 nM, 240 nM and 480 nM. Figure 43 shows the effect of different concentrations of primers on the nonspecific amplification products. The appearance of nonspecific products decreased when lower concentrations of primers were tested. However, nonspecific bands with 300 bp were still observable and exhibited higher intensities than the expected size of 84 bp.

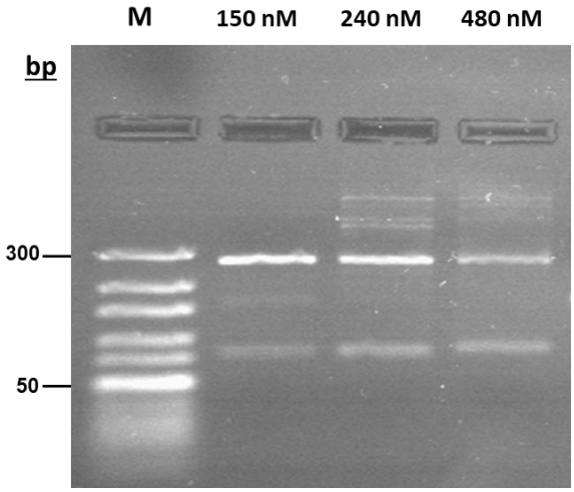

Figure 43. Optimization of RPA primer concentrations. M: Marker.

While these nonspecific products could impact the specificity of the amplification, our capture probe P (50) is only complementary to the ssDNA target sequence with 84 bp size. This ensures that the probe hybridizes to our ssDNA without interfering with other nonspecific products.

6.2. Asymmetric RPA amplification

In the previous experiments, lambda exonuclease treatment was selected as a suitable method for generating the ssDNA strand from PCR amplicons, as its signal amplitude was the highest. However, this method needs an additional enzymatic digestion step after amplification, and additional incubation time. This makes it unsuitable for PoC testing since it increases the complexity and increases the time needed for the assay.

To perform a simpler and more suitable method, we have selected Asymmetric Recombinase Polymerase Amplification (ARPA) to generate our ssDNA target strand in the field. ARPA is an amplification technique that uses different concentration ratios of forward and reverse primers [110,114]. In the ARPA reaction, the forward and reverse primers anneal on template DNA to amplify a dsDNA product at the initial amplification phase. While the amplification continues, the primer with a lower concentration is consumed, and the remaining primer with a higher concentration continues to generate the targeted ssDNA strand, see Figure 44. In this technique, our ssDNA target will be generated in the same reaction tube during the

amplification without the need to post-process the DNA products by lambda exonuclease treatment.

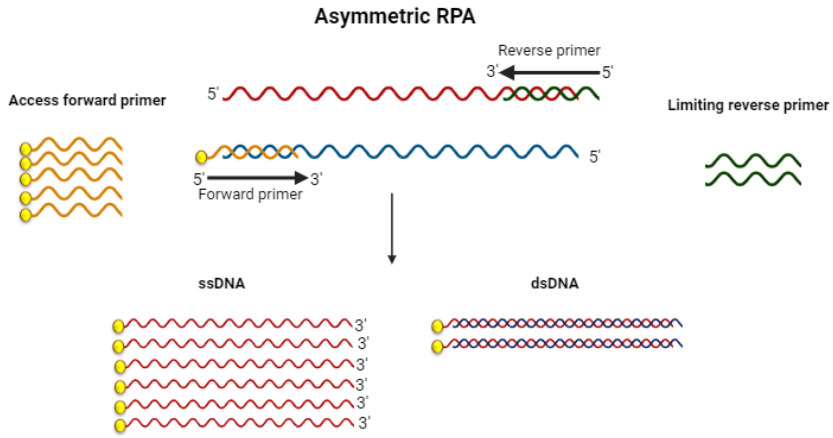

Figure 44. Principle of asymmetric RPA. Created with BioRender.com.

In our assay, the forward primer (F2) is the primer that generates the complementary ssDNA strand to our capture probe P (50). So we have chosen it as an access primer, while reverse primer (R1) acts as limiting primer. After that, we performed the asymmetric RPA using primer ratios at 1:20, 1:40 and 1:60 of forward and reverse primers for 30 minutes at 37°C. After ARPA amplification, we analyzed the amplicons by gel electrophoresis at 2% agarose concentration. Figure 45A shows the gel image of the product bands generated by ARPA. It can be seen that all three primer ratios tested showed nonspecific bands with different sizes. This suggests the low efficiency of the primers in specifically amplifying our target ssDNA using asymmetric RPA. However, the impact on the magnetic signals of these amplified products were not evaluated.

To evaluate it, we mixed the ARPA amplified products with 250 µl of 10× PBS buffer and transferred them to the ABICAP columns with the capture probe P (50) at 5 µM concentration for the hybridization reaction. Then, the MNPs were added to the PE filters for 3 minutes incubation time, followed by FMMD measurement using our magnetic reader. Figure 45B shows the signal amplitudes obtained from the ARPA amplified products at primer ratios of 1:20, 1:40 and 1:60. The magnetic measurement of all ARPA products showed a very low signal amplitude compared to the signal obtained from the positive control amplified product by PCR.

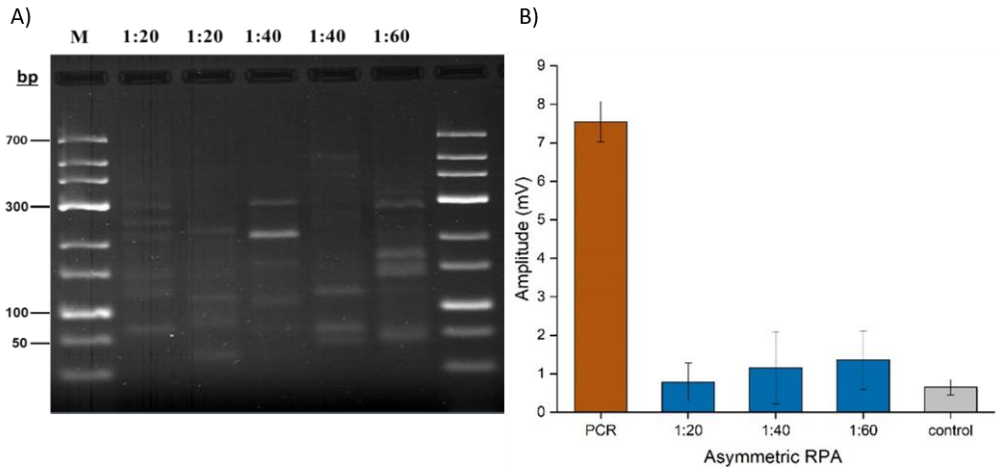

Figure 45. A) The gel image of primer ratios tested for asymmetric RPA. B) The signal amplitudes for asymmetric RPA products generated by different primer ratios. Error bars represent the standard deviation of three independent measurements.

Based on the results, the primers showed low efficiency in specifically amplifying our desired target ssDNA. This inefficiency might be due to the reasons we mentioned before, such as the repetitive nature of the target sequences and the lower binding stringency of primers at isothermal conditions. Moreover, the asymmetric RPA technique itself is prone to produce undesired amplification products due to the primer imbalance, as highlighted in a previous study [115]. Therefore, we conclude that amplifying our target ssDNA using asymmetric RPA strategy with the primer pair (F2/R1) is not suitable for our assay. Thus, new primers should be designed that might offer higher specificity.

We screened our selected DNA target sequence to find potential reverse primers. Then, four new reverse primers were designed to amplify products that contain complementary sequences to our capture probe P (50). The new reverse primer sequences are listed in Table 7.

Table 7. The designed reverse primer sequences with their expected amplicon sizes for screening.

Primer	**Sequence (5′ to 3′)**	**Expected amplicon size**	**Length (bp)**
R3	CACTCCACCTTCGGTTTCGCTCCTAAAGCTG	81	31
R4	GGCGTCGCGAAACCTTGATGGGGGAACC	107	28
R5	CTCCATCTTGGCGTCGCGAAACCTTGA	116	27
R6	CACATTCAGAAGCAAAATACACTGCGTC	166	28

To evaluate the primers' efficiency, we performed RPA amplification using the new reverse primers R3, R4, R5 and R6 against the forward primer F3. Five tubes were prepared with the new reverse primers and forward primer F3 at 480 nM final concentration. The same protocol was applied for RPA reaction as mentioned earlier. All tubes contained a mix of 20 µl of 2× reaction buffer, 9.2 µl of dNTPs, 5 µl of 10× basic E-mix, 2.5 µl of 20× core reaction mix and *Brucella* gDNA (0.02 ng/µl). The incubation time was 30 minutes at 37°C. After amplification, the amplified products were purified and analyzed by gel electrophoresis at 2% agarose concentration to evaluate primer efficiency.

Figure 46 shows the performance of the newly designed reverse primers. From the gel image, all primer pairs were successfully amplified with their expected amplicon size with different band intensities. In addition, all of them showed a nonspecific product with a size of about 300 bp except the primer pair (F3/R6), which produced a specific amplification product with a size of 166 bp. By evaluating the band intensities of expected amplicon size for all primer pairs, it is clear that increasing the product size from 81 bp to 166 bp increases the intensity of the bands. It is unclear why this behavior is observed in our results. We assume this might be related to the DNA polymerase activity, as it favors longer distances between primers to synthesize strands without frequently dissociating from the DNA template. In addition, more templates available for the polymerase to work on results in more efficient amplification for longer DNA products. Overall, the primer pair (F3/R6) showed optimal efficiency and specificity in our RPA amplification, compared with other pairs. Thus, this pair was selected for the next experiments. An additional image for validation of the specificity of the primer pair (F3/R6) can be found in Figure S10 in the supplement.

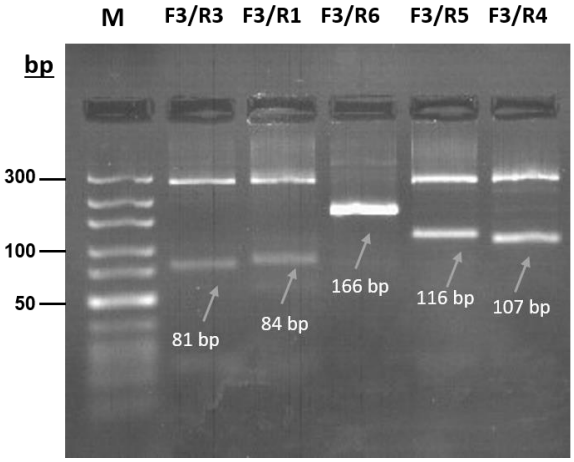

Figure 46. The agarose gel image of RPA products amplified by the new reverse primers.

Before we perform asymmetric RPA amplification for the selected primer pair (F3/R6), the impact of the new product with a size of 166 bp, which is longer than our previous amplicon size of 84 bp, needs to be evaluated in terms of hybridization efficiency and magnetic signals. The amplicons with a size of 166 bp were digested by lambda exonuclease enzyme to generate the ssDNA target strand complementary to our capture probe P (50). Then, the digested amplicons were mixed with 250 µl of 10× PBS buffer and added to the PE filters for hybridization reaction for 1 hour. Finally, the MNPs were added to hybridized strands for sensing the magnetic response. As shown in Figure 47, the signal amplitude of the product size of 166 bp was very low, compared with the previous product size of 84 bp. This indicates the lower hybridization efficiency of the new product size of 166 bp. This can be explained by the fact that longer ssDNA sequences have the potential to form more secondary structure than shorter sequences, which can hinder the probe's ability to hybridize with the complementary sequences. In addition, it might be that the lambda exonuclease treatment efficiency is lower with longer strands, leading to incomplete digestion of the amplicons.

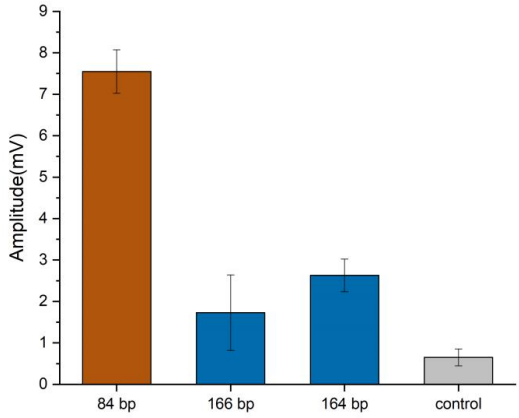

Figure 47. The signal amplitudes of the different sizes of ssDNA target. Error bars represent the standard deviation of three independent measurements.

To address that, we evaluated the hybridization efficiency using a synthesized oligonucleotide sequence T (164) that has the same sequence but with two base pairs shorter, due to the maximum oligonucleotide length that the manufacturer can produce, see Table 1 in the material and methods chapter. Here, we performed the hybridization at 5 µM concentration of T (164) and 5 µM of capture probe P (50) for 1 hour, and then magnetic measurement was done by FMMD. As shown in Figure 47, the signal amplitude of the synthesized T (164) was slightly higher than the digested RPA amplicon with a size of 166 bp. However, both exhibited very low signal amplitudes compared to those obtained from the PCR positive control with a size of 84 bp. This validates that the target length of 166 bp is unsuitable for hybridization with our capture probe P (50). In addition, the secondary structure analysis of the sequence confirms the high potential to form a secondary structure, see Figure S11 in the supplement.

In conclusion, the primer pair (F3/R6) showed specific amplification without any nonspecific bands. However, the great length of the amplified target sequence resulted in lower hybridization efficiency, which influenced the magnetic signals. This result indicates that even if it works properly, generating this ssDNA by asymmetric RPA will not be suitable for our assay using this specific primer pair. Therefore, a new strategy that maintains the use of the primer pair (F3/R6) but employs a different detection method of amplicon with the size of 166 bp is needed to enhance our assay performance. The new strategy will be addressed in the next section.

6.3. Detection of whole amplicon

Several studies have modified the two primers to produce dual-labeled amplicon that can be captured at one end and detected at the other. This is usually done by modifying one primer with labels such as 5-FAM antigenic label, Digoxigenin (DIG), or Fluorescein Isothiocyanate (FITC), which allow the amplicon to be captured by anti-FAM, anti-DIG, and anti-FITC antibodies immobilized onto the membrane [116]. Once the amplicon is captured at one end, it can be detected through other labels, such as biotin from the second modified primer, which streptavidin-nanoparticles can bind, enabling visual detection [117–119]. Another strategy is based on using primers with additional oligonucleotide sequences (tail) at their end. This tail sequence is used to hybridize with a complementary probe to capture the amplicon at one end, while the other end can be used for detection [120,121]. Comparing the two strategies, tail primers have several advantages over antibody labeling. Firstly, they are cost-effective, reducing the need for the high-cost antibodies and additional reagents. Secondly, they are more specific through the nature of the sequence complementary between ssDNA strands. In addition, they have reduced variability which leads to more consistent and reliable results. Thus, tail primers were selected as a suitable strategy to detect our amplified *Brucella* DNA.

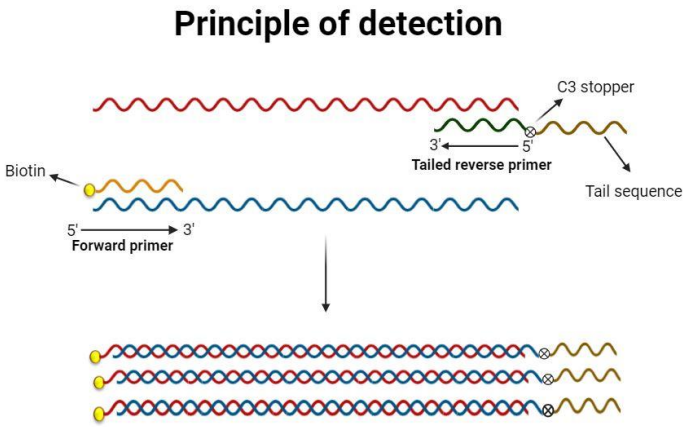

Figure 48. Principle of tailed-primer RPA amplification. Created with BioRender.com.

The new strategy is based on the detection of whole RPA amplified amplicon through the hybridization between a tail sequence and a capture probe immobilized onto our PE filter, see Figure 48. Here, we added short ssDNA tail sequences with different sizes at the 5` ends of the

reverse primer (R6). We incorporated a C3 spacer as a stopper between the tail and reverse primer sequences to prevent polymerase elongation [122]. The same modification of the forward primers with biotin is kept for MNP labeling. For the hybridization reaction, we designed a new capture probe complementary to the tail sequences, and added a poly (T) nucleotide with a size of 15 bp to the 3` ends to increase its length. The addition of poly (T) sequences improves the binding capacity and accessibility of the probe to the amplicon tail, which increases the hybridization efficiency. The new capture probe and tail primers are listed in Table 8.

Table 8. The new tailed-reverse primer and capture probe sequences.

Oligonucleotides	Sequence (5′ to 3′)	Length (bp)
R7	AGCGTGCAGGGAGAGTGGTA-C3-CACATTCAGAAGCAAAATACACTGC	45
R8	AGCGTGCAGGGAGAG-C3-CACATTCAGAAGCAAAATACACTGCGTC	43
P (Tail)	CTCTCCCTGCACGCT-TTTTTTTTTTTTTT	30

The new RPA-tailed primers (R7 and R8) were screened against all forward primers F2, F3, and F4, to select the suitable primer pair. All primers were at 480 nM final concentration. Each tube contained a mixture of 20 µl of 2× reaction buffer, 9.2 µl of dNTPs, 5 µl of 10× basic E-mix, 2.5 µl of 20× core reaction mix and *Brucella* gDNA (0.02 ng/µl). The samples were incubated in a heat block for 30 minutes at 37°C. Following RPA amplification, the products were purified and analyzed using gel electrophoresis with 2% agarose concentration. Figure 49 shows the amplification efficiency of the screened-tailed reverse primers. All primer pairs with the tailed primer R8 successfully amplified the expected product size with different intensities. However, no products were generated from all primer pairs with the tailed primer R7. We also observed the appearance of primer dimer in all primer pairs tested with high intensity. From the results, the tailed primer R8 has more efficiency in amplifying our target *Brucella* DNA, and the primer pair F4/R8 showed the highest intensity. Thus, this primer pair was selected for the next experiments.

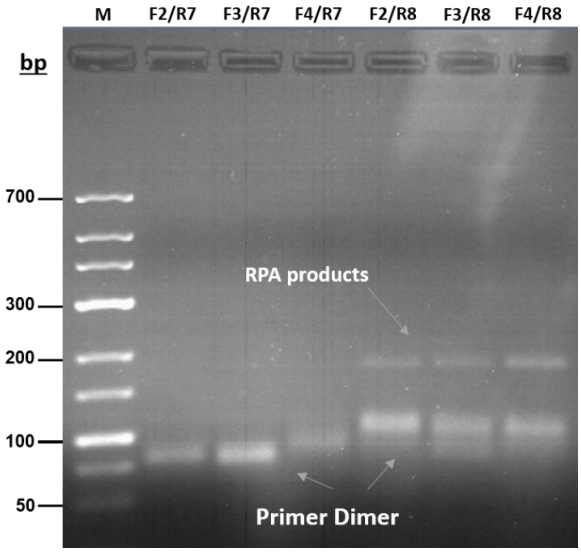

Figure 49. The agarose gel image of RPA products amplified by the tailed-reverse primers R7 and R8.

To investigate the impact of the new strategy on our FMMD measurement, we performed a hybridization reaction and magnetic detection using the RPA products amplified by the primer pair (F4/R8), and we used a non-template control (NTC) as a negative control. The samples were added into the PE filter containing the complementary capture probe P (tail) at 5 µM concentration for hybridization by gravity flow at a flow rate of ~200 µL/min. After hybridization, the PE filters were washed with 1× PBS to remove unbound RPA products. For magnetic detection, we incubated the PE filter with MNPs to allow their binding to biotinylated amplicon for 3 minutes. Finally, the PE filters were inserted into the measurement head of our portable magnetic reader to measure the signal amplitudes.

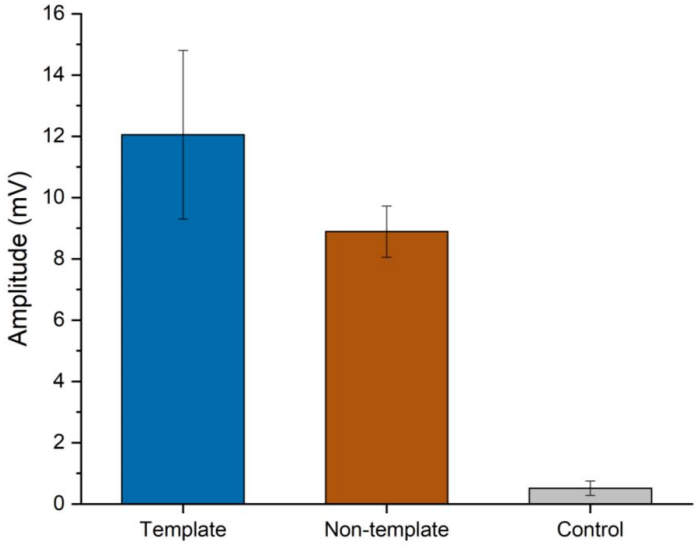

Figure 50. The signal amplitude of the RPA products amplified by the tailed-reverse primers. Error bars represent the standard deviation of three independent measurements.

As shown in Figure 50, the signal amplitude of the RPA products is slightly higher than the signals obtained from NTC and markedly higher than control. This indicates the efficient hybridization of the whole amplicon through the tail sequence and its complementary capture probe. However, NTC samples showed a very high signal amplitude compared to negative control. This can be explained by the non-specific interactions and the formation of stable secondary structures, such as primer dimers. The addition of tail sequences to the reverse primer increased its size and thus the potential of primers to interact with each other particularly at low temperatures such as 37°C increases, leading to primer dimer formation. When these primer dimers form, they bind to capture the probe through the tail sequence at one end, and MNPs bind to the biotinylated primer at the other. This leads to false positive results, which make it difficult to distinguish between true signals from the *Brucella* target DNA and artifacts caused by the primers. As a result, it reduces the reliability and specificity of our assay.

6.4. Reduction of primer dimer formation

In previous studies, primer dimer formation was observed in isothermal amplification techniques that require long primers (30-45 bases) and a high concentration of primers such as LAMP and RPA [123–125]. It influences the specificity and sensitivity of the amplification,

which causes false positive results, reduced efficiency and signal loss [126]. For LAMP amplification, several strategies based on destabilizing nucleic acid structure using chemical additives were used to prevent it and to improve the overall amplification specificity [127,128]. For RPA amplification, one method is widely used based on a probe system. In this system, an additional specific probe modified with tags such as biotin or FAM at the 5′ end, and a blocking modification at the 3′ end is designed to anneal to the amplicon between the binding sites of the primers [123,129]. Once the probe anneals to the amplicon, site-specific cleavage (THF cleavage) of the probe by endonuclease nfo enzyme occurs. This generates two fragments, one blocked short fragment and another long fragment that can be extended [119]. Another method is the use of a self-avoiding molecular recognition system (SAMRS), which involves incorporating SAMRS nucleotides such as 2-aminopurine-2′-deoxyriboside (A*), 2′-deoxy-2-thiothymidine (T*), 2′-deoxyinosine (G*), and N4-ethyl-2′-deoxycytidine (C*) into the primers [130]. This system has been employed to prevent the primer dimer formation in RPA amplification when dual labeled amplicon is required, particularly with RPA-based lateral flow biosensors [46,131]. One more strategy is the use of organic additives such as dimethyl sulfoxide (DMSO) and betaine [132]. These additives disrupt the hydrogen bonds and lower the melting temperature of the dsDNA [128]. Several studies showed the successful elimination of the primer dimer and the nonspecific products in several RPA amplification assays using those additives [133,134]. Comparing these strategies, organic additives are relatively inexpensive, simple to use, and do not require modification to primers or additional probe sequences.

In our assay, we evaluated three methods that may influence primer dimer formation. The first method was based on adjusting the primer concentrations at 150, 300, 450, and 600 nM. The second was based on performing RPA amplification using betaine at different concentrations (0.1, 0.25, 0.5, and 1 M). The last method was based on using DMSO at different concentrations (1, 3, 5, and 10%). *Brucella* genomic (0.02 ng/µl) and non-template samples were used to evaluate the effect of all three methods on the amplification efficiency and primer dimer reduction. All RPA reactions were incubated at 37°C for 30 minutes. Following the amplification, all RPA products were purified and loaded onto gel at 100 V for 1 hour, and then the intensity of bands was assessed using ImageJ.

Figure 51 shows the gel images of the methods used to reduce primer dimer formation using a template and non-template DNA. For the primer concentration optimization results on template DNA, all RPA products appeared at all concentrations tested with lower intensities at

concentrations 150 nM and 300 nM, see Figure 51A. For primer dimer, the intensities decreased with decreasing primer concentration from 600 to 300 nM, while no primer dimer was observed at 150 nM concentration. The same results were obtained when different primer concentrations were tested on samples without DNA but with a weak band observed at 150 nM concentration, see Figure 51B. By comparing the bands at a primer concentration of 150 nM with and without template DNA, we assume that the primers were consumed during the RPA amplification in the presence of template DNA, which led to the complete elimination of primer dimer. In the absence of a DNA template, the chances of primers binding to each other are higher, and thus, the weak band was observed. The results indicated that low primer concentration reduced primer dimer formation.

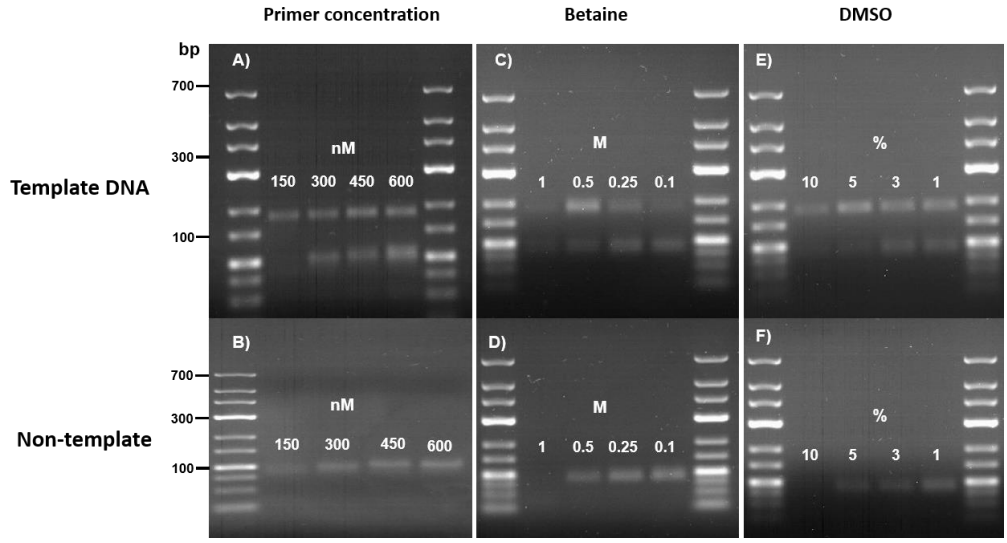

Figure 51. Agarose gel images show the effects of primer concentration optimization, DMSO, and betaine on primer dimer formation. A) The effect of primer concentration optimization on template DNA; B) Non-template DNA. C) The effect of betaine on template DNA; D) Non-template DNA. E) The effect of DMSO on template DNA; F) Non-template DNA.

For betaine results on template DNA, the bands showed inconsistency and low intensities at all concentrations tested; see Figure 51C. For primer dimer formation, the intensities decreased with increasing betaine concentration from 0.1 M to 1 M. In the absence of template DNA, the intensities of primer dimer bands decreased with increasing betaine concentration from 0.1 M to 0.5 M. No band was observed at the highest concentration of 1 M, see Figure 51D. These findings suggest that the betaine has a significant impact on RPA amplification efficiency, as it

reduces the yield of desired product and primer dimer formation even when low concentration is tested.

For DMSO results on template DNA, the bands were observed at all concentrations, while the intensities decreased with increasing DMSO concentration from 1 to 10%. In addition, increasing the concentration of DMSO reduced primer dimer formation at 5% concentration and eliminated it at 10 % concentration, see Figure 51E. DMSO also eliminated the primer dimer formation for non-template samples at the highest concentration of 10%, see Figure 51F. These results indicated that DMSO is efficient in eliminating primer dimer formation at 10% concentration for samples with and without template DNA. However, it reduced the yield of the desired products. To discuss these results, adding betaine and DMSO to RPA reactions completely prevented the primer dimer formation in NTC samples. However, the primer concentration optimization method reduced it with very low intensity but without complete elimination. We also found that all of them reduced product yield and band intensities. Betaine has the highest influence on amplification efficiency, as it reduced and inhibited the reaction even at low concentrations, like the findings of other studies [135,136].

To evaluate their effect on magnetic signals, we performed three RPA amplifications, followed by hybridization and FMMD measurement using our magnetic reader. We have selected the primer concentration at 150 nM for the first RPA amplification. In the second amplification, we added 10% DMSO to the reaction. For the final amplification, we added 1M betaine to the reaction. The selection of these concentrations was based on our previous results where we had the lowest primer dimer formation, see Figure 51. All RPA amplifications were conducted on samples containing *Brucella* gDNA, and on non-template DNA samples. After amplification, the RPA products were mixed with 250 µl of 10× PBS buffer, and then transferred to the PE filter to hybridize with the complementary capture probe P (tail) at 5 µM concentration by gravity flow. Finally, the MNPs incubated 3 minutes for magnetic labeling and then for FMMD measurement.

As shown in Figure 52, the signal amplitude of RPA amplified in the presence of gDNA was high when the primer concentration was tested at 150 nM, while the signal amplitude was slightly lower in the absence of gDNA. For DMSO-RPA products, the signal amplitude was markedly higher in the presence of gDNA compared to NTC samples. Betaine-RPA products also exhibited higher signal amplitude compared to NTC samples. Noticeably, a reduction in signal amplitude for target DNA was obtained in all optimization methods, compared to signal

amplitude shown in Figure 50. The reduction was about 23.57% for the primer optimization method, 23.07 % for DMSO, and 45.06% for betaine. This can be explained by their impact on the amplification yield in which the band intensities of the desired products decreased at those concentrations, see Figure 51. For NTC samples, lowering the primer concentration to 150 nM was inefficient in eliminating the primer dimer formation, as the signal amplitude was not significantly reduced. However, adding 10% DMSO and 1 M betaine eliminated the primer dimer formation, and the signal amplitude was very low in both, with 92.07% and 93.30% reduction percentages, respectively.

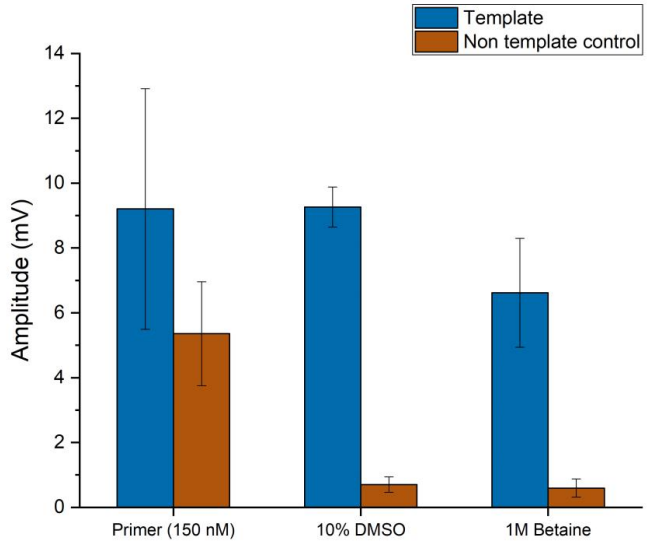

Figure 52. The effect of methods used for reducing primer dimers on signal amplitude. Error bars represent the standard deviation of two independent measurements.

Based on these results, the signal-to-background ratio resulting from the addition of 10% DMSO or 1M betaine to the RPA reaction is higher than that obtained using the primer concentration method. The reduction of primer formation and signal amplitude for NTC samples was similar in DMSO and betaine. However, the signal amplitude obtained from DMSO-RPA products was higher than that of betaine. Thus, we have selected DMSO-RPA for further optimization experiments.

6.5. Reaction conditions optimization of tailed-RPA amplification

After the elimination of the primer dimer, we optimized the reaction factors that influence the RPA amplification performance and magnetic sensing. We optimized reaction temperature, Magnesium Acetate (MgOAc) concentration, and incubation time to achieve optimal efficiency for our assay.

Optimizing the RPA reaction temperature is important for achieving consistent amplification and optimal enzyme activity. The recommended RPA reaction temperature for recombinase and polymerase enzymes to exhibit optimal activity is between 37°C and 42°C. However, numerous studies investigated temperatures outside this range, and they found that the minimum temperature necessary to yield a reliable positive result is above 30°C [110,137,138]. Interestingly, other studies demonstrated that RPA amplification can still produce detectable signals even at low temperatures such as 25°C [47,48]. Therefore, we investigated the effect of reaction incubation temperature on our RPA amplification to select the optimal temperature for our assay. The tubes were incubated for RPA amplification at 21, 30, 37, and 42°C reaction temperatures for 30 minutes. NTC samples at 37°C were used as a negative control. After amplification, all tubes were added to PE filters for hybridization reaction and magnetic measurement. Figure 53 shows the effect of amplification temperature on signal amplitude. The signal amplitude obtained from the target DNA was higher than the signal amplitude of NTC at all incubation temperatures. This indicates that RPA products can be detected even at low incubation temperatures such as 21 and 30°C. However, the signal amplitude at 37°C was the highest among all incubation temperatures. Thus, it was selected as an optimal incubation temperature for our assay.

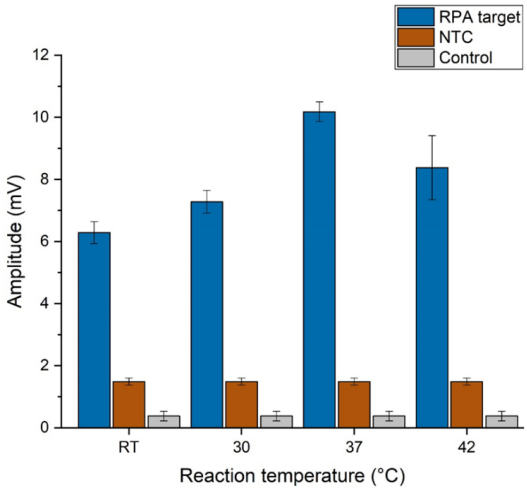

Figure 53. Effect of RPA incubation temperature on signal amplitudes. Error bars represent the standard deviation of two independent measurements.

MgOAc reagent is another important factor that has an influence on the sensitivity and specificity of RPA amplification. MgOAc is a cofactor for UvsX recombinase and Bacillus subtilis Pol I (Bsu) polymerase enzymes [139]. Magnesium ions (Mg^{2+}) enhance enzyme performance by stabilizing enzyme-DNA complexes and facilitating catalytic activity during amplification. The manufacturer (TwistDx) recommends a final concentration of 14 mM MgOAc for optimal RPA amplification. However, the studies have demonstrated that increasing the concentration of MgOAc above 14 mM enhances the yield of RPA products and thus enhances the overall sensitivity of the assay [140,141]. Therefore, we optimized our RPA amplification by testing MgOAc at 6 mM, 14 mM, 24 mM, and 36 mM concentrations. For each concentration, *Brucella* gDNA and NTC samples were tested. All RPA amplifications were incubated at 37°C for 30 minutes. After amplification, all tubes were added to PE filters for hybridization reaction and magnetic measurement. As shown in Figure 54A, the signal amplitudes of *Brucella* gDNA samples increased with higher MgOAc concentrations. Noticeably, the NTC samples exhibited higher signal amplitude at concentrations of 24 mM and 36 mM than at 6 mM and 14 mM. This indicates that increasing the concentration of MgOAc enhanced the polymerase activity. However, this enhancement might lead to an increased activity of (Bsu) DNA polymerase on the primer dimer. Another explanation is that when we increased the concentration of MgOAc, which contained Mg^{2+}, the ionic strength of the reaction mixture increased, and thus, the nonspecific interaction between primers increased,

which led to a more stable primer dimer formation. Similarly, other studies have reported that increasing the concentration of MgOAc produced nonspecific amplification products, which resulted in poor resolution for distinguishing between target DNA signals and background signals [142,143]. From this result, the signal-to-background ratio was the highest at 14 mM MgOAc concentration, and thus, we decided to keep it as a suitable concentration for our assay.

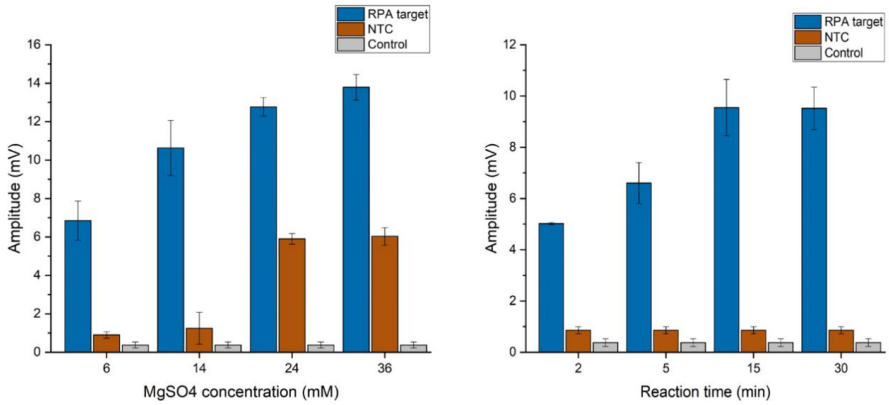

Figure 54. A) Effect of MgOAc concentration. B) Effect of reaction time on signal amplitude. Error bars represent the standard deviation of three independent measurements.

To determine the optimal RPA incubation time that produces the highest RPA product yield and magnetic signals, we performed RPA amplifications at different incubation times. The reaction tubes were incubated for RPA amplification at 2, 5, 15, 30 minutes at 37°C. After amplification, all tubes were transferred to PE filters for hybridization reaction and magnetic detection. As shown in Figure 54B, the signal amplitude increased gradually with increasing incubation time from 2 to 15 minutes. However, longer incubation time such as 30 minutes showed similar signal amplitude as at 15 minutes, indicating that increasing incubation time to more than 15 minutes does not enhance the amplification efficiency. Although the incubation times of 2 and 5 minutes were enough to produce detectable magnetic signals, 15 minutes showed the highest signal amplitude, and was thus selected as an optimal time for our assay.

6.6. Limit of detection and specificity

The limit of detection of our RPA-FMMD assay was determined under the previously optimized condition using a serial dilution ranging from 5 to 5 × 10^6 copies of the *Brucella* gDNA. The RPA amplification was conducted in a total volume of 50 µL. To prepare the

reaction mixture, we mixed 20 µL of 2× reaction buffer, 9.2 µL of dNTPs, 5 µL of 10× basic E-mix, 5 µl of DMSO and 2.4 µL of each primer. Then, 2.5 µL of 20× core reaction was added to the tube lid and mixed. Finally, the RPA amplification was initiated by adding 2.5 µL of magnesium acetate (MgOAc) and 1 µL of each prepared genomic DNA. The reaction tubes were incubated at 37°C for 15 minutes. After the amplification, the reaction tubes were added to PE filters containing the complementary capture probe P (tail) at a concentration of 5 µM for hybridization through the tail primer, using gravity flow at a rate of approximately 200 µL/min. Following hybridization, the PE filters were washed with 1× PBS to remove non hybridized RPA products. For magnetic detection, the PE filters were incubated with MNPs for 3 minutes to enable binding to the biotinylated RPA products. Finally, the PE filters were placed into the measurement head of our portable magnetic reader to measure the signal amplitudes. As shown in Figure 55, all concentrations ranging from 5×10^3 to 5×10^6 were detected by our RPA-FMMD assay. However, concentrations below 5×10^6 have shown very low signal amplitudes, similar to non-template controls. Based on the result, 5×10^3 copy numbers which correspond to approximately (9 fM) was determined as the limit of detection of our assay.

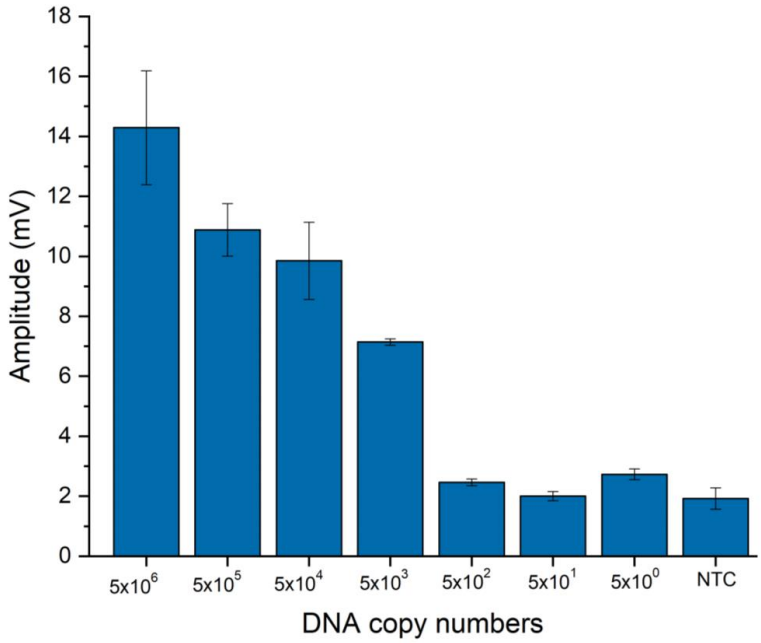

Figure 55. The signal amplitudes for different copy numbers of RPA-amplified *Brucella* DNA. Error bars represent the standard deviation of three independent measurements.

Evaluating the specificity of the RPA-FMMD assay in the presence of genomic DNA from different bacterial species is important to ensure accurate *Brucella* detection without cross-reactivity. Therefore, our RPA-FMMD assay specificity was further assessed by testing its performance against genomic DNA extracted from various pathogenic species, including *Campylobacter fetus subsp. venerealis (Cfv)*, *Campylobacter fetus subsp. fetus (Cff)*, the *Ovax Chlamydia vaccine strain*, *Escherichia coli (APEC)*, and *Salmonella enteritidis*. The amplification and magnetic detection were conducted under the optimized conditions established in the previous section. As shown in Figure 56, the signal amplitude was high only for the *Brucella* gDNA target, while all non-target bacterial genomes showed a very low signal amplitude. This low signal amplitude obtained from all bacterial species confirms that the RPA-FMMD assay is specific and accurately identifies *Brucella* in the presence of potentially interfering bacterial species.

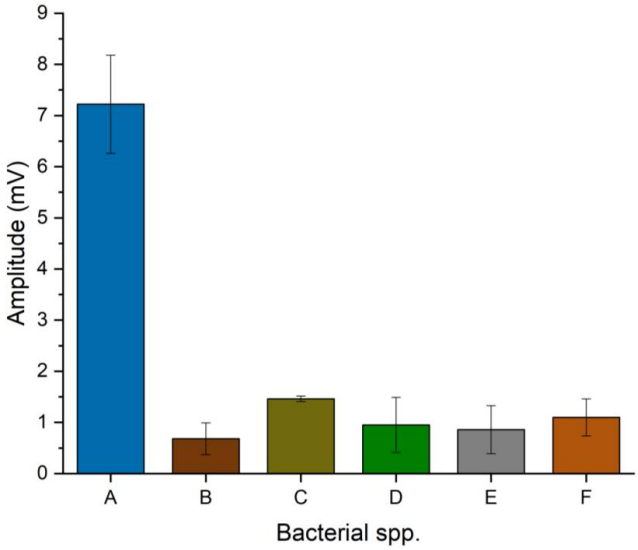

Figure 56. The signal amplitudes for *Brucella melitensis* and non-related bacterial genomic DNA amplified by RPA. (A) *Brucella melitensis* at 2 ng/µL, (B) *Ovax Chlamydia* at 5 ng/µL, (C) *Campylobacter fetus subsp. venerealis* (Cfv) at 27 ng/µL, (D) *Campylobacter fetus subsp. fetus* (Cff) at 55 ng/µL, (E) *Escherichia coli* (APEC) at 83 ng/µL, (F) *Salmonella enteritidis* at 84 ng/µL. Error bars represent the standard deviation of three independent measurements.

6.7. Performance comparison to existing methods

We created a table to compare our magnetic biosensor performance with the existing diagnostic methods used to detect *Brucella* pathogen. It includes conventional methods and new advanced techniques. We covered the key parameters such as assay time, safety, stage of infection, cost, sensitivity and specificity, see Table 9.

Table 9. Comparison of the properties of our magnetic biosensor with those of existing methods

Method	**Target Element**	**Assay Time**	**Safety**	**Stage of Infection**	**Cost**	**Sensitivity/LOD**	**Specificity**	**Ref.**
Blood culture	Living bacteria	Days to weeks	Low	Early to Acute	Moderate to High	10–90%	100%	[23,35,144]
Rose bengal	Antibodies	Minutes	Moderate	Acute to Chronic	Low	75–100%	39–100%	[4,5,145–147]
Standard agglutination	Antibodies	Hours to days	Moderate	Acute to Chronic	Low to Moderate	75–96%	44–99%	[148–151]
ELISA	Antibodies	Hours	Moderate	Acute to Chronic	Moderate to High	98.7%	98.4%	[152]
Quantum dot	Antibodies	2 h	Moderate	Acute to Chronic	High	96.15%	94.12%	[153]
Colorimetric	Antibodies	Hour	Moderate	Acute to Chronic	Moderate	98.33%	100%	[154]
PCR	DNA	Hours	High	Early to Chronic	Moderate to High	93-100%	98–100%	[35,155,156]
Colorimetric	DNA	2 h	High	Early to chronic	Low to Moderate	3.32 pg/mL	100%	[157,158]
Electrochemical	DNA	1 h	High	Early to Chronic	Moderate	2.7×10^{-20} mol dm^{-3}	100%	[159]
FMMD-PCR	DNA	* Less than 1 h	High	Early to Chronic	Low to Moderate	0.09 fM	100%	This study
FMMD_RPA	DNA	25 minutes	High	Early to Chronic	Low to Moderate	9 fM	100%	This study

Chapter 7

7. RPA Amplification in Temperature-Controlled Measurement Head

To improve the FMMD technique in terms of field nucleic acid testing, the integration of RPA amplification is vital advancement as it increases the mobile capabilities and functionalities of the portable magnetic reader without the need for any sample-preprocessing infrastructure. The magnetic reader sensor unit, referred to as Measurement Head (MH), consists of a nested configuration of coils that generates low and high frequency excitation signals, LF and HF excitation, respectively, and picks up the sample's magnetic response signal. The thermal energy in the MH is mainly produced by the resistive heat of the low frequency excitation coil, which is essential for FMMD signal acquisition. The peak current through the LF-coil is 240 mA, yielding a power dissipation of approximately 2.4 W, whereas the HF-coil current of 20 mA led to just 7 mW of heating power, 350-fold lower than the LF power. Thus, the LF excitation chain generates enough heat to be used as a temperature control input, and the HF power is negligible. We hypothesize that this thermal energy can be utilized to drive various biological assays, or isothermal amplification sample-pretreatment in the field, if controlled properly. Combining isothermal amplification with FMMD allows sensitive and selective magnetic detection and quantification of DNA in a single device without the need of additional instrumentation for the amplification process.

To investigate the practicability of this endeavor, we apply a simple pulse width modulation (PWM) control approach to regulate the temperature of the measurement head and to maintain it constant at a desired pre-set temperature. We utilize temperature feedback from the LF-coil surface, switch the LF coil current on and off by means of duty cycle control, and perform RPA inside the MH, directly at its sample position, and assess the basic performance from the controller perspective and from the perspective of its utilization for RPA.

The chapter is partly based on the original joint publication by the author and Max P. Jessing [160].

7.1. Controller performance

To test the feasibility of RPA amplification in the measurement head, it was necessary to examine the reliability of the temperature controller in a controlled test (lab) setting. While performing any NA amplification before as well as during FMMD signal acquisition, the sample to be amplified or measured is inside the sample bore of the MH. However, due to geometrical restrictions, sample and temperature sensors cannot be installed simultaneously at the current stage. Therefore, the temperature sensor used for feedback control was positioned on the surface of the LF-coil in the MH, a small distance from the center of the sample position. To help visualize this, a schematic of the measurement head, the temperature sensor and sample position, and the principle of the power to temperature conversion can be seen in Figure 57.

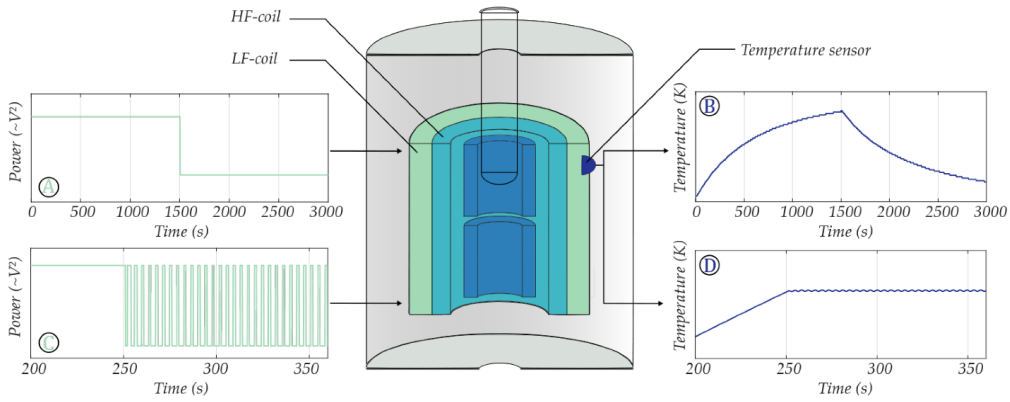

Figure 57. Schematic of the measurement head cross section, including the temperature sensor position. A) Uncontrolled low frequency power input step. B) Uncontrolled Temperature output corresponding to the input depicted in A. C) pulse width modulated low frequency power input. D) Adjustable temperature output corresponding to the PWM input depicted in C.[160]

Due to the distinct control and amplification positions, it is important to not only characterize the controller and controllable temperature ranges at the position of the feedback sensor, but also to test the temperature at the sample position that is not directly controlled. The feedback sensor behavior was characterized for 10 different feedback temperature settings (30, 37, 38, 39, 40, 41, 45, 48, 50, 53°C) set in ascending (heating) and descending (cooling) order between

room temperature and 53°C (Figure 58A, solid lines). The corresponding temperatures at sample position were recorded with an epoxy-passivated temperature sensor in DI-water simultaneously (Figure 58A, dashed lines).

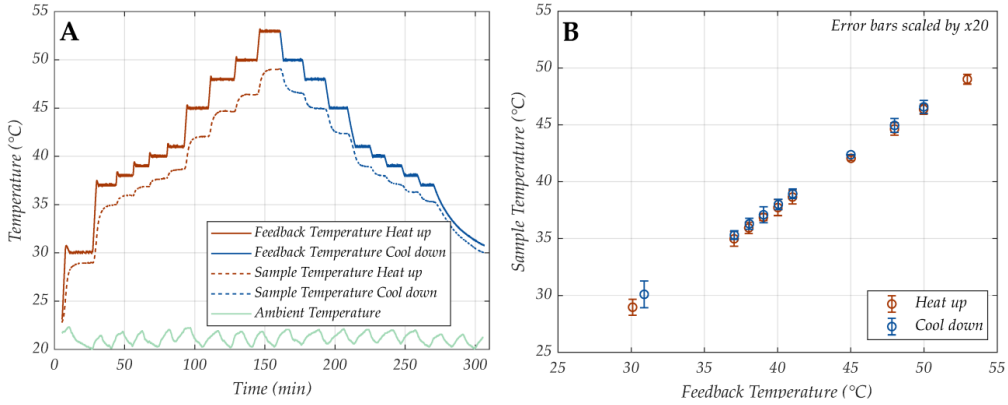

Figure 58. Linear dependency of controller temperature vs. sample position temperature. The standard deviation bars in are scaled by 20× and indicate the stability of the temperature control at sample position.[160]

To determine the sample position temperature for any feedback controller setting, first a "calibration" was performed. The temperature relation at the region of interest (sample position) was plotted against the temperature at the more accessible LF-surface location, which is suited for controlling (Figure 57B). This way, a linear relationship of T_s (sample temp.) and T_f (feedback temp.) could be ensured to select the necessary amplification temperatures at the sample position easily.

7.2. RPA amplification

As proof of concept, we conducted RPA amplification using the positive control template and oligo mix primers provided in the TwistAmp® Liquid Basic kit, which is expected to produce an amplicon of 289 bp. In our study, we tested the RPA amplification across a range of temperatures, including 21°C, 30°C, 37°C, 38°C, 45°C, and 50°C. This range of temperatures was chosen to investigate the amplification efficiency both within and outside the optimal operating temperature range of RPA. This way, we could assess how the variation of temperature, when being controlled by PWM, affects the performance of RPA amplification

from a biological perspective. The RPA amplification was performed both inside our temperature-controlled measurement head and in a water bath as a reference method. The temperature ranged from 30°C to 50°C, and the incubation time was 30 minutes.

Figure 60 shows the gel image of the RPA products amplified inside our measurement head and in a water bath, controlled to different temperatures. From the gel image, we confirm the successful RPA positive control amplification, as the expected amplicons with the size of 289 bp were observed at 37°C and 38°C in both our measurement head and water bath. When the amplification was tested outside the operating temperature of RPA, such as at low temperatures (21°C and 30°C) and at high temperatures (45°C and 50°C), no bands were observed. This can be explained by the decreased activity of the enzymes at lower temperatures and enzyme denaturation at higher temperatures, which result in inefficient amplification and therefore in absence of bands on the agarose gel. From this result, we conclude that our implementation of a PWM controller regulated and controlled the temperature of the measurement head sufficiently, as the bands were observed at optimal temperature range of RPA (37°C and 38°C), while no bands were observed at low and high temperatures.

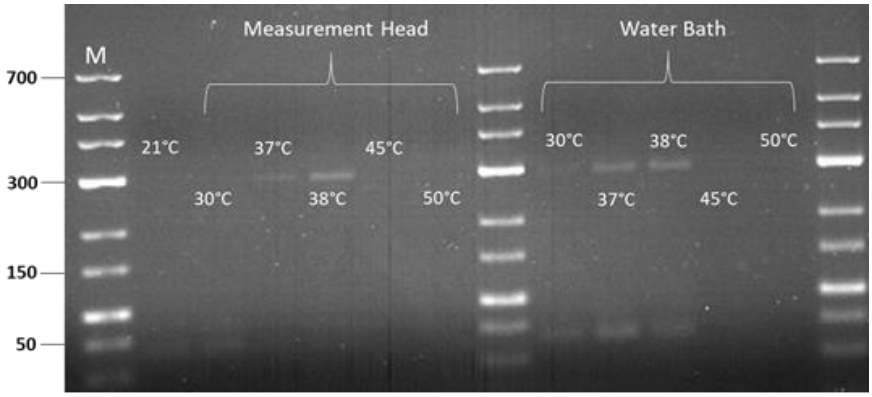

Figure 59. Gel image of RPA amplification inside measurement head and water bath at different incubation temperatures. M: Marker.[160]

To validate the temperature stability at the sample position in terms of the amplification performance, we performed RPA at different incubation times ranging from 10 to 30 minutes. Similar to previous investigations, the amplification was performed inside our measurement head and in a water bath at 38°C. After the amplification, the amplified products were purified and loaded into the gel for 1 hour. As shown in Figure 61, the band intensities for the RPA products amplified inside the measurement head and in the water bath were similar at all

incubation times. This confirms that the stability of the temperature controlled by PWM inside the measurement head and the water bath control performance are similar in terms of their potential for successful RPA.

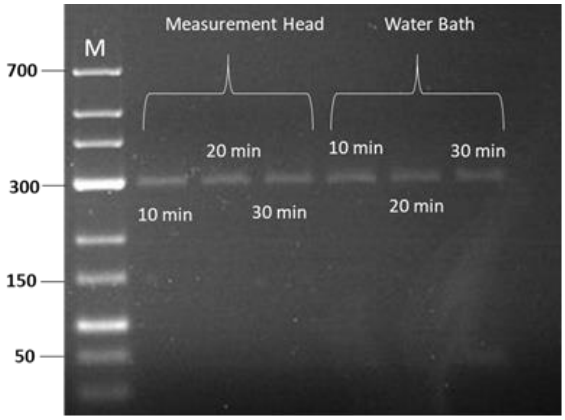

Figure 60. Gel image of RPA amplification inside measurement head and water bath at different incubation times. M: Marker.[160]

After the demonstration of the amplification inside our temperature-controlled MH using the positive control template and oligo mix primers, we performed another RPA amplification using authentic *Brucella* gDNA and our designed primers (F3/R6) at 600 nM concentration. The RPA amplification was tested at the optimal range of RPA amplification temperatures, including 37, 38, 39, and 40°C for 30 minutes. As shown in Figure 62, all RPA products were observed at all temperatures tested with high intensities. This validates that our setup can efficiently run RPA amplification at the optimal range of temperatures for actual assays.

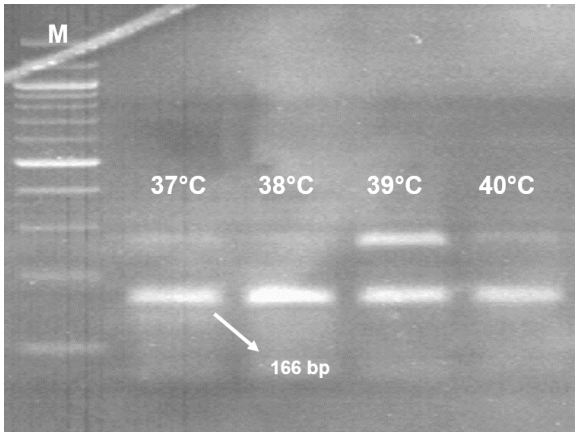

Figure 61. Gel image of RPA amplification inside measurement head at different incubation temperatures. M: Mark.

Chapter 8

8. Conclusions and future directions

In conclusion, we developed a new magnetic nanoparticle-based biosensor for detection and quantification of *Brucella* DNA by utilizing the unique non-linear and non-hysteretic magnetization characteristics of superparamagnetic NPs through frequency mixing magnetic detection technology. The use of superparamagnetic NPs as sensing elements allows the precise quantification of DNA hybridization events on a functionalized polyethylene filter. We successfully achieved a rapid detection time of less than 10 minutes and sensitive detection of *Brucella* DNA. The proposed magnetic biosensor, optimized and tested on synthetic and amplified gDNA, exhibited a high selectivity, robustness, and reproducibility, allowing for the reliable detection of *Brucella* DNA. A detection range from 19 nM to 1650 nM was found. When tested with products amplified from *Brucella* genomic DNA, the detection limit was as low as 55 copies.

The developed MNP biosensor has been enhanced in terms of portability and usability for PoC testing of *Brucella* DNA. The enhancement comes from the effective integration of the RPA amplification method with FMMD using the small-handled magnetic reader. The RPA-FMMD assay combines the unique properties of superparamagnetic NPs with the fast DNA amplification of RPA. The RPA-FMMD assay demonstrated a limit of detection of 9 fM with high specific detection of *Brucella* genomic DNA. The total assay time is less than 25 minutes, making it fast and suitable for field testing.

The feasibility of performing recombinase polymerase amplification in the measurement head of the magnetic reader device prior to FMMD signal acquisition at continuously constant ambient conditions was presented using a PWM approach with the inherently generated heat from the LF excitation coil of the system. This simple implementation has proven to be a valuable addition to the mobile functionality of the FMMD device for the RPA-based sample

preparation. For such an improvement, we could perform RPA amplification and magnetic sensing in our magnetic reader without additional devices.

The developed assay is a promising PoC method with several interesting features for DNA detection. The assay can be easily applied to detect any type of microbial pathogen and is not limited to *Brucella*. In addition, the inexpensive portable readout unit, the affordable magnetic nanoparticles, and the disposable polyethylene filters make it an attractive solution to perform large-scale field screening and ensure the accessibility of the technology to low-/middle-income countries. Moreover, the assay can be integrated with several isothermal amplification methods to enhance its practicality in the field.

Future work should focus on selecting a suitable PoC DNA extraction method that can be performed without using lab equipment. One of the methods could be using magnetic bead DNA extraction that allows for rapid purification of DNA in a highly efficient and specific manner. Another method is using magnetic ionic liquids (MIL), which are solvents with magnetic properties that bind to gDNA, and can be separated by an external magnet. Another improvement could be done by performing solid phase RPA amplification either on PE filter or on the shell of MNPs. By performing such an amplification particularly inside the temperature-controlled measurement head, it will improve the robustness and reliability and thus its possible contribution to global health care.

References

1. Refai, M. Incidence and Control of Brucellosis in the Near East Region. *Veterinary Microbiology* **2002**, *90*, 81–110, doi:10.1016/S0378-1135(02)00248-1.
2. Dadar, M.; Shahali, Y.; Whatmore, A.M. Human Brucellosis Caused by Raw Dairy Products: A Review on the Occurrence, Major Risk Factors and Prevention. *International Journal of Food Microbiology* **2019**, *292*, 39–47, doi:10.1016/j.ijfoodmicro.2018.12.009.
3. Aljanazreh, B.; Alzatari, K.; Tamimi, A.; Alsaafeen, M.H.; Hassouneh, W.; Ashhab, Y. Brucellosis Re-Emergence after a Decade of Quiescence in Palestine, 2015–2017: A Seroprevalence and Molecular Characterization Study. *Transboundary and Emerging Diseases* **2022**, *69*, e130–e140, doi:10.1111/tbed.14270.
4. Ruiz-Mesa, J.D.; Sánchez-Gonzalez, J.; Reguera, J.M.; Martín, L.; Lopez-Palmero, S.; Colmenero, J.D. Rose Bengal Test: Diagnostic Yield and Use for the Rapid Diagnosis of Human Brucellosis in Emergency Departments in Endemic Areas. *Clinical Microbiology and Infection* **2005**, *11*, 221–225, doi:10.1111/j.1469-0691.2004.01063.x.
5. Zakaria, A.M. Comparative Assessment of Sensitivity and Specificity of Rose Bengal Test and Modified In-House ELISA by Using IS711 Taqman Real Time PCR Assay as a Gold Standard for the Diagnosis of Bovine Brucellosis. *Biomedical and Pharmacology Journal* **2018**, *11*, 951–957.
6. Mainar-Jaime, R.C.; Muñoz, P.M.; de Miguel, M.J.; Grilló, M.J.; Marín, C.M.; Moriyón, I.; Blasco, J.M. Specificity Dependence between Serological Tests for Diagnosing Bovine Brucellosis in Brucella-Free Farms Showing False Positive Serological Reactions Due to Yersinia Enterocolitica O:9. *Can Vet J* **2005**, *46*, 913–916.
7. Hasanjani Roushan, M.R.; Marashi, S.M.A.; Moulana, Z. Polymerase Chain Reaction–Based Assays for the Diagnosis of Active and Relapsed Cases of Human Brucellosis. *Am J Trop Med Hyg* **2016**, *95*, 1272–1276, doi:10.4269/ajtmh.16-0344.
8. Yu, W.L.; Nielsen, K. Review of Detection of Brucella Sp. by Polymerase Chain Reaction. *Croat Med J* **2010**, *51*, 306–313, doi:10.3325/cmj.2010.51.306.
9. Navarro, E.; Escribano, J.; Fernández, J.A.; Solera, J. Comparison of Three Different PCR Methods for Detection of Brucella Spp. in Human Blood Samples. *FEMS Immunology & Medical Microbiology* **2002**, *34*, 147–151, doi:10.1111/j.1574-695X.2002.tb00616.x.
10. Syedmoradi, L.; Daneshpour, M.; Alvandipour, M.; Gomez, F.A.; Hajghassem, H.; Omidfar, K. Point of Care Testing: The Impact of Nanotechnology. *Biosensors and Bioelectronics* **2017**, *87*, 373–387, doi:10.1016/j.bios.2016.08.084.
11. Tang, C.; He, Z.; Liu, H.; Xu, Y.; Huang, H.; Yang, G.; Xiao, Z.; Li, S.; Liu, H.; Deng, Y.; et al. Application of Magnetic Nanoparticles in Nucleic Acid Detection. *Journal of Nanobiotechnology* **2020**, *18*, 62, doi:10.1186/s12951-020-00613-6.
12. Yari, P.; Rezaei, B.; Dey, C.; Chugh, V.K.; Veerla, N.V.R.K.; Wang, J.-P.; Wu, K. Magnetic Particle Spectroscopy for Point-of-Care: A Review on Recent Advances. *Sensors* **2023**, *23*, 4411, doi:10.3390/s23094411.
13. Krause, H.-J.; Wolters, N.; Zhang, Y.; Offenhäusser, A.; Miethe, P.; Meyer, M.H.F.; Hartmann, M.; Keusgen, M. Magnetic Particle Detection by Frequency Mixing for Immunoassay Applications. *Journal of Magnetism and Magnetic Materials* **2007**, *311*, 436–444, doi:10.1016/j.jmmm.2006.10.1164.

14. Cleaveland, S.; Laurenson, M.K.; Taylor, L.H. Diseases of Humans and Their Domestic Mammals: Pathogen Characteristics, Host Range and the Risk of Emergence. *Philosophical Transactions of the Royal Society of London. Series B: Biological Sciences* **2001**, doi:10.1098/rstb.2001.0889.

15. Rahman, M.T.; Sobur, M.A.; Islam, M.S.; Ievy, S.; Hossain, M.J.; El Zowalaty, M.E.; Rahman, A.T.; Ashour, H.M. Zoonotic Diseases: Etiology, Impact, and Control. *Microorganisms* **2020**, *8*, 1405, doi:10.3390/microorganisms8091405.

16. Debnath, F.; Chakraborty, D.; Deb, A.K.; Saha, M.K.; Dutta, S. Increased Human-Animal Interface & Emerging Zoonotic Diseases: An Enigma Requiring Multi-Sectoral Efforts to Address. *Indian J Med Res* **2021**, *153*, 577–584, doi:10.4103/ijmr.IJMR_2971_20.

17. Tomley, F.M.; Shirley, M.W. Livestock Infectious Diseases and Zoonoses. *Philosophical Transactions of the Royal Society B: Biological Sciences* **2009**, *364*, 2637–2642, doi:10.1098/rstb.2009.0133.

18. COVID-19 Deaths | WHO COVID-19 Dashboard Available online: https://data.who.int/dashboards/covid19/cases (accessed on 9 July 2024).

19. Slingenbergh, J.; Gilbert, M.; Balogh De, K.; Wint, W. Ecological Sources of Zoonotic Diseases: -EN- -FR- -ES-. *Rev. Sci. Tech. OIE* **2004**, *23*, 467–484, doi:10.20506/rst.23.2.1492.

20. Rohr, J.R.; Barrett, C.B.; Civitello, D.J.; Craft, M.E.; Delius, B.; DeLeo, G.A.; Hudson, P.J.; Jouanard, N.; Nguyen, K.H.; Ostfeld, R.S.; et al. Emerging Human Infectious Diseases and the Links to Global Food Production. *Nat Sustain* **2019**, *2*, 445–456, doi:10.1038/s41893-019-0293-3.

21. Esposito, M.M.; Turku, S.; Lehrfield, L.; Shoman, A. The Impact of Human Activities on Zoonotic Infection Transmissions. *Animals* **2023**, *13*, 1646, doi:10.3390/ani13101646.

22. Shaheen, M.N.F. The Concept of One Health Applied to the Problem of Zoonotic Diseases. *Reviews in Medical Virology* **2022**, *32*, e2326, doi:10.1002/rmv.2326.

23. Franco, M.P.; Mulder, M.; Gilman, R.H.; Smits, H.L. Human Brucellosis. *The Lancet Infectious Diseases* **2007**, *7*, 775–786, doi:10.1016/S1473-3099(07)70286-4.

24. Laine, C.G.; Johnson, V.E.; Scott, H.M.; Arenas-Gamboa, A.M. Global Estimate of Human Brucellosis Incidence - Volume 29, Number 9—September 2023 - Emerging Infectious Diseases Journal - CDC., doi:10.3201/eid2909.230052.

25. Khurana, S.K.; Sehrawat, A.; Tiwari, R.; Prasad, M.; Gulati, B.; Shabbir, M.Z.; Chhabra, R.; Karthik, K.; Patel, S.K.; Pathak, M.; et al. Bovine Brucellosis – a Comprehensive Review. *Veterinary Quarterly* **2021**, *41*, 61–88, doi:10.1080/01652176.2020.1868616.

26. Jamil, T.; Khan, A.U.; Saqib, M.; Hussain, M.H.; Melzer, F.; Rehman, A.; Shabbir, M.Z.; Khan, M.A.; Ali, S.; Shahzad, A.; et al. Animal and Human Brucellosis in Pakistan. *Front. Public Health* **2021**, *9*, doi:10.3389/fpubh.2021.660508.

27. Liu, Z.; Gao, L.; Wang, M.; Yuan, M.; Li, Z. Long Ignored but Making a Comeback: A Worldwide Epidemiological Evolution of Human Brucellosis. *Emerging Microbes & Infections* **2024**, *13*, 2290839, doi:10.1080/22221751.2023.2290839.

28. Georgi, E.; Walter, M.C.; Pfalzgraf, M.-T.; Northoff, B.H.; Holdt, L.M.; Scholz, H.C.; Zoeller, L.; Zange, S.; Antwerpen, M.H. Whole Genome Sequencing of Brucella Melitensis Isolated from 57 Patients in Germany Reveals High Diversity in Strains from Middle East. *PLoS One* **2017**, *12*, e0175425, doi:10.1371/journal.pone.0175425.

29. Cross, A.R.; Baldwin, V.M.; Roy, S.; Essex-Lopresti, A.E.; Prior, J.L.; Harmer, N.J. Zoonoses under Our Noses. *Microbes and Infection* **2019**, *21*, 10–19, doi:10.1016/j.micinf.2018.06.001.

30. Mailles, A.; Garin-Bastuji, B.; Lavigne, J.P.; Jay, M.; Sotto, A.; Maurin, M.; Pelloux, I.; O'Callaghan, D.; Mick, V.; Vaillant, V.; et al. Human Brucellosis in France in the 21st Century:

Results from National Surveillance 2004–2013. *Médecine et Maladies Infectieuses* **2016**, *46*, 411–418, doi:10.1016/j.medmal.2016.08.007.

31. Moreno, E.; Blasco, J.-M.; Moriyón, I. Facing the Human and Animal Brucellosis Conundrums: The Forgotten Lessons. *Microorganisms* **2022**, *10*, 942, doi:10.3390/microorganisms10050942.
32. Di Bonaventura, G.; Angeletti, S.; Ianni, A.; Petitti, T.; Gherardi, G. Microbiological Laboratory Diagnosis of Human Brucellosis: An Overview. *Pathogens* **2021**, *10*, 1623, doi:10.3390/pathogens10121623.
33. Pfukenyi, D.M.; Meletis, E.; Modise, B.; Ndengu, M.; Kadzviti, F.W.; Dipuo, K.; Moesi, K.; Kostoulas, P.; Matope, G. Evaluation of the Sensitivity and Specificity of the Lateral Flow Assay, Rose Bengal Test and the Complement Fixation Test for the Diagnosis of Brucellosis in Cattle Using Bayesian Latent Class Analysis. *Preventive Veterinary Medicine* **2020**, *181*, 105075, doi:10.1016/j.prevetmed.2020.105075.
34. Sanjuan-Jimenez, R.; Colmenero, J.D.; Morata, P. Lessons Learned with Molecular Methods Targeting the BCSP-31 Membrane Protein for Diagnosis of Human Brucellosis. *Clinica Chimica Acta* **2017**, *469*, 1–9, doi:10.1016/j.cca.2017.03.014.
35. Yagupsky, P.; Morata, P.; Colmenero, J.D. Laboratory Diagnosis of Human Brucellosis. *Clin Microbiol Rev* **2019**, *33*, e00073-19, doi:10.1128/CMR.00073-19.
36. García-Bernalt Diego, J.; Fernández-Soto, P.; Muro, A. The Future of Point-of-Care Nucleic Acid Amplification Diagnostics after COVID-19: Time to Walk the Walk. *International Journal of Molecular Sciences* **2022**, *23*, 14110, doi:10.3390/ijms232214110.
37. De Felice, M.; De Falco, M.; Zappi, D.; Antonacci, A.; Scognamiglio, V. Isothermal Amplification-Assisted Diagnostics for COVID-19. *Biosensors and Bioelectronics* **2022**, *205*, 114101, doi:10.1016/j.bios.2022.114101.
38. Srivastava, P.; Prasad, D. Isothermal Nucleic Acid Amplification and Its Uses in Modern Diagnostic Technologies. *3 Biotech* **2023**, *13*, 200, doi:10.1007/s13205-023-03628-6.
39. Zhao, Y.; Chen, F.; Li, Q.; Wang, L.; Fan, C. Isothermal Amplification of Nucleic Acids. *Chem. Rev.* **2015**, *115*, 12491–12545, doi:10.1021/acs.chemrev.5b00428.
40. Oliveira, B.B.; Veigas, B.; Baptista, P.V. Isothermal Amplification of Nucleic Acids: The Race for the Next "Gold Standard." *Frontiers in Sensors* **2021**, *2*.
41. Notomi, T.; Mori, Y.; Tomita, N.; Kanda, H. Loop-Mediated Isothermal Amplification (LAMP): Principle, Features, and Future Prospects. *J Microbiol.* **2015**, *53*, 1–5, doi:10.1007/s12275-015-4656-9.
42. Zhang, K.; Zhang, H.; Cao, H.; Jiang, Y.; Mao, K.; Yang, Z. Rolling Circle Amplification as an Efficient Analytical Tool for Rapid Detection of Contaminants in Aqueous Environments. *Biosensors* **2021**, *11*, 352, doi:10.3390/bios11100352.
43. Piepenburg, O.; Williams, C.H.; Stemple, D.L.; Armes, N.A. DNA Detection Using Recombination Proteins. *PLOS Biology* **2006**, *4*, e204, doi:10.1371/journal.pbio.0040204.
44. James, A.; Macdonald, J. Recombinase Polymerase Amplification: Emergence as a Critical Molecular Technology for Rapid, Low-Resource Diagnostics. *Expert Review of Molecular Diagnostics* **2015**, *15*, 1475–1489, doi:10.1586/14737159.2015.1090877.
45. Lobato, I.M.; O'Sullivan, C.K. Recombinase Polymerase Amplification: Basics, Applications and Recent Advances. *Trends Analyt Chem* **2018**, *98*, 19–35, doi:10.1016/j.trac.2017.10.015.
46. Mukama, O.; Nie, C.; Habimana, J.D.D.; Meng, X.; Ting, Y.; Songwe, F.; Al Farga, A.; Mugisha, S.; Rwibasira, P.; Zhang, Y.; et al. Synergetic Performance of Isothermal Amplification Techniques and Lateral Flow Approach for Nucleic Acid Diagnostics. *Analytical Biochemistry* **2020**, *600*, 113762, doi:10.1016/j.ab.2020.113762.

47. Sun, K.; Xing, W.; Yu, X.; Fu, W.; Wang, Y.; Zou, M.; Luo, Z.; Xu, D. Recombinase Polymerase Amplification Combined with a Lateral Flow Dipstick for Rapid and Visual Detection of Schistosoma Japonicum. *Parasites & Vectors* **2016**, *9*, 476, doi:10.1186/s13071-016-1745-5.

48. Ma, Q.; Liu, H.; Ye, F.; Xiang, G.; Shan, W.; Xing, W. Rapid and Visual Detection of *Mycobacterium Tuberculosis* Complex Using Recombinase Polymerase Amplification Combined with Lateral Flow Strips. *Molecular and Cellular Probes* **2017**, *36*, 43–49, doi:10.1016/j.mcp.2017.08.004.

49. Wahed, A.A.E.; Patel, P.; Faye, O.; Thaloengsok, S.; Heidenreich, D.; Matangkasombut, P.; Manopwisedjaroen, K.; Sakuntabhai, A.; Sall, A.A.; Hufert, F.T.; et al. Recombinase Polymerase Amplification Assay for Rapid Diagnostics of Dengue Infection. *PLOS ONE* **2015**, *10*, e0129682, doi:10.1371/journal.pone.0129682.

50. Larrea-Sarmiento, A.; Stack, J.P.; Alvarez, A.M.; Arif, M. Multiplex Recombinase Polymerase Amplification (RPA) Assay Developed Using Unique Genomic Regions and Coupled with a Lateral Flow Device for Rapid on-Site Detection of Genus Clavibacter and C. Nebraskensis 2020, 2020.08.22.262824.

51. Lv, R.; Lu, N.; Wang, J.; Li, Y.; Qi, Y. Recombinase Polymerase Amplification for Rapid Detection of Zoonotic Pathogens: An Overview. *Zoonoses* **2022**, doi:10.15212/ZOONOSES-2022-0002.

52. Lillis, L.; Siverson, J.; Lee, A.; Cantera, J.; Parker, M.; Piepenburg, O.; Lehman, D.A.; Boyle, D.S. Factors Influencing Recombinase Polymerase Amplification (RPA) Assay Outcomes at Point of Care. *Molecular and Cellular Probes* **2016**, *30*, 74–78, doi:10.1016/j.mcp.2016.01.009.

53. Tan, M.; Liao, C.; Liang, L.; Yi, X.; Zhou, Z.; Wei, G. Recent Advances in Recombinase Polymerase Amplification: Principle, Advantages, Disadvantages and Applications. *Front. Cell. Infect. Microbiol.* **2022**, *12*, doi:10.3389/fcimb.2022.1019071.

54. Pourshahidi, A.M. Frequency Mixing Magnetic Detection for Characterization and Multiplex Detection of Superparamagnetic Nanoparticles.

55. Gloag, L.; Mehdipour, M.; Chen, D.; Tilley, R.D.; Gooding, J.J. Advances in the Application of Magnetic Nanoparticles for Sensing. *Advanced Materials* **2019**, *31*, 1904385, doi:10.1002/adma.201904385.

56. Wu, K.; Saha, R.; Su, D.; Krishna, V.D.; Liu, J.; Cheeran, M.C.-J.; Wang, J.-P. Magnetic-Nanosensor-Based Virus and Pathogen Detection Strategies before and during COVID-19. *ACS Appl. Nano Mater.* **2020**, *3*, 9560–9580, doi:10.1021/acsanm.0c02048.

57. Luiz, M.T.; Dutra, J.A.P.; Viegas, J.S.R.; de Araújo, J.T.C.; Tavares Junior, A.G.; Chorilli, M. Hybrid Magnetic Lipid-Based Nanoparticles for Cancer Therapy. *Pharmaceutics* **2023**, *15*, 751, doi:10.3390/pharmaceutics15030751.

58. Etli, E.; Akar, A. Magnetic Nanoparticles for Diagnosis and Treatment. *Med-Science* **2022**, *11*, 934, doi:10.5455/medscience.2021.10.338.

59. Cole, A.J.; Yang, V.C.; David, A.E. Cancer Theranostics: The Rise of Targeted Magnetic Nanoparticles. *Trends Biotechnol* **2011**, *29*, 323–332, doi:10.1016/j.tibtech.2011.03.001.

60. Pietschmann, J.; Voepel, N.; Voß, L.; Rasche, S.; Schubert, M.; Kleines, M.; Krause, H.-J.; Shaw, T.M.; Spiegel, H.; Schroeper, F. Development of Fast and Portable Frequency Magnetic Mixing-Based Serological SARS-CoV-2-Specific Antibody Detection Assay. *Frontiers in Microbiology* **2021**, *12*.

61. Rettcher, S.; Jungk, F.; Kühn, C.; Krause, H.-J.; Nölke, G.; Commandeur, U.; Fischer, R.; Schillberg, S.; Schröper, F. Simple and Portable Magnetic Immunoassay for Rapid Detection and Sensitive Quantification of Plant Viruses. *Appl Environ Microbiol* **2015**, *81*, 3039–3048, doi:10.1128/AEM.03667-14.

62. Pietschmann, J.; Spiegel, H.; Krause, H.-J.; Schillberg, S.; Schröper, F. Sensitive Aflatoxin B1 Detection Using Nanoparticle-Based Competitive Magnetic Immunodetection. *Toxins* **2020**, *12*, 337, doi:10.3390/toxins12050337.

63. Pietschmann, J.; Dittmann, D.; Spiegel, H.; Krause, H.-J.; Schröper, F. A Novel Method for Antibiotic Detection in Milk Based on Competitive Magnetic Immunodetection. *Foods* **2020**, *9*, 1773, doi:10.3390/foods9121773.

64. Meyer, M.H.F.; Hartmann, M.; Krause, H.-J.; Blankenstein, G.; Mueller-Chorus, B.; Oster, J.; Miethe, P.; Keusgen, M. CRP Determination Based on a Novel Magnetic Biosensor. *Biosensors and Bioelectronics* **2007**, *22*, 973–979, doi:10.1016/j.bios.2006.04.001.

65. Meyer, M.H.F.; Stehr, M.; Bhuju, S.; Krause, H.-J.; Hartmann, M.; Miethe, P.; Singh, M.; Keusgen, M. Magnetic Biosensor for the Detection of Yersinia Pestis. *Journal of Microbiological Methods* **2007**, *68*, 218–224, doi:10.1016/j.mimet.2006.08.004.

66. Achtsnicht, S.; Pourshahidi, A.M.; Offenhäusser, A.; Krause, H.-J. Multiplex Detection of Different Magnetic Beads Using Frequency Scanning in Magnetic Frequency Mixing Technique. *Sensors* **2019**, *19*, 2599, doi:10.3390/s19112599.

67. Pourshahidi, A.M.; Achtsnicht, S.; Nambipareechee, M.M.; Offenhäusser, A.; Krause, H.-J. Multiplex Detection of Magnetic Beads Using Offset Field Dependent Frequency Mixing Magnetic Detection. *Sensors* **2021**, *21*, 5859, doi:10.3390/s21175859.

68. Bikulov, T.; Offenhäusser, A.; Krause, H.-J. Passive Mixer Model for Multi-Contrast Magnetic Particle Spectroscopy. *International Journal on Magnetic Particle Imaging IJMPI* **2023**, *9*, doi:10.18416/IJMPI.2023.2303087.

69. Moreno, E. Retrospective and Prospective Perspectives on Zoonotic Brucellosis. *Frontiers in Microbiology* **2014**, *5*.

70. Rodolakis, A.; Yousef Mohamad, K. Zoonotic Potential of Chlamydophila. *Veterinary Microbiology* **2010**, *140*, 382–391, doi:10.1016/j.vetmic.2009.03.014.

71. Sahin, O.; Yaeger, M.; Wu, Z.; Zhang, Q. Campylobacter-Associated Diseases in Animals. *Annual Review of Animal Biosciences* **2017**, *5*, 21–42, doi:10.1146/annurev-animal-022516-022826.

72. Jajere, S.M. A Review of Salmonella Enterica with Particular Focus on the Pathogenicity and Virulence Factors, Host Specificity and Antimicrobial Resistance Including Multidrug Resistance. *Vet World* **2019**, *12*, 504–521, doi:10.14202/vetworld.2019.504-521.

73. Kathayat, D.; Lokesh, D.; Ranjit, S.; Rajashekara, G. Avian Pathogenic Escherichia Coli (APEC): An Overview of Virulence and Pathogenesis Factors, Zoonotic Potential, and Control Strategies. *Pathogens* **2021**, *10*, 467, doi:10.3390/pathogens10040467.

74. Zuker, M. Mfold Web Server for Nucleic Acid Folding and Hybridization Prediction. *Nucleic Acids Research* **2003**, *31*, 3406–3415, doi:10.1093/nar/gkg595.

75. Holländer, A. Surface Oxidation inside of Macroscopic Porous Polymeric Materials. *Surface and Coatings Technology* **2005**, *200*, 561–564, doi:10.1016/j.surfcoat.2005.01.091.

76. Abuawad, A.; Ashhab, Y.; Offenhäusser, A.; Krause, H.-J. DNA Sensor for the Detection of Brucella Spp. Based on Magnetic Nanoparticle Markers. *International Journal of Molecular Sciences* **2023**, *24*, 17272, doi:10.3390/ijms242417272.

77. Morales, M.A.; Halpern, J.M. Guide to Selecting a Biorecognition Element for Biosensors. *Bioconjugate Chem.* **2018**, *29*, 3231–3239, doi:10.1021/acs.bioconjchem.8b00592.

78. Monis, P.T.; Giglio, S. Nucleic Acid Amplification-Based Techniques for Pathogen Detection and Identification. *Infect Genet Evol* **2006**, *6*, 2–12, doi:10.1016/j.meegid.2005.08.004.

79. Chern, E. c.; Siefring, S.; Paar, J.; Doolittle, M.; Haugland, R. a. Comparison of Quantitative PCR Assays for Escherichia Coli Targeting Ribosomal RNA and Single Copy Genes. *Letters in Applied Microbiology* **2011**, *52*, 298–306, doi:10.1111/j.1472-765X.2010.03001.x.

80. Luo, R.F.; Scahill, M.D.; Banaei, N. Comparison of Single-Copy and Multicopy Real-Time PCR Targets for Detection of Mycobacterium Tuberculosis in Paraffin-Embedded Tissue. *Journal of Clinical Microbiology* **2010**, *48*, 2569–2570, doi:10.1128/JCM.02449-09.

81. Margulis, M.; Danielli, A. Rapid and Sensitive Detection of Repetitive Nucleic Acid Sequences Using Magnetically Modulated Biosensors. *ACS Omega* **2019**, *4*, 11749–11755, doi:10.1021/acsomega.9b01071.

82. Treangen, T.J.; Abraham, A.-L.; Touchon, M.; Rocha, E.P.C. Genesis, Effects and Fates of Repeats in Prokaryotic Genomes. *FEMS Microbiol Rev* **2009**, *33*, 539–571, doi:10.1111/j.1574-6976.2009.00169.x.

83. Rashid, J.I.A.; Yusof, N.A. The Strategies of DNA Immobilization and Hybridization Detection Mechanism in the Construction of Electrochemical DNA Sensor: A Review. *Sensing and Bio-Sensing Research* **2017**, *16*, 19–31, doi:10.1016/j.sbsr.2017.09.001.

84. Nimse, S.B.; Song, K.; Sonawane, M.D.; Sayyed, D.R.; Kim, T. Immobilization Techniques for Microarray: Challenges and Applications. *Sensors (Basel)* **2014**, *14*, 22208–22229, doi:10.3390/s141222208.

85. Teh, H.F.; Gong, H.; Dong, X.-D.; Zeng, X.; Lai Kuan Tan, A.; Yang, X.; Tan, S.N. Electrochemical Biosensing of DNA with Capture Probe Covalently Immobilized onto Glassy Carbon Surface. *Analytica Chimica Acta* **2005**, *551*, 23–29, doi:10.1016/j.aca.2005.07.008.

86. Wang, Z.; Li, R.-X. Fabrication of DNA Micropatterns on the Polycarbonate Surface of Compact Discs. *Nanoscale Res Lett* **2007**, *2*, 69, doi:10.1007/s11671-006-9032-6.

87. Elschner, T.; Scholz, F.; Miethe, P.; Heinze, T. Rapid Flow Through Immunoassay for CRP Determination Based on Polyethylene Filters Modified with ω-Aminocellulose Carbamate. *Macromolecular Bioscience* **2014**, *14*, 1539–1546, doi:10.1002/mabi.201400179.

88. Kim, K.; Chen, W.C.W.; Heo, Y.; Wang, Y. Polycations and Their Biomedical Applications. *Progress in Polymer Science* **2016**, *60*, 18–50, doi:10.1016/j.progpolymsci.2016.05.004.

89. Spedding, G. The World's Most Popular Assay? A Review of the Ninhydrin-Based Free Amino Nitrogen Reaction (FAN Assay) Emphasizing the Development of Newer Methods and Conditions for Testing Alcoholic Beverages. *Journal of the American Society of Brewing Chemists* **2013**, *71*, 83–89, doi:10.1094/ASBCJ-2013-0411-01.

90. Friedman, M. Applications of the Ninhydrin Reaction for Analysis of Amino Acids, Peptides, and Proteins to Agricultural and Biomedical Sciences. *J. Agric. Food Chem.* **2004**, *52*, 385–406, doi:10.1021/jf030490p.

91. Peterson, A.W.; Heaton, R.J.; Georgiadis, R.M. The Effect of Surface Probe Density on DNA Hybridization. *Nucleic Acids Res* **2001**, *29*, 5163–5168.

92. Rao, A.N.; Grainger, D.W. Biophysical Properties of Nucleic Acids at Surfaces Relevant to Microarray Performance. *Biomater. Sci.* **2014**, *2*, 436–471, doi:10.1039/C3BM60181A.

93. Yesil, M.; Donmez, S.; Arslan, F. Development of an Electrochemical DNA Biosensor for Detection of Specific Mycobacterium Tuberculosis Sequence Based on Poly(L-Glutamic Acid) Modified Electrode. *J Chem Sci* **2016**, *128*, 1823–1829, doi:10.1007/s12039-016-1159-0.

94. Aladag, N.; Ozkan-Ariksoysal, D.; Gezen-Ak, D.; Yilmazer, S.; Ozsoz, M. An Electrochemical DNA Biosensor for the Detection of the Apa I Polymorphism in the Vitamin D Receptor Gene Using Meldola's Blue as a Hybridization Indicator. *Electroanalysis* **2010**, *22*, 590–598, doi:10.1002/elan.200900405.

95. He, Z.; Wu, L.; Fields, M.W.; Zhou, J. Use of Microarrays with Different Probe Sizes for Monitoring Gene Expression. *Applied and Environmental Microbiology* **2005**, *71*, 5154–5162, doi:10.1128/AEM.71.9.5154-5162.2005.

96. Relógio, A.; Schwager, C.; Richter, A.; Ansorge, W.; Valcárcel, J. Optimization of Oligonucleotide-Based DNA Microarrays. *Nucleic Acids Research* **2002**, *30*, e51, doi:10.1093/nar/30.11.e51.

97. Rivas, L.; Reuterswärd, P.; Rasti, R.; Herrmann, B.; Mårtensson, A.; Alfvén, T.; Gantelius, J.; Andersson-Svahn, H. A Vertical Flow Paper-Microarray Assay with Isothermal DNA Amplification for Detection of Neisseria Meningitidis. *Talanta* **2018**, *183*, 192–200, doi:10.1016/j.talanta.2018.02.070.

98. Kane, M.D.; Jatkoe, T.A.; Stumpf, C.R.; Lu, J.; Thomas, J.D.; Madore, S.J. Assessment of the Sensitivity and Specificity of Oligonucleotide (50mer) Microarrays. *Nucleic Acids Res* **2000**, *28*, 4552–4557.

99. Wong, K.L.; Liu, J. Factors and Methods to Modulate DNA Hybridization Kinetics. *Biotechnology Journal* **2021**, *16*, 2000338, doi:10.1002/biot.202000338.

100. S. Swenson, C.; H. Lackey, H.; J. Reece, E.; M. Harris, J.; M. Heemstra, J.; M. Peterson, E. Evaluating the Effect of Ionic Strength on PNA:DNA Duplex Formation Kinetics. *RSC Chemical Biology* **2021**, *2*, 1249–1256, doi:10.1039/D1CB00025J.

101. Ariffin, E.Y.; Lee, Y.H.; Futra, D.; Tan, L.L.; Karim, N.H.A.; Ibrahim, N.N.N.; Ahmad, A. An Ultrasensitive Hollow-Silica-Based Biosensor for Pathogenic Escherichia Coli DNA Detection. *Anal Bioanal Chem* **2018**, *410*, 2363–2375, doi:10.1007/s00216-018-0893-1.

102. Jia, Y.; Chen, S.; Wang, Q.; Li, J. Recent Progress in Biosensor Regeneration Techniques. *Nanoscale* **2024**, *16*, 2834–2846, doi:10.1039/D3NR05456J.

103. Rizzi, G.; Lee, J.-R.; Guldberg, P.; Dufva, M.; Wang, S.X.; Hansen, M.F. Denaturation Strategies for Detection of Double Stranded PCR Products on GMR Magnetic Biosensor Array. *Biosensors and Bioelectronics* **2017**, *93*, 155–160, doi:10.1016/j.bios.2016.09.031.

104. Singh, S.; Kaushal, A.; Gautam, H.; Gupta, S.; Kumar, A. Ultrasensitive Nanohybrid DNA Sensor for Detection of Pathogen to Prevent Damage of Heart Valves. *Sensors and Actuators B: Chemical* **2017**, *246*, 300–304, doi:10.1016/j.snb.2017.02.043.

105. Citartan, M.; Tang, T.-H.; Tan, S.-C.; Gopinath, S.C.B. Conditions Optimized for the Preparation of Single-Stranded DNA (ssDNA) Employing Lambda Exonuclease Digestion in Generating DNA Aptamer. *World J Microbiol Biotechnol* **2011**, *27*, 1167–1173, doi:10.1007/s11274-010-0563-8.

106. Marimuthu, C.; Tang, T.-H.; Tominaga, J.; Tan, S.-C.; B. Gopinath, S.C. Single-Stranded DNA (ssDNA) Production in DNA Aptamer Generation. *Analyst* **2012**, *137*, 1307–1315, doi:10.1039/C2AN15905H.

107. Gao, Y.; Wolf, L.K.; Georgiadis, R.M. Secondary Structure Effects on DNA Hybridization Kinetics: A Solution versus Surface Comparison. *Nucleic Acids Research* **2006**, *34*, 3370–3377, doi:10.1093/nar/gkl422.

108. Civit, L.; Fragoso, A.; O'Sullivan, C.K. Evaluation of Techniques for Generation of Single-Stranded DNA for Quantitative Detection. *Analytical Biochemistry* **2012**, *431*, 132–138, doi:10.1016/j.ab.2012.09.003.

109. Botella, J.R. Point-of-Care DNA Amplification for Disease Diagnosis and Management. *Annu. Rev. Phytopathol.* **2022**, *60*, 1–20, doi:10.1146/annurev-phyto-021621-115027.

110. Li, J.; Macdonald, J.; Stetten, F. von Review: A Comprehensive Summary of a Decade Development of the Recombinase Polymerase Amplification. *Analyst* **2018**, *144*, 31–67, doi:10.1039/C8AN01621F.

111. Wu, L.; Ye, L.; Wang, Z.; Cui, Y.; Wang, J. Utilization of Recombinase Polymerase Amplification Combined with a Lateral Flow Strip for Detection of Perkinsus Beihaiensis in the Oyster Crassostrea Hongkongensis. *Parasites & Vectors* **2019**, *12*, 360, doi:10.1186/s13071-019-3624-3.

112. Jarvi, S.I.; Atkinson, E.S.; Kaluna, L.M.; Snook, K.A.; Steel, A. Development of a Recombinase Polymerase Amplification (RPA-EXO) and Lateral Flow Assay (RPA-LFA) Based on the ITS1 Gene for the Detection of Angiostrongylus Cantonensis in Gastropod Intermediate Hosts. *Parasitology* **2021**, *148*, 251–258, doi:10.1017/S0031182020002139.

113. Fuller, S.L.; Savory, E.A.; Weisberg, A.J.; Buser, J.Z.; Gordon, M.I.; Putnam, M.L.; Chang, J.H. Isothermal Amplification and Lateral-Flow Assay for Detecting Crown-Gall-Causing Agrobacterium Spp. *Phytopathology®* **2017**, *107*, 1062–1068, doi:10.1094/PHYTO-04-17-0144-R.

114. Wang, Y.; Li, X.; Xi, D.; Wang, X. Visual Detection of Fusarium Proliferatum Based on Asymmetric Recombinase Polymerase Amplification and Hemin/G-Quadruplex DNAzyme. *RSC Advances* **2019**, *9*, 37144–37147, doi:10.1039/C9RA05709A.

115. Farrera-Soler, L.; Gonse, A.; Kim, K.T.; Barluenga, S.; Winssinger, N. Combining Recombinase Polymerase Amplification and DNA-Templated Reaction for SARS-CoV-2 Sensing with Dual Fluorescence and Lateral Flow Assay Output. *Biopolymers* **2022**, *113*, e23485, doi:10.1002/bip.23485.

116. Ma, B.; Li, J.; Chen, K.; Yu, X.; Sun, C.; Zhang, M. Multiplex Recombinase Polymerase Amplification Assay for the Simultaneous Detection of Three Foodborne Pathogens in Seafood. *Foods* **2020**, *9*, 278, doi:10.3390/foods9030278.

117. Jiang, W.; Ren, Y.; Han, X.; Xue, J.; Shan, T.; Chen, Z.; Liu, Y.; Wang, Q. Recombinase Polymerase Amplification-Lateral Flow (RPA-LF) Assay Combined with Immunomagnetic Separation for Rapid Visual Detection of Vibrio Parahaemolyticus in Raw Oysters. *Anal Bioanal Chem* **2020**, *412*, 2903–2914, doi:10.1007/s00216-020-02532-9.

118. Sun, N.; Wang, Y.; Yao, X.; Chen, F.; Gao, D.; Wang, W.; Li, X. Visual Signal Generation for the Detection of Influenza Viruses by Duplex Recombinase Polymerase Amplification with Lateral Flow Dipsticks. *Anal Bioanal Chem* **2019**, *411*, 3591–3602, doi:10.1007/s00216-019-01840-z.

119. Zhou, Q.; Liu, Y.; Wang, Z.; Wang, H.; Zhang, X.; Lu, Q. Rapid On-Site Detection of the Bursaphelenchus Xylophilus Using Recombinase Polymerase Amplification Combined With Lateral Flow Dipstick That Eliminates Interference From Primer-Dependent Artifacts. *Front. Plant Sci.* **2022**, *13*, doi:10.3389/fpls.2022.856109.

120. Al-Madhagi, S.; Joda, H.; Jauset-Rubio, M.; Ortiz, M.; Katakis, I.; O'Sullivan, C.K. Isothermal Amplification Using Modified Primers for Rapid Electrochemical Analysis of Coeliac Disease Associated DQB1*02 HLA Allele. *Analytical Biochemistry* **2018**, *556*, 16–22, doi:10.1016/j.ab.2018.06.013.

121. Jauset-Rubio, M.; Svobodová, M.; Mairal, T.; McNeil, C.; Keegan, N.; El-Shahawi, M.S.; Bashammakh, A.S.; Alyoubi, A.O.; O'Sullivan, C.K. Aptamer Lateral Flow Assays for Ultrasensitive Detection of β-Conglutin Combining Recombinase Polymerase Amplification and Tailed Primers. *Anal. Chem.* **2016**, *88*, 10701–10709, doi:10.1021/acs.analchem.6b03256.

122. AL-Madhagi, S.; O'Sullivan, C.K.; Prodromidis, M.I.; Katakis, I. Combination of Ferrocene Decorated Gold Nanoparticles and Engineered Primers for the Direct Reagentless Determination of Isothermally Amplified DNA. *Microchim Acta* **2021**, *188*, 117, doi:10.1007/s00604-021-04771-8.

123. Wu, H.; Zhao, P.; Yang, X.; Li, J.; Zhang, J.; Zhang, X.; Zeng, Z.; Dong, J.; Gao, S.; Lu, C. A Recombinase Polymerase Amplification and Lateral Flow Strip Combined Method That Detects

Salmonella Enterica Serotype Typhimurium With No Worry of Primer-Dependent Artifacts. *Front. Microbiol.* **2020**, *11*, doi:10.3389/fmicb.2020.01015.

124. Meagher, R.J.; Priye, A.; Light, Y.K.; Huang, C.; Wang, E. Impact of Primer Dimers and Self-Amplifying Hairpins on Reverse Transcription Loop-Mediated Isothermal Amplification Detection of Viral RNA. *Analyst* **2018**, *143*, 1924–1933, doi:10.1039/c7an01897e.

125. Wang, D.-G.; Brewster, J.D.; Paul, M.; Tomasula, P.M. Two Methods for Increased Specificity and Sensitivity in Loop-Mediated Isothermal Amplification. *Molecules* **2015**, *20*, 6048–6059, doi:10.3390/molecules20046048.

126. Wang, Y.; Liu, D.; Deng, J.; Wang, Y.; Xu, J.; Ye, C. Loop-Mediated Isothermal Amplification Using Self-Avoiding Molecular Recognition Systems and Antarctic Thermal Sensitive Uracil-DNA-Glycosylase for Detection of Nucleic Acid with Prevention of Carryover Contamination. *Analytica Chimica Acta* **2017**, *996*, 74–87, doi:10.1016/j.aca.2017.10.022.

127. Özay, B.; McCalla, S.E. A Review of Reaction Enhancement Strategies for Isothermal Nucleic Acid Amplification Reactions. *Sensors and Actuators Reports* **2021**, *3*, 100033, doi:10.1016/j.snr.2021.100033.

128. Kim, S.-H.; Lee, S.-Y.; Kim, U.; Oh, S.-W. Diverse Methods of Reducing and Confirming False-Positive Results of Loop-Mediated Isothermal Amplification Assays: A Review. *Analytica Chimica Acta* **2023**, *1280*, 341693, doi:10.1016/j.aca.2023.341693.

129. Ivanov, A.V.; Safenkova, I.V.; Zherdev, A.V.; Dzantiev, B.B. Recombinase Polymerase Amplification Assay with and without Nuclease-Dependent-Labeled Oligonucleotide Probe. *Int J Mol Sci* **2021**, *22*, 11885, doi:10.3390/ijms222111885.

130. Hoshika, S.; Chen, F.; Leal, N.A.; Benner, S.A. Self-Avoiding Molecular Recognition Systems (SAMRS). *Nucleic Acids Symposium Series* **2008**, *52*, 129–130, doi:10.1093/nass/nrn066.

131. Wang, Y.; Jiao, W.; Wang, Y.; Wang, Y.; Shen, C.; Qi, H.; Shen, A.-D. Graphene Oxide and Self-Avoiding Molecular Recognition Systems-Assisted Recombinase Polymerase Amplification Coupled with Lateral Flow Bioassay for Nucleic Acid Detection. *Microchim Acta* **2020**, *187*, 667, doi:10.1007/s00604-020-04637-5.

132. Jensen, M.A.; Fukushima, M.; Davis, R.W. DMSO and Betaine Greatly Improve Amplification of GC-Rich Constructs in De Novo Synthesis. *PLOS ONE* **2010**, *5*, e11024, doi:10.1371/journal.pone.0011024.

133. Guo, Q.; Zhou, K.; Chen, C.; Yue, Y.; Shang, Z.; Zhou, K.; Fu, Z.; Liu, J.; Lin, J.; Xia, C.; et al. Development of a Recombinase Polymerase Amplification Assay for Schistosomiasis Japonica Diagnosis in the Experimental Mice and Domestic Goats. *Front. Cell. Infect. Microbiol.* **2021**, *11*, doi:10.3389/fcimb.2021.791997.

134. Salazar, A.; Ochoa-Corona, F.M.; Talley, J.L.; Noden, B.H. Recombinase Polymerase Amplification (RPA) with Lateral Flow Detection for Three Anaplasma Species of Importance to Livestock Health. *Sci Rep* **2021**, *11*, 15962, doi:10.1038/s41598-021-95402-y.

135. Poulton, K.; Webster, B. Development of a Lateral Flow Recombinase Polymerase Assay for the Diagnosis of *Schistosoma Mansoni* Infections. *Analytical Biochemistry* **2018**, *546*, 65–71, doi:10.1016/j.ab.2018.01.031.

136. Ma, C.; Wang, Y.; Zhang, P.; Shi, C. Accelerated Isothermal Nucleic Acid Amplification in Betaine-Free Reaction. *Analytical Biochemistry* **2017**, *530*, 1–4, doi:10.1016/j.ab.2017.04.017.

137. Rosser, A.; Rollinson, D.; Forrest, M.; Webster, B.L. Isothermal Recombinase Polymerase Amplification (RPA) of Schistosoma Haematobium DNA and Oligochromatographic Lateral Flow Detection. *Parasites Vectors* **2015**, *8*, 446, doi:10.1186/s13071-015-1055-3.

138. Li, Z.; Pinto Torres, J.E.; Goossens, J.; Stijlemans, B.; Sterckx, Y.G.-J.; Magez, S. Development of a Recombinase Polymerase Amplification Lateral Flow Assay for the Detection of Active

Trypanosoma Evansi Infections. *PLoS Negl Trop Dis* **2020**, *14*, e0008044, doi:10.1371/journal.pntd.0008044.

139. Munawar, M.A. Critical Insight into Recombinase Polymerase Amplification Technology. *Expert Review of Molecular Diagnostics* **2022**, *22*, 725–737, doi:10.1080/14737159.2022.2109964.

140. Xiang, S.; Zhang, H.; Cha, X.; Lin, Y.; Shang, Y. A New Duplex Recombinase Polymerase Amplification (D-RPA) Method for the Simultaneous and Rapid Detection of Shigella and Bacillus Cereus in Food. *Foods* **2023**, *12*, 1889, doi:10.3390/foods12091889.

141. Naveen, K.P.; Bhat, A.I. Reverse Transcriptase Loop-Mediated Isothermal Amplification and Reverse Transcriptase Recombinase Amplification Assays for Rapid and Sensitive Detection of Cardamom Vein Clearing Virus. *3 Biotech* **2020**, *10*, 250, doi:10.1007/s13205-020-02238-w.

142. Valloly, P.; Roy, R. Nucleic Acid Quantification with Amplicon Yield in Recombinase Polymerase Amplification 2022, 2022.06.28.497931.

143. Thoeny, V.; Melnik, E.; Huetter, M.; Asadi, M.; Mehrabi, P.; Schalkhammer, T.; Pulverer, W.; Maier, T.; Mutinati, G.C.; Lieberzeit, P.; et al. Recombinase Polymerase Amplification in Combination with Electrochemical Readout for Sensitive and Specific Detection of PIK3CA Point Mutations. *Analytica Chimica Acta* **2023**, *1281*, 341922, doi:10.1016/j.aca.2023.341922.

144. Al Dahouk, S.; Nöckler, K. Implications of Laboratory Diagnosis on Brucellosis Therapy. *Expert Review of Anti-infective Therapy* **2011**, *9*, 833–845, doi:10.1586/eri.11.55.

145. Ekiri, A.B.; Kilonzo, C.; Bird, B.H.; VanWormer, E.; Wolking, D.J.; Smith, W.A.; Masanja, H.; Kazwala, R.R.; Mazet, J.A.K. Utility of the Rose Bengal Test as a Point-of-Care Test for Human Brucellosis in Endemic African Settings: A Systematic Review. *J Trop Med* **2020**, *2020*, 6586182, doi:10.1155/2020/6586182.

146. Gwida, M.M.; El-Gohary, A.H.; Melzer, F.; Tomaso, H.; Rösler, U.; Wernery, U.; Wernery, R.; Elschner, M.C.; Khan, I.; Eickhoff, M.; et al. Comparison of Diagnostic Tests for the Detection of Brucella Spp. in Camel Sera. *BMC Res Notes* **2011**, *4*, 525, doi:10.1186/1756-0500-4-525.

147. Lukambagire, A.S.; Mendes, Â.J.; Bodenham, R.F.; McGiven, J.A.; Mkenda, N.A.; Mathew, C.; Rubach, M.P.; Sakasaka, P.; Shayo, D.D.; Maro, V.P.; et al. Performance Characteristics and Costs of Serological Tests for Brucellosis in a Pastoralist Community of Northern Tanzania. *Sci Rep* **2021**, *11*, 5480, doi:10.1038/s41598-021-82906-w.

148. Memish, Z.A.; Almuneef, M.; Mah, M.W.; Qassem, L.A.; Osoba, A.O. Comparison of the Brucella Standard Agglutination Test with the ELISA IgG and IgM in Patients with Brucella Bacteremia. *Diagnostic Microbiology and Infectious Disease* **2002**, *44*, 129–132, doi:10.1016/S0732-8893(02)00426-1.

149. Abernethy, D.A.; Menzies, F.D.; McCullough, S.J.; McDowell, S.W.J.; Burns, K.E.; Watt, R.; Gordon, A.W.; Greiner, M.; Pfeiffer, D.U. Field Trial of Six Serological Tests for Bovine Brucellosis. *The Veterinary Journal* **2012**, *191*, 364–370, doi:10.1016/j.tvjl.2011.03.008.

150. Camacho-Martínez, J.C.; Rios-Lugo, M.J.; Gaytán-Hernández, D.; Hernández-Mendoza, H. Comparison of a Brucella Enzyme Immunoassay and the Standard Agglutination with 2-Mercaptoethanol Test in the Diagnosis and Monitoring of Brucellosis in Mexican Patients. *Clin Lab* **2020**, *66*, doi:10.7754/Clin.Lab.2020.190932.

151. McGiven, J.A.; Tucker, J.D.; Perrett, L.L.; Stack, J.A.; Brew, S.D.; MacMillan, A.P. Validation of FPA and cELISA for the Detection of Antibodies to Brucella Abortus in Cattle Sera and Comparison to SAT, CFT, and iELISA. *Journal of Immunological Methods* **2003**, *278*, 171–178, doi:10.1016/S0022-1759(03)00201-1.

152. Xu, N.; Wang, W.; Chen, F.; Li, W.; Wang, G. ELISA Is Superior to Bacterial Culture and Agglutination Test in the Diagnosis of Brucellosis in an Endemic Area in China. *BMC Infectious Diseases* **2020**, *20*, 11, doi:10.1186/s12879-019-4729-1.

153. Li, L.; Yin, D.; Xu, K.; Liu, Y.; Song, D.; Wang, J.; Zhao, C.; Song, X.; Li, J. A Sandwich Immunoassay for Brucellosis Diagnosis Based on Immune Magnetic Beads and Quantum Dots. *Journal of Pharmaceutical and Biomedical Analysis* **2017**, *141*, 79–86, doi:10.1016/j.jpba.2017.03.002.

154. Lu, J.; Li, C.; Zhang, E.; Hou, S.; Xiao, K.; Li, X.; Zhang, L.; Wang, Z.; Chen, C.; Li, C.; et al. Novel Vertical Flow Immunoassay with Au@PtNPs for Rapid, Ultrasensitive, and On-Site Diagnosis of Human Brucellosis. *ACS Omega* **2023**, *8*, 29534–29542, doi:10.1021/acsomega.3c03381.

155. Al-Nakkas, A.; Mustafa, A.S.; Wright, S.G. Large-Scale Evaluation of a Single-Tube Nested PCR for the Laboratory Diagnosis of Human Brucellosis in Kuwait. *Journal of Medical Microbiology* **2005**, *54*, 727–730, doi:10.1099/jmm.0.45772-0.

156. Che, L.; Qi, C.; Bao, W.; Ji, X.; Liu, J.; Du, N.; Gao, L.; Zhang, K.; Li, Y. Monitoring the Course of Brucella Infection with qPCR-Based Detection. *International Journal of Infectious Diseases* **2019**, *89*, 66–71, doi:10.1016/j.ijid.2019.09.013.

157. Sattarahmady, N.; Kayani, Z.; Heli, H. Highly Simple and Visual Colorimetric Detection of Brucella Melitensis Genomic DNA in Clinical Samples Based on Gold Nanoparticles. *J IRAN CHEM SOC* **2015**, *12*, 1569–1576, doi:10.1007/s13738-015-0629-5.

158. Ahangari, A.; Mahmoodi, P.; Mohammadzadeh, A. Biosensors Functionalized with Nanoparticles for Rapid Detection of Brucella. *Microchemical Journal* **2022**, *181*, 107697, doi:10.1016/j.microc.2022.107697.

159. Rahi, A.; Sattarahmady, N.; Heli, H. An Ultrasensitive Electrochemical Genosensor for Brucella Based on Palladium Nanoparticles. *Analytical Biochemistry* **2016**, *510*, 11–17, doi:10.1016/j.ab.2016.07.012.

160. Jessing, M.P.; Abuawad, A.; Bikulov, T.; Abresch, J.R.; Offenhäusser, A.; Krause, H.-J. Isothermal Amplification Using Temperature-Controlled Frequency Mixing Magnetic Detection-Based Portable Field-Testing Platform. *Sensors* **2024**, *24*, 4478, doi:10.3390/s24144478.

Supplementary materials

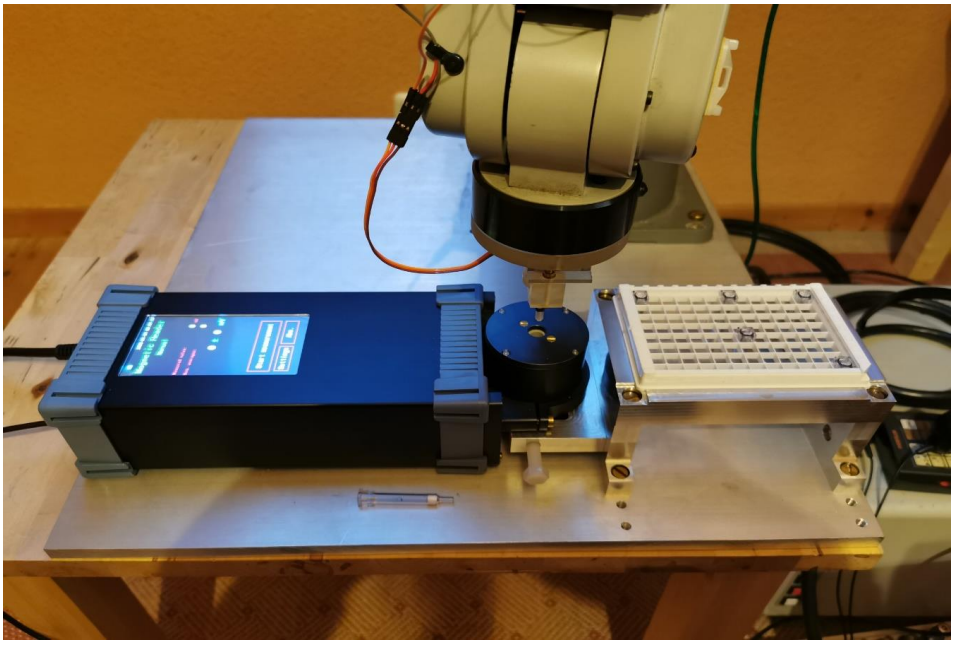

Figure S1. The micro-robot arm system, magnetic reader and 96 well rack.

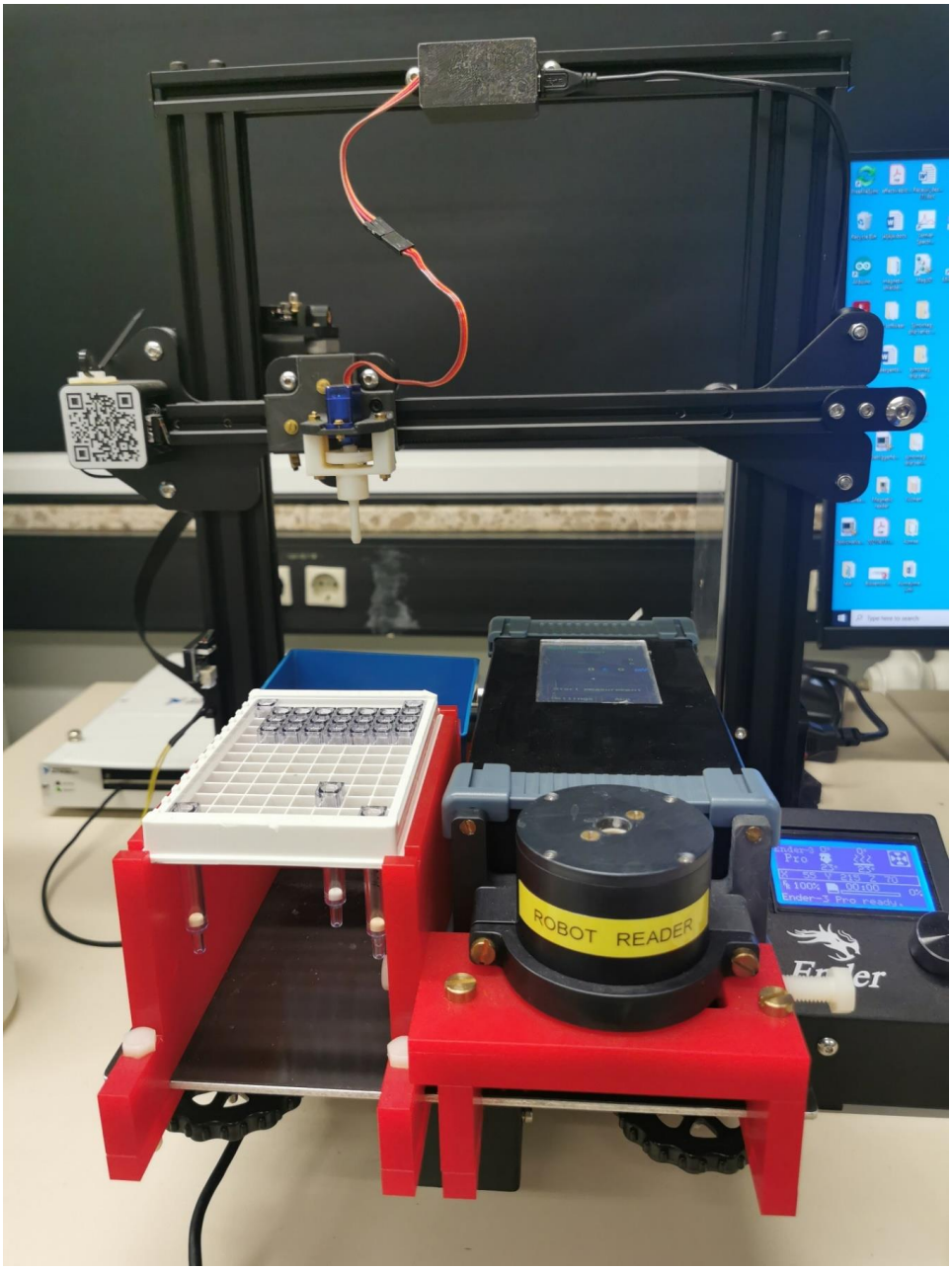

Figure S2. The 3D printer ender-3 system, magnetic reader and 96 well rack.

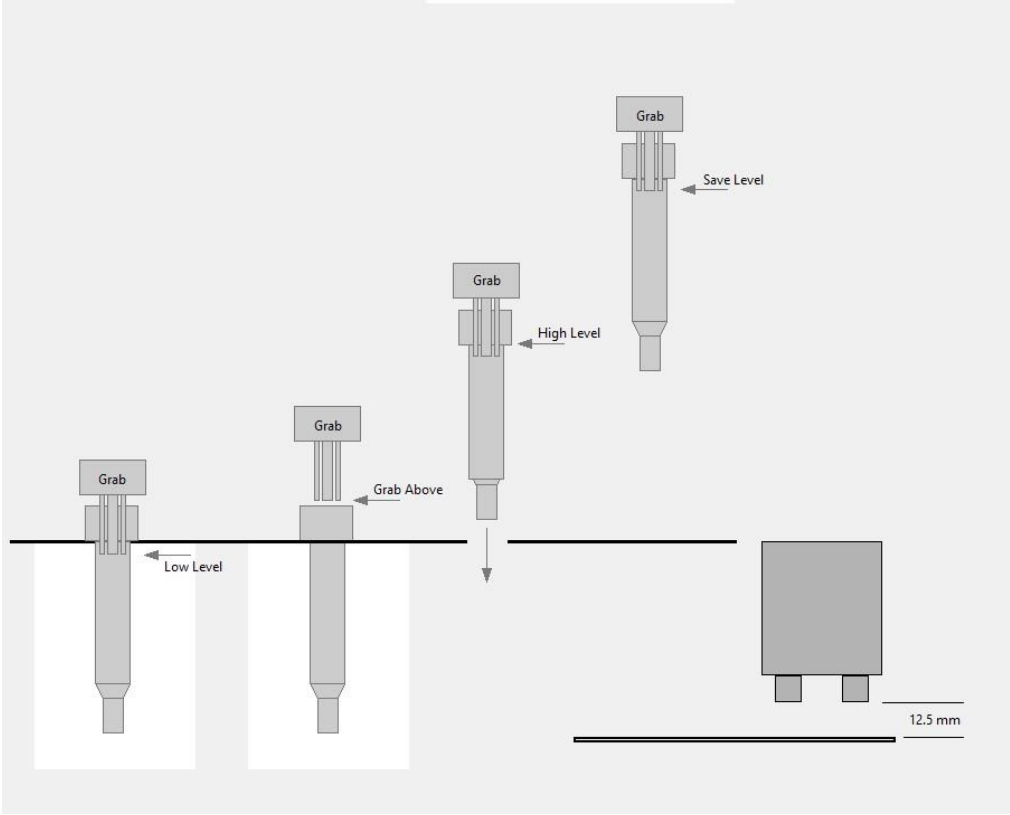

Figure S3. The movement of grabber.

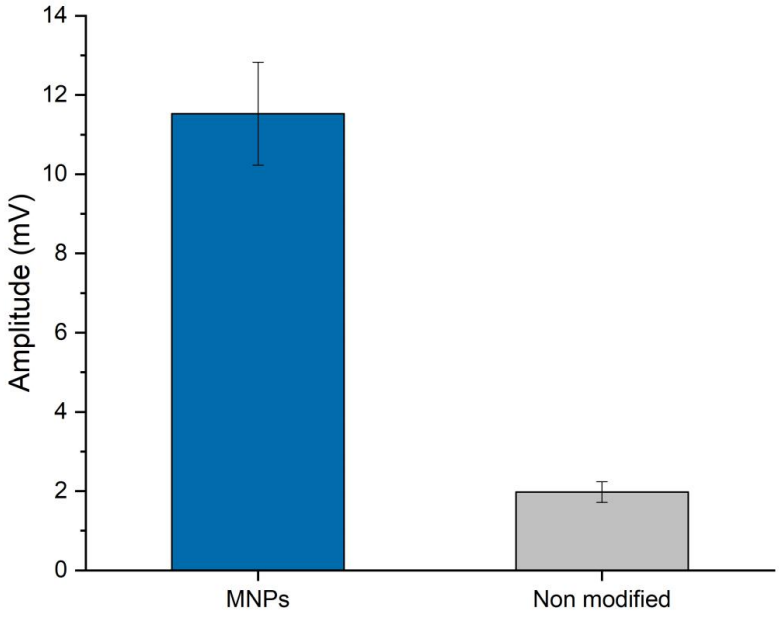

Figure S4. The signal amplitudes of MNPs in the absence of DNA on PE filters coated with PEI. Error bars represent the standard deviation of two independent measurements.

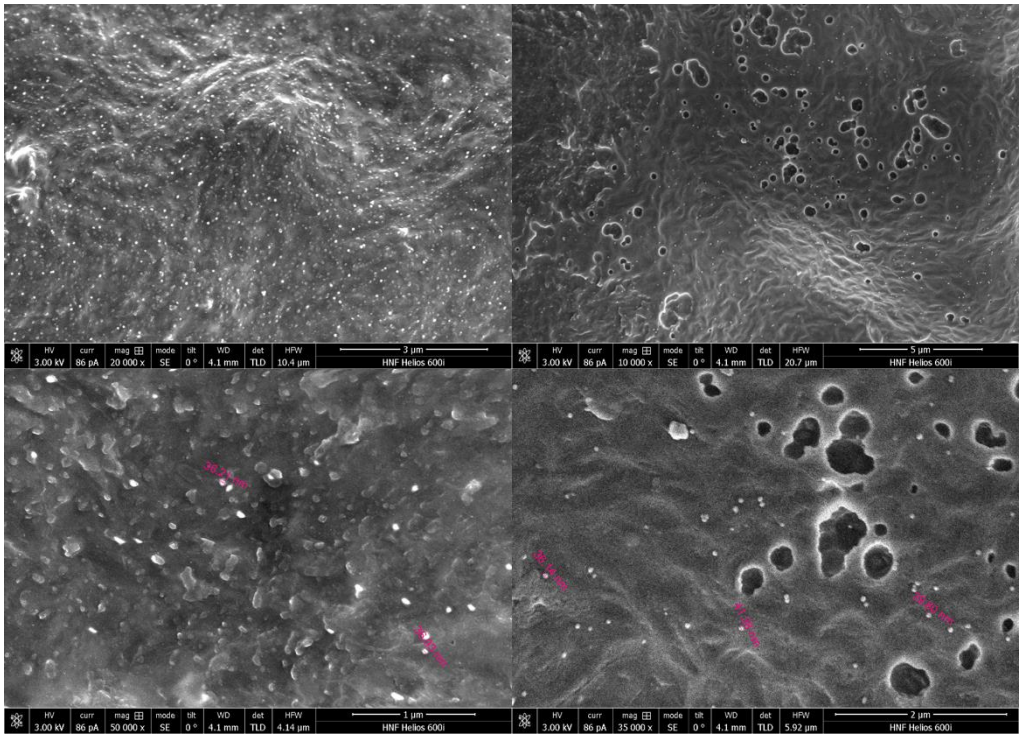

Figure S5. SEM images of gold nanoparticles bound to the immobilized capture probes on an amine-functionalized PE filters.

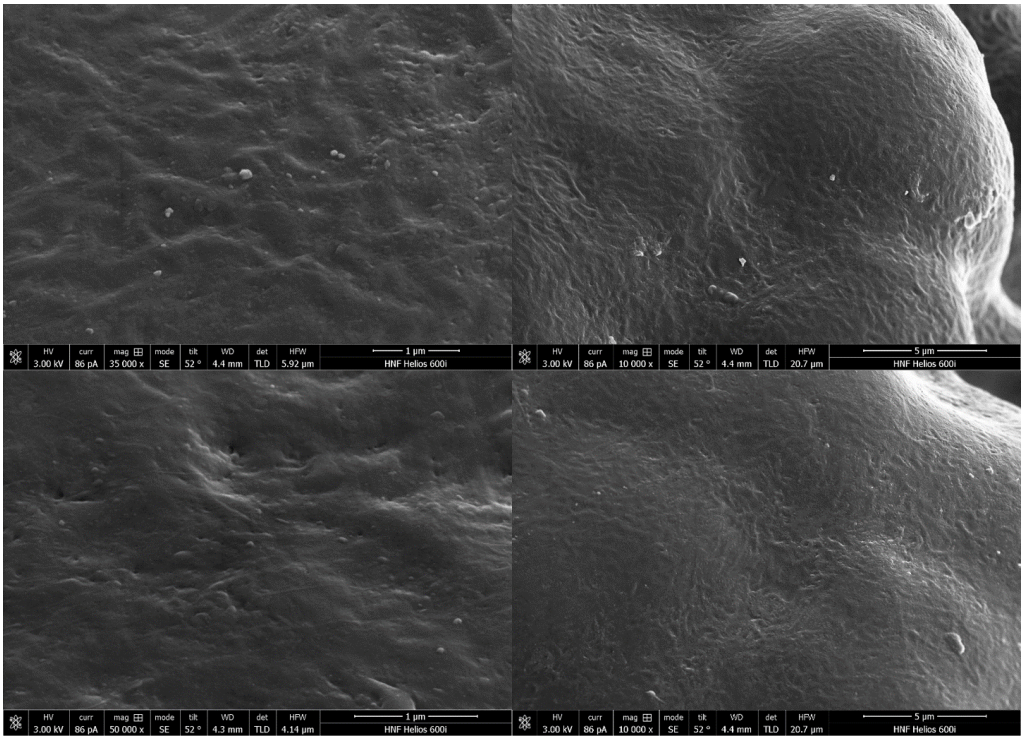

Figure S6. SEM images of gold nanoparticles bound to the immobilized capture probes on non-functionalized PE filters.

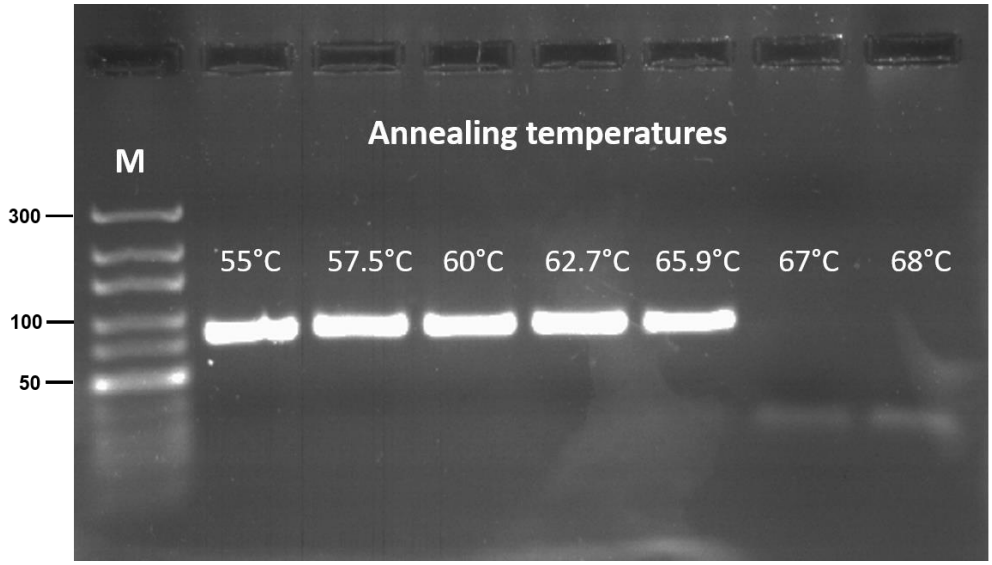

Figure S7. The Annealing temperatures of PCR.

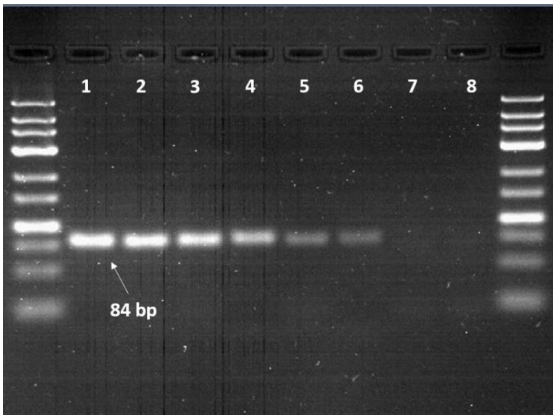

Figure S8. Agarose gel images for the PCR of amplified *Brucella* DNA (84 bp) with different copy numbers. Lane 1: $5x10^6$. Lane 2: $5x10^5$. Lane 3: $5x10^4$. Lane 4: $5x10^3$. Lane 5: $5x10^2$. Lane 6: $5x10^1$. Lane 7: $5x10^0$. Lane 8: Non-template control.

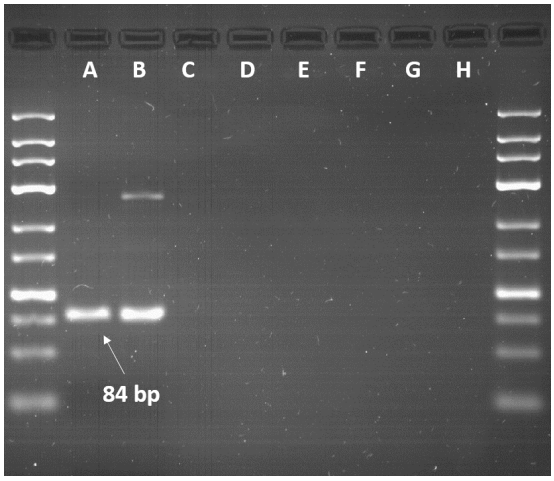

Figure S9. Agarose gel images for the PCR of *Brucella* DNA and non-related bacterial genomes (A) *Brucella* positive control, (B) *Brucella melitensis* at 2 ng/µL, (C) *Ovax Chlamydia* at 5 ng/µl, (D*) Campylobacter fetus subsp. venerealis (Cfv)* at 27 ng/µl, (E) *Campylobacter fetus subsp. fetus (Cff)* at 55 ng/µl, (F) *Escherichia coli (APEC)* at 83 ng/µl, (G) *Salmonella enteritidis* at 84 ng/µl, (H) Non-template control.

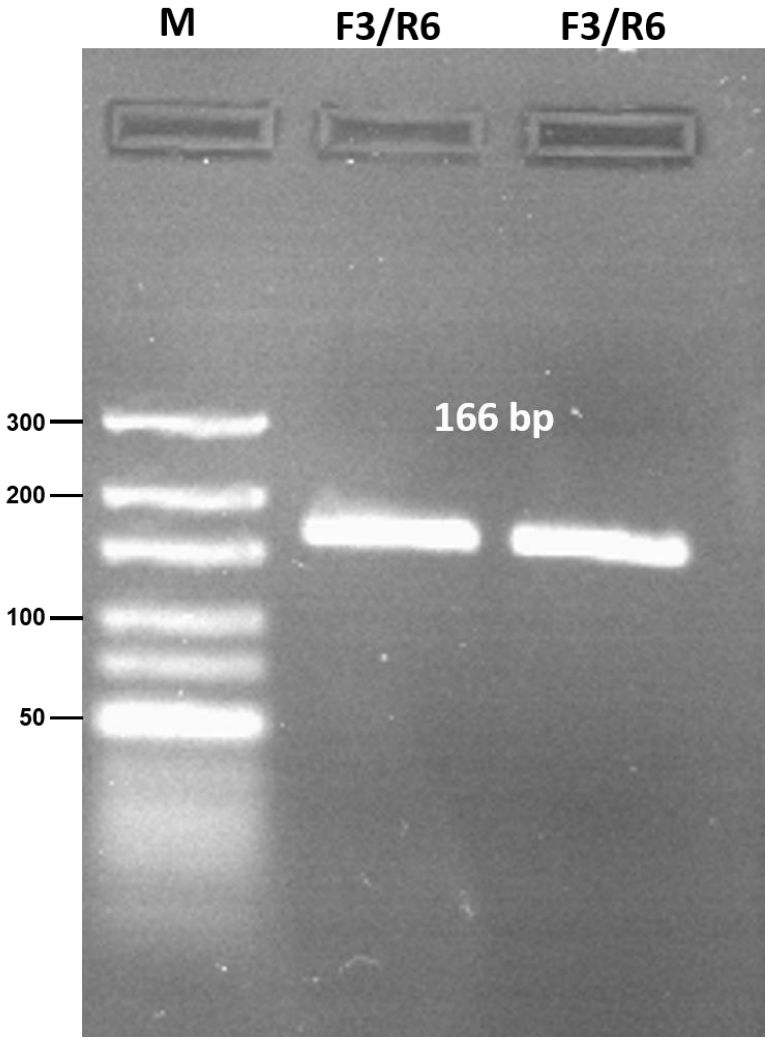

Figure S10. The RPA products amplified by F3/R6 primer pair.

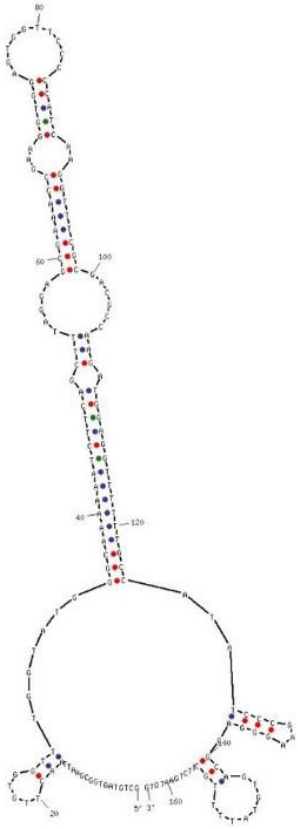

Figure S11. Secondary structure of the ssDNA with the size of 166 bp.

List of Tables

List of Figures

Abbreviations

ARPA	Asymmetric Recombinase Polymerase Amplification
bp	Base Pair
BSA	Bovine Serum Albumin in PBS
CDC	Centers for Disease Control and Prevention
CV	Coefficient of Variations
DIG	Digoxigenin
DMSO	Dimethyl Sulfoxide
DNA	Deoxyribonucleic Acid
dNTPs	Deoxyribonucleoside Triphosphates
EDA	Ethylenediamine
FITC	Fluorescein Isothiocyanate
FMMD	Frequency Mixing Magnetic Detection
gDNA	Genomic DNA
HF	High Frequency
LAMP	Loop-Mediated Isothermal Amplification
LF	Low Frequency
LOD	Limit of Detection
MB	Magnetic Beads
MERS	Middle East Respiratory Syndrome
MH	Measurement Head
MgOAc	Magnesium Acetate
MNPs	Magnetic Nanoparticles
NA	Nucleic Acid
NAATs	Nucleic Acid Amplification Tests
NP	Nanoparticle
NTC	Non-Template Control
PBS	Phosphate Buffer Solution
PCR	Polymerase Chain Reaction
PE	Polyethylene
PEI	Polyethyleneimine

PEG	Polyethylene Glycol
POC	Point of Care
PWM	Pulse Width Modulation
RBT	Rose Bengal Test
RCA	Rolling Circle Amplification
RNA	Ribonucleic Acid
RPA	Recombinase Polymerase Amplification
RP	Ruhemann's Purple
SAMRS	Self-Avoiding Molecular Recognition System
SARS	Severe Acute Respiratory Syndrome
SAT	Standard Agglutination Test
SDA	Strand Displacement Amplification
SEM	Scanning Electron Microscope
SP	Superparamagnetism
SPION	Superparamagnetic Iron Oxide Nanoparticles
SPN	Superparamagnetic Nanoparticles
spp.	Species
ssDNA	Single-Stranded DNA
SSBs	Single Stranded DNA-Binding Proteins
Tm	Melting Temperature
µL	Microliter
µM	Micromolar

List of Publications

- **Abdalhalim Abuawad**, Yaqoub Ashhab, Andreas Offenhäusser, and Hans-Joachim Krause. "**DNA Sensor for the Detection of Brucella spp. Based on Magnetic Nanoparticle Markers**." International journal of molecular sciences 24, no. 24 (2023): 17272.

  Author Contributions:
  Abuawad: conceptualization, methodology, data curation, investigation, visualization, validation, writing—original draft, writing—review and editing; **Ashhab**: conceptualization, methodology, investigation, validation, supervision, writing—review and editing; **Offenhäusser**: resources, supervision; **Krause**: conceptualization, methodology, investigation, validation, resources, supervision, writing—review and editing.

- Max P. Jessing†, **Abdalhalim Abuawad** †, Timur Bikulov, Jan R. Abresch, Andreas Offenhäusser, and Hans-Joachim Krause. "**Isothermal Amplification Using Temperature-Controlled Frequency Mixing Magnetic Detection-Based Portable Field-Testing Platform.**" *Sensors* 24, no. 14 (2024): 4478.

  Author Contributions:
  Conceptualization, **Jessing** and **Abuawad**; methodology, **Jessing**, **Abuawad** and **Bikulov**; software, **Abresch** and **Jessing**; validation, **Jessing** and **Abuawad**; formal analysis, **Jessing**; data curation, **Jessing**; writing—original draft preparation, **Jessing** and **Abuawad**; writing—review and editing, all authors; visualization, **Jessing**; supervision, **Krause** and **Offenhäusser**; project administration, **Krause**; funding acquisition, **Krause.**

† These authors contributed equally to this work

Conference contribution

- **Abdalhalim Abuawad**; Yaqoub Ashhab; Andreas Offenhäusser; Hans-Joachim Krause; Magnetic nanoparticle-based sensor for detection of Brucella DNA at point of care. (Short talk and Poster) at the 4th European BioSensor Symposium 2023.

List of Patents

Abdalhalim Abuawad, Max Jesssing, Hans-Joachim Krause, Florian Schröper. “Apparatus and method for combined amplification and detection of a solution”. European patent: EP24153492.4, submitted (24.01.2024).

Acknowledgements

I would like to express my deepest gratitude to all those who supported me throughout this journey.

First of all, I would like to thank **Prof. Dr. Andreas Offenhäusser** for giving me the opportunity to work at the IBI-3 Institute. I am grateful for the supervision and resources that enabled me to achieve my research goals.

Prof. Dr. Hans-Joachim Krause, thank you for your continuous support, patience, and motivation and always being available for guidance. I have learned so much from you professionally and personally throughout this journey. I enjoyed working under your supervision as a member of your group (Magnetic field sensors group). I appreciate all your support.

Dr. Yaqoub Ashhab, thank you for your continuous trust in me. You have consistently provided invaluable support and guidance. Your advice and ideas for experiments and interpretations helped to guide this thesis in the right direction.

I am grateful to **Prof. Dr. Lothar Elling** for supporting my application to the faculty and agreeing to be a second referee for this thesis.

Dieter Lomparski, thank you for the design and software development of the automated measurement system. Our conversations at the coffee table were will not be forgotten.

Many thanks to **Max Jessing** for contributing to our joint patent and publication. I truly enjoyed working with you and appreciated your collaboration.

My friend **Ali Mohammad Pourshahidi**, your friendship has made my journey enjoyable.

Special thanks to **Faranak Eivazi** and **Timur Bikulov** for the great time and atmosphere at the institute, the discussions, and the willingness to help.

To my family and lovely parents, your lifelong support and guidance have been helpful in shaping who I am today. Thank you for your endless love and for always being there for me.

Assalla, thank you for encouraging and standing by me through every challenge. Your patience and support have been my greatest sources of strength. I am truly grateful for having you in my life.

Eleina, your presence has brought happiness and meaning to my life.

Band / Volume 99
Structure of two-dimensional multilayers and topological superconductors: surfactant mediated growth, intercalation, and doping
Y.-R. Lin (2023), x, 111 pp
ISBN: 978-3-95806-716-5

Band / Volume 100
Frequency mixing magnetic detection for characterization and multiplex detection of superparamagnetic nanoparticles
A. M. Pourshahidi (2023), X, 149 pp
ISBN: 978-3-95806-727-1

Band / Volume 101
Unveiling the relaxation dynamics of Ag/HfO2 based diffusive memristors for use in neuromorphic computing
S. A. Chekol (2023), x, 185 pp
ISBN: 978-3-95806-729-5

Band / Volume 102
Analysis and quantitative comparison of neural network dynamics on a neuron-wise and population level
R. Gutzen (2024), xii, 252 pp
ISBN: 978-3-95806-738-7

Band / Volume 103
3D Scaffolds with Integrated Electrodes for Neuronal Cell Culture
J. Abu Shihada (2024), vii, 163 pp
ISBN: 978-3-95806-756-1

Band / Volume 104
Advances in Photoemission Orbital Tomography
A. Haags (2024), ix, 254 pp
ISBN: 978-3-95806-766-0

Band / Volume 105
Quantitative investigation of point defects and their dynamics in focused ion beam-prepared group III-nitride lamellas by off-axis electron holography
K. Ji (2024), 164 pp
ISBN: 978-3-95806-782-0

Band / Volume 106
NeuCoNS and Stacked-Net: Facilitating the Communication for Accelerated Neuroscientific Simulations
R. Kleijnen (2024), xx, 110, xxi-xxxiv pp
ISBN: 978-3-95806-788-2

Band / Volume 107
Construction of a Spiking Network Model of Macaque Primary Visual Cortex: Towards Digital Twins
A. Kurth (2024), xvi, 207 pp
ISBN: 978-3-95806-800-1

Band / Volume 108
Spin selectivity of chiral molecules on surfaces
M.R. Safari (2025), xiv, 165 pp
ISBN: 978-3-95806-810-0

Band / Volume 109
Redox-based Random Access Memory Arrays for Computing-In-Memory and Neuromorphic Computing
H. Chen (2025), x, 154 pp
ISBN: 978-3-95806-814-8

Band / Volume 110
Mechanics of deep neural networks beyond the Gaussian limit
K. Fischer (2025), xvi, 138 pp
ISBN: 978-3-95806-815-5

Band / Volume 111
Characteristics of plastically deformed *fcc* and *bcc* High-Entropy Alloys
T. Meenen (2025), x, 115 pp
ISBN: 978-3-95806-820-9

Band / Volume 112
Software-Configurable Analog-To-Digital Converters for Configurable Pulse Detection
L. Krystofiak (2025), xvii, 113 pp, xxix
ISBN: 978-3-95806-826-1

Band / Volume 113
Development of Superparamagnetic Based Biological Sensor for the Detection of Brucella DNA Using Frequency Mixing Magnetic Detection
A. Abuawad (2025), X, 129 pp
ISBN: 978-3-95806-836-0

Weitere ***Schriften des Verlags im Forschungszentrum Jülich*** unter
http://wwwzb1.fz-juelich.de/verlagextern1/index.asp

Information
Band / Volume 113
ISBN 978-3-95806-836-0

Mitglied der Helmholtz-Gemeinschaft

JÜLICH
Forschungszentrum